THE ASTROPHYSICAL JOURNAL SUPPLEMENT SERIES, 133:345–393, 2001 April
© 2001. The American Astronomical Society. All rights reserved. Printed in U.S.A.

A HIGH-RESOLUTION SURVEY OF INTERSTELLAR K I ABSORPTION

DANIEL E. WELTY[1,2]
University of Chicago, Astronomy and Astrophysics Center, 5640 South Ellis Avenue, Chicago, IL 60637; welty@oddjob.uchicago.edu

AND

L. M. HOBBS[2]
University of Chicago, Yerkes Observatory, Williams Bay, WI 53191; hobbs@yerkes.uchicago.edu
Received 2000 June 22; accepted 2000 October 6

ABSTRACT

We present high-resolution (FWHM $\sim$0.4–1.8 km s^{-1}) spectra, obtained with the AAT UHRF, the McDonald Observatory 2.7 m coudé spectrograph, and/or the KPNO coudé feed, of interstellar K I absorption toward 54 Galactic stars. These new K I spectra reveal complex structure and narrow, closely blended components in many lines of sight. Multicomponent fits to the line profiles yield estimates for the column densities, line widths, and velocities for 319 individual interstellar cloud components. The median component width (FWHM) and the true median separation between adjacent components are both $\lesssim$1.2 km s^{-1}. The median and maximum individual component K I column densities, about 4×10^{10} and 10^{12} cm^{-2}, correspond to individual component hydrogen column densities of about 2×10^{20} and 10^{21} cm^{-2} and $E(B-V) \sim 0.03$ and 0.17, respectively. If T is typically $\sim$100 K, then at least half the individual components have subsonic internal turbulent velocities. We also reexamine the relationships between the column densities of K I, Na I, C I, Li I, H_{tot}, H_2, and CH. The four trace neutral species exhibit essentially linear relationships with each other over wide ranges in overall column density. If C is uniformly depleted by 0.4 dex, then Li, Na, and K are each typically depleted by 0.6–0.7 dex. The total line of sight values for N(K I) and N(Na I) show roughly quadratic dependences on $N(H_{tot})$, but the relationships for the ensemble of *individual* clouds could be significantly steeper. These quadratic (or steeper) dependences appear to rule out significant contributions to the ionization from cosmic rays, X-rays, and/or charge exchange with C II in most cases. Charge exchange with negatively charged large molecules may often be more important than radiative recombination in neutralizing most singly ionized atomic species in cool H I clouds, however—suggesting that the true n_e, n_H, and thermal pressures may be significantly smaller than the values estimated by considering only radiative recombination. Both N(CH) and $N(H_2)$ are nearly linearly proportional to N(K I) and N(Na I) [except for 10^{15} cm^{-2} $\lesssim N(H_2) \lesssim 10^{19}$ cm^{-2}, over which H_2 makes the transition to the self-shielded regime]. Those relationships appear also to hold for many individual components and component groups, suggesting that high-resolution spectra of K I and Na I can be very useful for interpreting lower resolution molecular data. The scatter about all these mean relationships is generally small ($\lesssim$0.1–0.2 dex), if certain consistently "discrepant" sight lines are excluded—suggesting that both the relative depletions and the relative ionization of Li, C, Na, and K are generally within factors of 2 of their mean values. Differences noted for sight lines in Sco-Oph, in the Pleiades, near the Orion Trapezium, and in the LMC and SMC may be due to differences in the strength and/or shape of the ambient radiation fields, perhaps amplified by the effects of charge transfer with large molecules.

Subject headings: ISM: abundances — ISM: atoms — ISM: kinematics and dynamics — line: profiles
On-line material: machine-readable tables

1. INTRODUCTION

In cool, neutral, predominantly atomic interstellar clouds at $T \sim 80$ K, the thermal widths (FWHM) of the absorption lines due to commonly observed elements range from 0.24 km s^{-1} (for ^{65}Zn) to 0.73 km s^{-1} (for ^{7}Li), and the internal turbulent motions may be comparable to the sound speed ($\sim$0.7 km s^{-1}). High spectral resolution ($R \gtrsim 200,000$, or FWHM $\lesssim 1.5$ km s^{-1}) is therefore required to discern and to determine the properties of individual interstellar clouds. High-resolution (FWHM $\sim$ 0.3–1.25 km s^{-1}) surveys of the interstellar absorption lines of Na I (Welty, Hobbs, & Kulkarni 1994, hereafter WHK) and Ca II (Welty, Morton, & Hobbs 1996, hereafter WMH) have revealed complex velocity structure in many lines of sight probing the Galactic disk and low halo, with a median separation between adjacent components (assumed to represent individual clouds) of approximately 1.2 km s^{-1}. Furthermore, those adjacent components may have very different properties [e.g., line widths, N(Na I)/N(Ca II) ratios]. The median line width for the components seen in Na I is about 1.2 km s^{-1} (FWHM); if $T \sim 80$ K (as inferred from observations of H_2), then at least 40% of the clouds have subsonic internal turbulent motions. The typically larger line widths for Ca II (even for components at the same velocities as those seen in Na I) suggest that Ca II generally occupies a somewhat larger volume, characterized by a larger T and/or turbulence.

Unfortunately, the relatively strong Na I D lines (at 5890 and 5896 Å) typically exhibit at least some saturation for lines of sight with total hydrogen column densities N(H) higher than about 10^{21} cm^{-2}—making it difficult to discern and characterize individual components even in high-resolution spectra. While the absorption from Ca II is

[1] Visiting observer, Kitt Peak National Observatory.
[2] Visiting observer, McDonald Observatory.

seldom saturated, large variations in both the calcium depletion and the calcium ionization balance make N(Ca II) a less reliable indicator of N(H). Because potassium is less abundant than either sodium or calcium by about a factor of 15 (and because the photoionization rate for K I is larger than that for Na I), significantly higher N(H) are required for K I to be detectable. High-resolution observations of the K I line at 7698 Å therefore can reveal the detailed interstellar component structure where the Na I D lines are saturated—providing information on the higher N(H) clouds which dominate many lines of sight. Spectra of K I recently have been used, for example, to delineate some of the cool H I clouds in a section of the local ISM (Trapero et al. 1992, 1995) and to extend studies of small-scale spatial structure in the ISM to higher N(H) clouds (Lauroesch & Meyer 1999).

Combining and comparing high-resolution spectra of K I, Na I, and other species can provide additional insights into the properties of interstellar clouds. First, we can determine the detailed component structure over a wider range of individual component column densities—K I reveals the strongest components, while Na I reveals additional lower column density components—enabling more accurate interpretation of lower resolution UV spectra of other similarly distributed species (e.g., Welty et al. 1999a, 1999b; Snow et al. 2000). Comparisons of individual component line widths, for species of different atomic weight, can yield estimates for the temperature and turbulence in the individual clouds (e.g., Dunkin & Crawford 1999) and/or information on cloud structure (Barlow et al. 1995; WMH). Comparisons of column densities of various trace neutral species can yield values for the relative elemental abundances and depletions (particularly valuable for Li, Na, and K, whose dominant first ions have no accessible lines) and constraints on grain scattering properties (e.g., Hobbs 1974c, 1976; Jenkins & Shaya 1979; Chaffee & White 1982). Ratios of trace and dominant species provide information on the processes affecting the ionization balance in interstellar clouds (e.g., Hobbs 1974b, 1976; Chaffee & White 1982; Lepp et al. 1988).

In this paper, we discuss spectra of interstellar K I, observed at resolutions of 0.4–0.6 and/or 1.2–1.8 km s^{-1}, toward 54 relatively bright Galactic stars. In most cases, these new spectra are characterized by higher resolution, higher S/N, and (therefore) higher sensitivity than previously available K I spectra. In §§ 2 and 3, we describe the procedures used to obtain, reduce, and analyze the spectra. In § 4, we discuss the statistical properties of the ensemble of individual components detected in K I and compare the K I absorption with that due to other species. We estimate typical depletions for Li, Na, and K and explore the effects of charge exchange with large molecules on the abundances of various trace neutral species in diffuse H I clouds. In an Appendix, we list the column density measurements for H_{tot}, H_2, Na I, K I, C I, Li I, and CH used for those comparisons.

2. OBSERVATIONS AND DATA REDUCTION

2.1. *Program Stars*

The 54 stars observed for interstellar K I absorption are listed in Table 1 in approximately increasing right ascension order, with Galactic coordinates, V magnitude, spectral type, and $E(B-V)$ as in WHK and WMH, who provide references for those data. Nineteen of the stars in the present K I survey were included in the Na I survey (WHK); a slightly different set of 19 was included in the Ca II survey (WMH). For those stars not in those two previous surveys, we have generally taken the relevant stellar data from the Bright Star Catalogue or its supplement (Hoffleit 1982; Hoffleit, Saladyga, & Wlasuk 1983) and have calculated $E(B-V)$ using the intrinsic colors tabulated by Johnson (1963). For stars within 300 pc, the distances correspond to the parallaxes measured by *Hipparcos* (ESA 1997); estimates for more distant stars are based on the absolute magnitudes and intrinsic colors listed by Blauuw (1963) and Johnson (1963), respectively.

Because higher N(H) are required for K I to be detectable (vs. Na I and Ca II), the stars observed for this survey of K I are (on average) more distant and more heavily reddened than those observed in the two previous surveys. The average and median distances (520 and 360 pc) are roughly 40% larger in the present survey, and the average and median $E(B-V)$ (0.29 and 0.22 mag) are about 3 times larger. In order to extend the range of well-determined K I column densities beyond that covered in previous surveys, we included both lightly reddened stars [10 with $E(B-V) \leq 0.06$ mag] and heavily reddened stars [10 with $E(B-V) \geq 0.50$ mag]. K I spectra for a set of 35 sight lines with 0.3 mag $\lesssim E(B-V) \lesssim 1.2$ mag, sampling so-called "translucent" clouds, will be presented in a future paper (Welty, Morton, & Snow 2001b, in preparation).

2.2. *Instrumental Setups*

Because the instrumental setups employed for these observations of K I are very similar to those used for the Na I and Ca II surveys, we will give only brief summaries here; more extensive descriptions may be found in WHK and WMH.

High-resolution K I spectra, with $\Delta v = 0.56 \pm 0.04$ km s^{-1} (FWHM), were obtained for 18 stars with the McDonald Observatory (McD) 2.7 m telescope and coudé spectrograph during two runs in 1989 October and 1995 September. As for the Na I spectra reported by WHK, the echelle grating was used in the double-pass configuration, with the TI2 CCD placed at the "scanner" focus. A quartz lamp was used for flat-field exposures; Th-Ar and potassium hollow cathode lamps were used to determine the wavelength scale. At this high resolution, only about 2.54 Å (99 km s^{-1} near the K I line at 7698.974 Å) was recorded on the CCD—which nonetheless provided sufficient wavelength coverage for all lines of sight except that toward 6 Cas, where the interstellar K I absorption spans about 90 km s^{-1}. The resolution was determined from the widths of the thorium lines in the Th-Ar exposures, assuming an intrinsic width of 0.55 km s^{-1} (see WHK), and was checked via comparisons with higher resolution UHRF spectra for ζ Oph and μ Sgr. S/N $\sim$ 100 was achieved in 180 minutes for ξ Per, which has $V \sim 4.0$.

Slightly higher resolution K I spectra, with $\Delta v = 0.40$–0.55 km s^{-1} (FWHM), were obtained for 7 stars with the Ultra-High Resolution Facility (UHRF) on the 3.9 m Anglo-Australian Telescope on 1994 June 9 and 1995 June 19 by M. Lemoine and R. Ferlet, who have graciously allowed the spectra to be presented here. The UHRF uses a 31.6 g mm^{-1} echelle grating in conjunction with a grating cross-disperser and a long focal length camera to achieve resolutions of 0.3–1.0 km s^{-1} (Diego et al. 1995). The 35-

TABLE 1

STELLAR DATA

Star	Name	l^a	b^a	V	Type	$E(B-V)$	Distance (pc)	Spectra[b]
HD 2905	κ Cas	120 50	+00 08	4.16	B1 Iae	0.33	900	K, M
HD 21291	...	141 30	+02 53	4.23	B9 Ia	0.40	1060	K, M
HD 22192	ψ Per	149 10	−06 05	4.23	B5 Ve	0.10	215	K
HD 23630	η Tau	166 40	−23 28	2.87	B7 III	0.03	113	K
HD 23850	27 Tau	167 00	−23 15	3.62	B8 III	0.00	117	K2
HD 24760	ε Per	157 21	−10 06	2.89	B0.5 III	0.10	165	K2
HD 23180	o Per	160 22	−17 44	3.82	B1 III	0.32	360	K, M
HD 24398	ζ Per	162 17	−16 42	2.85	B1 Ib	0.31	360	M
HD 24912	ξ Per	160 22	−13 07	4.03	O8 III	0.33	700	K, M
HD 27778	62 Tau	172 46	−17 23	6.36	B3 V	0.39	225	K2
HD 31964	ε Aur	162 47	+01 11	2.99	A8 Iab	0.37	1020	K2, M
HD 35149	23 Ori	199 10	−17 52	5.00	B1 V	0.11	295	K, M
HD 35411	η Ori	204 52	−20 24	3.35	B0.5 Vnn	0.11	276	K
HD 36861	λ Ori	195 03	−12 00	3.39	O	...	450	K, M
HD 37128	ε Ori	205 13	−17 15	1.69	B0 Ia	0.06	450	K
HD 37468	σ Ori	206 49	−17 20	3.80	O9.5 V	0.06	450	K
HD 37742	ζ Ori	206 27	−16 36	1.77	O9.5 Ib	0.06	250	M
HD 38771	κ Ori	214 31	−18 30	2.05	B0.5 Ia	0.04	221	K
HD 40111	139 Tau	183 58	+00 50	4.83	B0.5 II	0.19	780	K
HD 41117	χ^2 Ori	189 41	−00 52	4.60	B2 Iae	0.48	980	K2
HD 58350	η CMa	242 37	−06 29	2.45	B5 Ia	0.01	765	K2
HD 89688	23 Sex	241 01	+46 17	6.66	B2 IV	0.16	785	K2
HD 91316	ρ Leo	234 53	+52 46	3.85	B1 Ib	0.05	950	K2
HD 146010......	...	37 29	+44 01	6.75	A1 IV	0.10	89	K2
HD 141637......	1 Sco	346 06	+21 43	4.68	B1.5 Vn	0.19	160	K
HD 143275......	δ Sco	350 06	+22 29	2.30	B0.2 IV	0.19	125	K
HD 144217......	β^1 Sco	353 11	+23 36	2.62	B1 V	0.20	163	K
HD 144470......	ω^1 Sco	352 45	+22 46	3.96	B1 V	0.22	130	K2
HD 145502......	ν Sco	354 37	+22 42	4.01	B2 IV	0.28	135	K
HD 147084......	o Sco	352 20	+18 03	4.55	A4 II/III	0.72	170	K, A
HD 147165......	σ Sco	351 19	+17 00	2.89	B2 III	0.37	225	K2
HD 147933......	ρ Oph	353 41	+17 41	4.63	B1 V	0.48	120	K, A
HD 148184......	χ Oph	357 56	+20 41	4.40	B1.5 Ve	0.53	150	K, A
HD 148605......	22 Sco	353 06	+15 48	4.80	B3 V	0.08	120	K
HD 149757......	ζ Oph	6 17	+23 36	2.56	O9.5 Vnn	0.32	140	K, M, A
HD 154090......	...	350 50	+04 17	4.87	B1 Iae	0.45	1060	A
HD 154368......	...	349 58	+03 13	6.13	O9 Ia	0.78	1000	K
HD 164353......	67 Oph	29 44	+12 38	3.97	B5 Ib	0.11	740	K2
HD 165024......	θ Ara	343 20	−13 49	3.66	B2 Ib	0.09	660	A
HD 166937......	μ Sgr	10 00	−01 36	3.85	B2 III	0.46	165	M, A
HD 174638......	β Lyr	63 11	+14 47	3.52	B7 Ve	0.12	270	K2
HD 193267......	P Cyg	75 49	+01 19	4.80	B1Pe	0.63	1500	K
HD 197345......	α Cyg	84 17	+02 00	1.25	A2 Ia	0.09	500	K, M
HD 198183......	λ Cyg	78 05	−04 20	4.54	B6 IV	0.03	270	K
HD 198478......	55 Cyg	85 45	+01 29	4.84	B3 Iae	0.54	1010	M
HD 206165......	9 Cep	102 16	+07 15	4.73	B2 Ib	0.47	640	M
HD 206267......	...	99 17	+03 44	5.62	O6e	0.53	810	K
HD 207198......	...	103 08	+06 59	5.95	O9 IIe	0.62	1040	K
HD 207260......	ν Cep	102 19	+05 56	4.30	A2 Iab	0.51	780	M
HD 209975......	19 Cep	104 52	+05 23	5.11	O9 Ib	0.36	1060	K
HD 210839......	λ Cep	103 50	+02 37	5.06	O6 Iab	0.55	840	K, M
HD 212571......	π Aqr	65 59	−44 44	4.64	B1 Ve	0.22	330	K
HD 217675......	o And	102 12	−16 06	3.62	B6 IIIp	0.05	212	K, M
HD 223385......	6 Cas	115 43	+00 13	5.43	A3 Iae	0.67	1600	M

[a] Units of degrees and arcminutes.

[b] K = KPNO coudé feed (1993–1999; FWHM = 1.4–1.8 km s^{-1}); K2 = KPNO coudé feed (2000; FWHM = 1.2 km s^{-1}); A = AAT UHRF (1994, 1995; FWHM = 0.4–0.55 km s^{-1}); M = McDonald 2.7 m (1989, 1995; FWHM = 0.56 km s^{-1}).

slice image slicer (Diego 1993) and Tektronix CCD (1024 × 1024, 24 μm pixels) were used for all the observations reported here. All exposures were binned by 4 pixels perpendicular to the dispersion. Because of the large number of CCD rows filled by the stellar spectrum and the clean response of the CCD, flat-fielding was not required (cf. WMH). The spectral resolution, $\Delta v = 0.40$ km s^{-1} (1994) and 0.55 km s^{-1} (1995), was determined via scans of a stabilized He-Ne laser line at 6328.160 Å and by examination of the widths of the thorium lines in the Th-Ar exposures used for wavelength calibration. Because the interstellar K I absorption is detectable over only fairly narrow velocity intervals along these seven lines of sight, the 6.78 Å wavelength coverage recorded on the CCD was quite sufficient. S/N $\sim$ 370 was achieved in 40 minutes for ζ Oph, which has $V \sim 2.6$.

K I spectra with a resolution $\Delta v = 1.4$–1.8 km s^{-1} (FWHM) were obtained for 37 stars with the 0.9 m coudé feed (CF) telescope and 2.1 m coudé spectrograph of the Kitt Peak National Observatory during various runs from 1993 to 1999. To achieve the desired high resolution, we used the echelle grating, cross-dispersed via grism 730 in first order, camera 6, and a 70–90 μm entrance slit, corresponding to 0\.5–0\.6 on the sky. An RG-610 filter eliminated the grism's second-order contributions. Two different CCDs were used (T1KA: 1024 $\times$ 1024, 24 μm pixels in 1993; F3KB: 1024 $\times$ 3072, 15 μm pixels thereafter). The CCD was positioned so that lines of constant wavelength fell along columns; most exposures were binned by 2 pixels perpendicular to the dispersion. Flat-field exposures were obtained using a quartz lamp; the wavelength calibration was established via a Th-Ar lamp. For the 1993 observations, a significant extra "background" signal of about 110 $\pm$ 10 counts per unbinned pixel per hour was present; it was removed during the data reductions and appears to have had no significant effect on the extracted spectra. As a rough benchmark, we achieved S/N $\sim$ 115 in 50 minutes in "typical" seeing for ξ Per; the achievable S/N appears to have been limited to less than about 200 in several of the runs due to residual fringing remaining after flat-fielding.

The spectral resolution characterizing those CF K I spectra is somewhat poorer than that achieved with a similar setup at the Ca II K line (WMH). In general, it was very difficult to obtain a good focus in the order containing the K I line; even at the "best" focus, the thorium lines in the Th-Ar spectra were noticeably asymmetric (perhaps suggestive of some astigmatism?) for all runs except the one in 1994. The effective instrumental profile was first estimated by fitting the profiles of the thorium lines in the Th-Ar lamp exposures with one or two Gaussian components, then refined via comparisons with higher resolution spectra obtained at the AAT and/or McDonald (for which the instrumental profiles are narrower and much more symmetric). ζ Oph, whose K I profile is dominated by two narrow components separated by about 1 km s^{-1}, was observed during most runs; λ Cep, HD 21291, and ϵ Aur, whose K I profiles include several narrow, well-defined components, were each observed during several runs. For the 1994 CF spectra, the instrumental profile may be represented by a single Gaussian function, with FWHM = 1.4 $\pm$ 0.1 km s^{-1}. For the other CF runs, the instrumental profile is modeled with two Gaussian functions, generally with individual FWHM $\sim$ 1.0–1.2 km s^{-1}, separation $\sim$0.8–1.2 km s^{-1}, and relative strengths 0.15–0.3 : 1.0—corresponding to effective resolutions of about 1.55–1.8 km s^{-1}.

K I spectra for 13 stars in this survey were obtained with the CF in 2000 February, using a very similar instrumental setup (grism 780-2 and the 3° wedge were used for cross-dispersion), not long after the spectrograph had been realigned. The realignment appears to have greatly improved the focus, the instrumental profile, and the resolution near the K I line—the thorium lines in the Th-Ar spectra were symmetric and indicated a resolution of about 1.2 km s^{-1}, even when using a slit width of 130 μm (0\.9). These 13 sight lines are noted by a "K2" in the last column of Table 1.

2.3. *Data Reduction*

The initial processing of the CCD images from all three telescopes and the extraction of one-dimensional spectra were carried out using various IRAF routines, as for the Na I and Ca II data described by WHK and WMH. Wavelength calibration was accomplished via exposures of Th-Ar hollow cathode lamps, using the thorium rest wavelengths of Palmer & Engelman (1983). For the CF spectra, quadratic fits to the 6–12 lines found in the K I order yield typical residuals of 1–2 mÅ, or 0.04–0.08 km s^{-1}. Calibration exposures were usually obtained at the beginning, middle, and end of each night; in general, the zero points agree to within 10 mÅ, or 0.4 km s^{-1} (and usually much better), and the dispersions agree to within 0.03% for any individual night. At the higher McD and UHRF resolutions, only 4–6 Th-Ar lines with previously known wavelengths were generally found within the $\sim$2.5–6.8 Å spectral range recorded on the CCDs; linear fits to those lines yield typical residuals of 0.3–0.9 mÅ, or 0.01–0.04 km s^{-1}. For the UHRF observations, calibration spectra were usually obtained immediately before and/or immediately after each stellar exposure; the zero points agree to within 6 mÅ, or 0.23 km s^{-1}, and the dispersions agree to within 0.03% for each night. Comparisons of both the interstellar line profiles and the telluric absorption features, for lines of sight observed with more than one of the three systems, suggest very slight systematic differences in velocity zero point. We have adjusted the UHRF, McD, and CF velocities by +0.3, −0.1, and +0.2 km s^{-1}, respectively, where the absolute zero points were established via comparisons with Na I (WHK). There is therefore good agreement in both velocity scale and zero point between these K I spectra and the Na I and Ca II spectra reported by WHK and WMH. For example, for 24 "corresponding" components identified in the profile analysis (§ 4.1.3), v(K I) − v(Ca II) is 0.08 $\pm$ 0.17 km s^{-1} (mean $\pm$ standard deviation).

The wavelength-calibrated spectra were normalized by fitting Legendre polynomials to regions free of interstellar absorption. In all cases, sufficient continuum was present on both sides of the interstellar features (though, as noted above, some very weak K I absorption is present outside the observed range for 6 Cas). The relatively weak telluric absorption lines present near the interstellar K I lines were fitted (or predicted, via observations of stars displaying no interstellar K I, when "buried" within the interstellar absorption) and removed. The S/N determined in the continuum fits and the total equivalent width of the interstellar K I absorption measured from the normalized spectra are given in the second and third columns of Table 2. Entries on the first, second, and third lines for each star are from CF, McD, and UHRF spectra, respectively. The median S/Ns achieved, for the three data sets, are $\sim$120, 100, and 190, respectively. Those median S/Ns yield 2 σ equivalent width uncertainties or limits for narrow absorption lines, including contributions from both photon noise and continuum placement uncertainty, of about 1.0 mÅ (CF), 0.5 mÅ (McD), and 0.25 mÅ (UHRF), which correspond to unsaturated K I column densities of 5.6, 2.8, and 1.4 $\times$ 10^9 cm^{-2}, respectively. For the 13 lines of sight observed both with the CF and at higher resolution, the K I

TABLE 2

K I EQUIVALENT WIDTHS AND COMPONENT STRUCTURES

Star	S/N	W_λ (mÅ)	Comp	$v_\odot$ (km s^{-1})	N (10^{10} cm^{-2})	b (km s^{-1})
κ Cas	110	79.4	1	−24.95	4.8	1.81
	95	79.3	2	−22.26	3.8	[0.50]
	...	...	3	−21.16	13.1	[0.70]
			4	−19.27	5.2	1.32
			5	−16.01	1.9	[1.30]
			6	−14.39	8.8	0.60
			7	−12.87	2.5	[0.70]
			8	−10.79	2.7	[1.40]
			9	−6.77	5.2	0.57
			10	−5.63	3.6	2.11
HD 21291......	115	142.6	1	−17.14	1.0	0.76
	110	141.2	2	−14.04	0.2	[0.40]
	...	...	3	−12.31	8.4	0.73
			4	−10.52	14.4	0.66
			5	−8.72	3.1	[0.80]
			6	−7.43	4.2	[0.50]
			7	−5.95	8.9	0.74
			8	−4.14	9.4	0.62
			9	−2.03	2.5	(0.70)
			10	−0.47	48.5	[0.70]
			11	0.59	27.0	0.76
			12	2.71	1.2	0.23
ψ Per	115	20.8	1	−6.90	0.6	(0.80)
	...	...	2	−4.02	2.9	[0.40]
	...	...	3	−2.56	2.5	[0.60]
			4	−0.87	1.9	(1.00)
			5	2.37	3.5	0.38
			6	6.57	1.1	0.73
η Tau	220	0.5	1	16.76	0.3	0.96
27 Tau	110	3.2	1	16.22	1.6	1.25
ϵ Per...........	145	1.6	1	7.06	0.9	0.63
o Per	135	98.1	1	10.50	12.5	0.60
	100	95.5	2	11.52	10.0	0.44
	...	...	3	13.45	44.3	0.72
			4	14.74	22.5	0.62
			5	15.72	3.9	(0.60)
ζ Per...........	...	...	1	11.48	2.2	(1.00)
	100	67.6	2	13.25	26.0	0.68
	...	...	3	14.54	42.7	0.80
			4	16.40	0.1	(0.50)
ξ Per	200	59.9	1	6.71	17.6	0.56
	100	57.6	2	8.30	4.3	(1.20)
	...	...	3	9.62	7.0	[0.50]
			4	10.46	6.0	0.33
			5	11.32	2.4	(1.00)
			6	14.55	2.0	(1.00)
			7	15.23	2.1	(0.50)
62 Tau	85	83.6	1	12.60	2.2	(0.60)
	...	...	2	14.14	13.6	0.40
	...	...	3	15.22	19.2	(0.70)
			4	17.36	14.2	(0.80)
			5	18.62	17.5	0.40
			6	20.20	1.8	(0.70)
ϵ Aur	210	88.3	1	−3.18	0.4	(0.70)

TABLE 2—*Continued*

Star	S/N	W_λ (mÅ)	Comp	$v_\odot$ (km s^{-1})	N (10^{10} cm^{-2})	b (km s^{-1})
	140	93.4	2	−1.17	1.6	[0.50]
	…	…	3	0.60	48.8	0.83
			4	2.56	1.2	[0.50]
			5	4.30	2.8	[1.10]
			6	5.54	8.5	0.61
			7	6.65	1.6	(0.70)
			8	8.25	2.7	0.75
			9	9.87	0.9	[0.50]
			10	11.38	1.4	[0.50]
			11	12.62	9.7	0.67
23 Ori........	70	43.0	1	20.62	1.5	(1.00)
	60	45.7	2	21.95	12.6	0.80
	…	…	3	24.09	16.9	1.32
			4	26.87	0.3	(1.00)
η Ori	140	15.4	1	6.48	3.6	0.79
	…	…	2	8.55	4.8	1.06
	…	…	3	25.13	0.9	0.88
λ Ori	90	40.1	1	22.63	1.5	[1.00]
	110	37.0	2	24.31	8.0	0.94
	…	…	3	25.82	6.8	(0.80)
			4	26.75	5.3	0.37
			5	27.54	3.1	[1.00]
ϵ Ori	180	3.4	1	11.12	0.7	1.31
	…	…	2	17.17	0.3	0.56
	…	…	3	24.63	1.0	0.92
σ Ori.........	135	6.6	1	19.79	2.1	0.75
	…	…	2	24.12	1.7	1.00
ζ Ori	…	…	1	23.42	1.7	0.53
	150	5.3	2	26.70	1.4	0.48
κ Ori.........	135	5.9	1	17.78	0.6	(0.60)
	…	…	2	20.28	2.9	1.13
139 Tau......	65	21.1	1	6.73	0.5	(0.80)
	…	…	2	12.84	0.9	(0.80)
	…	…	3	15.29	7.2	[0.60]
			4	17.90	1.2	(0.80)
			5	21.48	1.7	[0.70]
			6	23.14	1.9	[0.70]
χ^2 Ori........	95	168.6	1	4.70	0.7	(0.80)
	…	…	2	8.97	26.9	1.85
	…	…	3	10.80	18.6	0.57
			4	12.48	9.8	(1.00)
			5	15.12	77.8	[1.25]
			6	17.54	14.0	[1.00]
			7	19.91	4.7	0.65
			8	22.08	1.0	(0.80)
η CMa	160	2.0	1	15.32	0.3	(1.00)
	…	…	2	20.23	0.3	(1.00)
	…	…	3	23.52	0.4	(1.00)
23 Sex........	55	61.3	1	−3.26	1.0	(0.70)
	…	…	2	3.25	11.1	0.79
	…	…	3	6.13	48.1	0.75
			4	8.1	0.6	(0.70)
ρ Leo	280	2.5	1	−12.57	0.2	(1.20)
	…	…	2	−10.91	0.2	[0.60]

TABLE 2—*Continued*

Star	S/N	W_λ (mÅ)	Comp	$v_\odot$ (km s^{-1})	N (10^{10} cm^{-2})	b (km s^{-1})
	...	...	3	−8.45	0.3	[1.10]
			4	−6.87	0.1	(0.80)
			5	−4.74	0.2	[1.09]
			6	−0.99	0.3	[0.44]
			7	18.51	0.3	0.57
HD 146010......	55	38.5	1	−18.16	3.0	[0.40]
	...	...	2	−16.08	31.1	0.64
1 Sco............	170	16.6	1	−16.69	1.1	0.69
	...	...	2	−13.95	0.8	(0.80)
	...	...	3	−8.39	5.6	[0.50]
			4	−6.40	2.0	(1.00)
δ Sco............	155	26.5	1	−14.81	1.5	1.08
	...	...	2	−10.90	16.4	1.03
β^1 Sco	150	20.9	1	−10.95	1.9	(0.60)
	...	...	2	−8.95	11.5	0.74
ω^1 Sco..........	170	23.6	1	−23.50	0.2	(0.80)
	...	...	2	−17.49	0.3	(0.70)
	...	...	3	−12.49	0.7	[0.50]
			4	−11.11	6.5	0.44
			5	−9.65	2.2	(0.70)
			6	−8.35	3.6	0.49
			7	−5.85	1.7	1.14
ν Sco............	120	38.2	1	−12.56	5.2	0.60
	...	...	2	−10.23	7.5	[1.00]
	...	...	3	−8.49	9.2	[0.50]
			4	−6.90	2.2	(0.80)
			5	−4.01	0.8	(1.00)
o Sco	105	121.0	1	−11.80	2.3	0.31
	...	...	2	−9.54	0.9	(0.30)
	190	126.4	3	−7.84	35.3	[0.60]
			4	−7.17	20.6	(0.60)
			5	−6.19	57.4	[0.70]
			6	−4.38	0.3	(0.50)
σ Sco	175	21.8	1	−14.23	0.4	(0.70)
	...	...	2	−8.75	0.8	1.23
	...	...	3	−6.26	8.1	0.75
			4	−4.62	3.8	0.54
			5	−3.13	0.6	(0.60)
ρ Oph	100	87.3	1	−13.37	1.5	0.93
	...	...	2	−11.19	0.6	[0.30]
	90	85.4	3	−10.39	3.7	[0.40]
			4	−9.03	29.7	0.62
			5	−8.02	48.1	[0.60]
			6	−6.83	16.7	0.44
			7	−6.19	1.3	(0.60)
χ Oph...........	110	68.0	1	−13.11	1.1	[0.60]
	...	...	2	−11.78	25.9	0.52
	240	66.7	3	−10.94	35.4	0.60
			4	−9.02	9.2	0.86
			5	−7.77	0.3	[0.60]
22 Sco	40	5.0	1	−7.53	2.8	0.87
ζ Oph...........	360	61.6	1	−19.09	1.0	0.96
	70	61.6	2	−16.50	1.2	[0.80]
	370	60.4	3	−14.98	40.9	0.57

TABLE 2—*Continued*

Star	S/N	W_λ (mÅ)	Comp	$v_\odot$ (km s^{-1})	N (10^{10} cm^{-2})	b (km s^{-1})
			4	−13.96	27.2	0.43
			5	−12.73	1.1	0.58
HD 154090	...	...	1	−12.29	0.5	[0.70]
	...	...	2	−9.79	23.6	0.57
	120	111.3	3	−8.54	18.0	[0.50]
			4	−7.59	8.1	[0.50]
			5	−6.24	5.7	0.66
			6	−4.76	0.7	(0.60)
			7	−2.57	30.4	0.58
			8	−1.68	12.4	1.35
HD 154368	120	199.1	1	−20.95	32.9	1.20
	...	...	2	−18.69	1.4	(1.00)
	...	...	3	−15.10	5.8	0.62
			4	−13.93	1.5	(1.00)
			5	−7.20	3.9	(0.80)
			6	−4.62	59.7	0.96
			7	−2.15	105.0	0.87
			8	0.31	8.9	(0.80)
			9	3.02	1.7	(1.00)
			10	6.18	4.2	1.15
67 Oph	145	38.3	1	−20.86	4.1	1.10
	...	...	2	−17.94	2.3	[0.80]
	...	...	3	−15.84	2.1	(0.70)
			4	−14.67	4.8	[0.40]
			5	−12.62	6.5	0.79
			6	−10.62	2.5	[1.00]
			7	−8.11	1.2	0.83
θ Ara	...	...	1	−4.43	0.9	0.61
	...	...	2	−3.01	4.0	[0.60]
	195	28.4	3	−2.25	3.7	[0.40]
			4	−1.15	4.3	0.87
			5	0.66	3.5	0.69
			6	2.38	0.2	[0.30]
			7	4.19	1.1	0.39
μ Sgr	...	...	1	−9.79	1.8	0.99
	125	41.0	2	−7.06	7.3	1.09
	80	41.9	3	−5.65	21.3	0.66
			4	−4.48	1.8	(0.70)
β Lyr	170	23.5	1	−23.78	2.2	[0.40]
	...	...	2	−22.33	5.3	0.82
	...	...	3	−20.99	2.4	(0.70)
			4	−19.00	3.2	[0.35]
			5	−17.87	0.8	(0.50)
			6	−14.37	0.5	1.58
P Cyg	125	43.4	1	−19.14	2.8	1.23
	...	...	2	−16.64	4.2	0.93
	...	...	3	−14.11	2.2	(1.00)
			4	−12.25	1.6	(0.60)
			5	−10.59	4.6	[0.60]
			6	−9.33	5.8	[0.60]
			7	−7.89	3.7	(1.50)
			8	−5.26	1.1	(1.50)
			9	0.51	0.7	[0.50]
α Cyg	300	15.6	1	−21.64	1.7	0.62
	125	14.1	2	−12.93	3.8	0.54
	...	...	3	−8.19	1.3	0.49
			4	−4.19	0.2	(0.50)
			5	−2.74	0.6	0.43

TABLE 2—*Continued*

Star	S/N	W_λ (mÅ)	Comp	$v_\odot$ (km s^{-1})	N (10^{10} cm^{-2})	b (km s^{-1})
			6	1.27	0.6	0.42
λ Cyg	95	2.8	1	−9.91	1.7	1.59
55 Cyg	...	...	1	−24.75	1.3	1.25
	85	127.2	2	−21.05	0.8	[0.80]
	...	...	3	−18.91	7.1	0.63
			4	−17.15	9.4	[0.70]
			5	−16.13	19.4	[0.70]
			6	−14.20	7.6	0.82
			7	−12.40	6.8	(1.00)
			8	−10.78	21.5	[0.55]
			9	−10.04	23.7	[0.70]
			10	−5.95	5.8	2.20
			11	−2.21	0.4	(0.80)
			12	−0.85	0.5	(0.80)
9 Cep	...	...	1	−27.67	0.4	(0.80)
	110	192.4	2	−25.88	1.9	[0.80]
	...	...	3	−24.20	29.3	0.65
			4	−22.95	1.3	(0.80)
			5	−20.44	6.9	0.96
			6	−18.40	8.4	0.77
			7	−16.68	8.6	0.67
			8	−14.89	39.0	0.82
			9	−13.52	13.8	0.47
			10	−12.50	8.1	(0.80)
			11	−11.57	8.2	[0.50]
			12	−10.18	33.6	0.77
			13	−8.98	4.6	(0.80)
			14	−6.63	0.7	(1.00)
HD 206267	125	198.1	1	−21.71	1.1	(1.00)
	...	...	2	−18.74	29.3	[0.70]
	...	...	3	−17.11	49.1	(0.80)
			4	−15.69	35.4	(0.80)
			5	−13.57	26.8	0.64
			6	−11.98	26.0	(1.00)
			7	−9.69	31.1	0.81
			8	−7.25	2.7	(1.00)
HD 207198	120	236.7	1	−21.36	4.8	(1.00)
	...	...	2	−19.37	29.8	0.62
	...	...	3	−17.14	19.9	(1.00)
			4	−15.28	62.3	1.15
			5	−12.89	70.4	0.90
			6	−10.15	19.1	[0.80]
			7	−8.33	46.1	0.74
			8	−7.02	4.8	(1.00)
ν Cep	...	...	1	−23.76	5.7	0.88
	125	206.6	2	−21.64	36.3	[0.88]
	...	...	3	−20.59	17.3	0.49
			4	−19.30	17.7	[0.70]
			5	−17.69	36.7	0.64
			6	−16.49	33.0	[0.80]
			7	−14.99	18.4	0.68
			8	−13.63	4.7	(0.80)
			9	−12.11	7.3	0.54
			10	−10.48	17.0	0.52
			11	−8.91	1.0	0.45
19 Cep	115	95.1	1	−18.37	12.0	[1.50]
	...	...	2	−15.49	12.2	0.81
	...	...	3	−13.41	8.2	[0.80]
			4	−11.39	19.4	[0.90]

TABLE 2—*Continued*

Star	S/N	W_λ (mÅ)	Comp	$v_\odot$ (km s^{-1})	N (10^{10} cm^{-2})	b (km s^{-1})
			5	−9.42	7.7	(1.00)
			6	−6.91	3.3	0.73
λ Cep	90	161.6	1	−34.60	11.2	0.81
	85	157.0	2	−32.87	1.3	[0.60]
	...	...	3	−31.07	1.9	0.53
			4	−17.26	3.9	0.97
			5	−15.35	41.5	0.58
			6	−13.40	39.4	0.66
			7	−11.00	12.3	[1.10]
			8	−9.57	3.9	[0.60]
			9	−8.39	1.8	(0.80)
			10	−6.55	1.6	(1.00)
			11	−5.21	7.6	0.60
			12	−2.70	9.7	0.53
			13	−1.50	0.7	(0.80)
π Aqr	95	8.3	1	−13.23	1.6	1.88
	...	...	2	−5.74	2.7	1.58
	...	...	3	−1.59	0.8	(0.60)
o And......	145	9.9	1	−19.97	1.8	0.79
	140	11.0	2	−10.66	0.6	0.81
	...	...	3	−8.37	3.1	0.89
			4	−6.21	0.7	0.76
6 Cas	...	...	1	−38.76	0.9	0.40
	70	146.5	2	−31.26	1.2	(0.80)
	...	...	3	−30.22	2.4	[0.50]
			4	−28.49	45.4	0.76
			5	−26.28	4.8	(1.00)
			6	−24.92	5.0	[0.80]
			7	−23.26	3.8	(0.80)
			8	−21.93	8.9	0.74
			9	−19.92	5.9	[1.20]
			10	−17.43	11.8	0.60
			11	−14.70	2.5	(1.20)
			12	−12.43	3.6	(1.20)
			13	−10.90	3.3	[0.60]
			14	−9.86	8.4	[0.80]
			15	−7.72	1.3	(1.20)
			16	−4.91	0.6	(1.00)
			17	8.52	1.4	1.30
			18	22.20	0.4	[0.50]

NOTE.—Table 2 is also available in machine-readable form in the electronic edition of the *Astrophysical Journal.*

equivalent widths generally agree within their mutual 2 σ uncertainties, and the ratio of equivalent widths (CF vs. McD/UHRF) is 1.01 ± 0.05 (mean ± standard deviation)—i.e., there are no apparent systematic differences in equivalent width.

3. RESULTS

3.1. *Spectra and Profile Analysis*

The normalized K I spectra are shown in Figures 1–9, where the order is the same as in Table 1. For lines of sight observed both with the CF and at higher resolution, the CF spectrum is shown at the top, with the McD or UHRF spectrum offset below. The source of each spectrum is indicated at the right, just above the continuum. At the bottom of each panel, we show the corresponding Na I D1 or D2 spectrum. Nineteen of the Na I spectra are from WHK (FWHM = 0.5 km s^{-1}), 22 were obtained with the CF at resolutions of about 1.5–2.5 km s^{-1} (including three—λ Ori, ρ Oph, HD 206267—by Watson & Meyer 1996), and another nine, with resolutions of about 1.0–2.0 km s^{-1}, were originally presented by Hobbs (PEPSIOS; Hobbs 1969, 1975, 1976). We note that some of the higher resolution Na I profiles show clear evidence for narrow, hyperfine-split components, as discussed by WHK (see, e.g., α Cyg). All the PEPSIOS Na I spectra have been shifted by −0.55 km s^{-1} (see WHK and § 3.2 below), and slight adjustments were made to the K I velocities from the three observatories (as noted above), but the Na I and K I profiles for individual stars have not otherwise been shifted in velocity to force alignment. Some telluric absorption features may be present in the PEPSIOS Na I profiles. For o Sco ($v \sin i \sim 10$ km s^{-1}), the dotted lines show the stellar

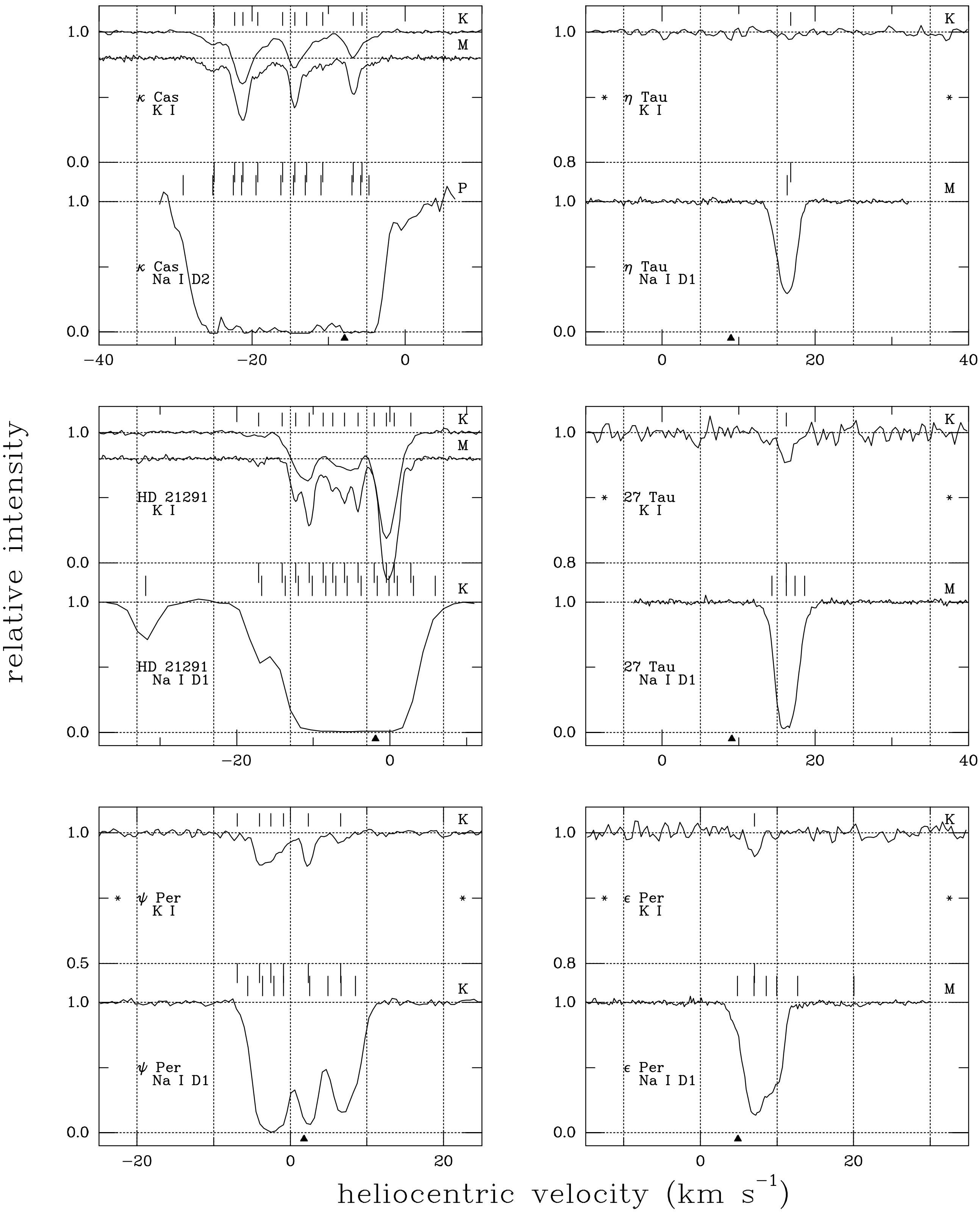

FIG. 1.—Interstellar K I and Na I profiles. The vertical scale has been expanded in some cases to show weaker lines more clearly (noted by an asterisk near both vertical axes). The sources of the spectra have been noted at the right, just above the continuum [M = McDonald 2.7 m coudé (FWHM = 0.56 km s^{-1} for K I, FWHM = 0.50 km s^{-1} for Na I); K = KPNO coudé feed (FWHM = 1.2–1.8 km s^{-1} for K I, FWHM = 1.5–2.5 km s^{-1} for Na I); A = AAT UHRF (FWHM = 0.4–0.55 km s^{-1}); P = PEPSIOS (FWHM ∼ 1.0–2.0 km s^{-1})]. Tick marks above the spectra indicate the components found in fitting the profiles; the K I components are repeated above the Na I spectra for comparison. Some telluric absorption may be present in the PEPSIOS Na I profiles. The solid triangles denote $v_{LSR} = 0$ km s^{-1}.

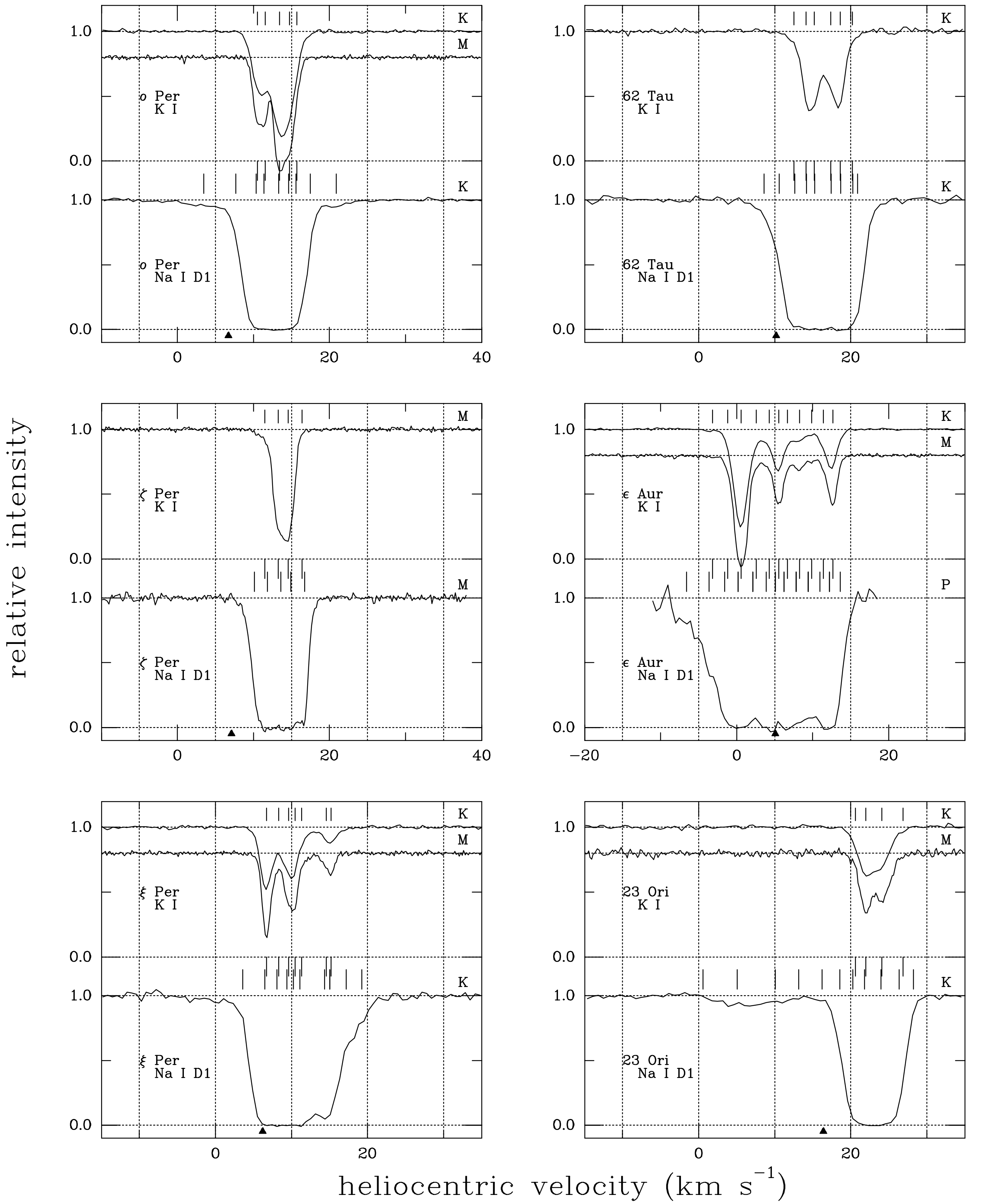

FIG. 2.—Interstellar K I and Na I profiles (as for Fig. 1)

absorption present for both K I and Na I (Hobbs 1975). We have chosen the Na I and K I reference wavelengths to be the weighted means of the wavelengths of the individual hyperfine subcomponents (5889.9509 Å, 5895.9242 Å, 7698.974 Å) to facilitate comparisons between the Na I and K I profiles.

We have used the method of profile fitting to determine column densities (N), line widths ($b \sim$ FWHM/1.665), and velocities (v) for the discernible individual interstellar clouds contributing to the observed line profiles. As in the Na I and Ca II surveys, we have assumed that each cloud/component may be represented by a symmetric Voigt line profile and

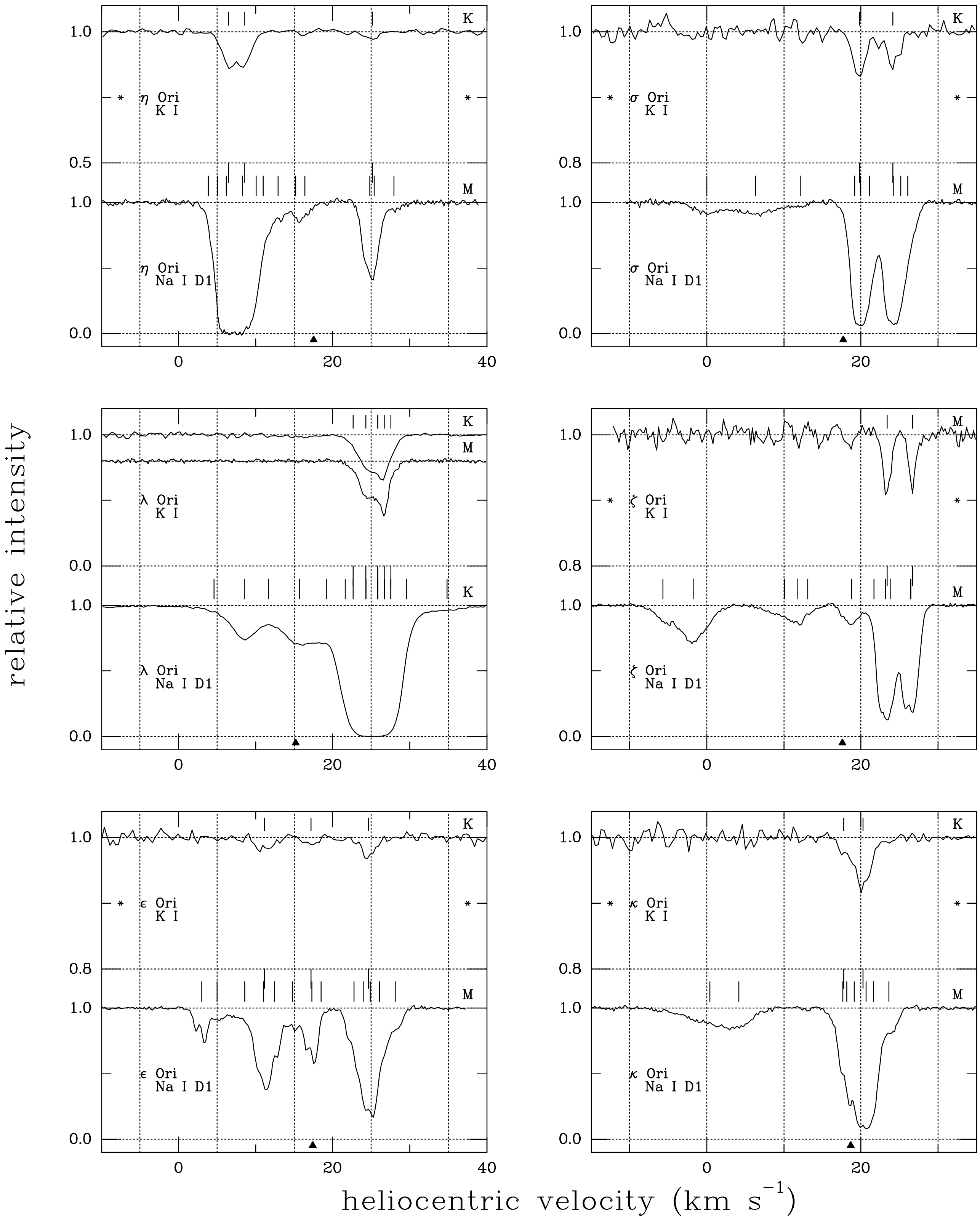

FIG. 3.—Interstellar K I and Na I profiles (as for Fig. 1)

have adopted the minimum number of components needed to adequately fit the observed profiles, given the S/N achieved in each case. We used either a one or two-Gaussian instrumental profile, as described above, to fit the profiles observed with the different spectrographs. The rest wavelengths and oscillator strengths of the two K I hyperfine components are listed in Appendix A of WHK. While the individual hyperfine components (separated by 0.35 km s^{-1}) are not resolved in these spectra, inclusion of the hyperfine structure does significantly affect the derived

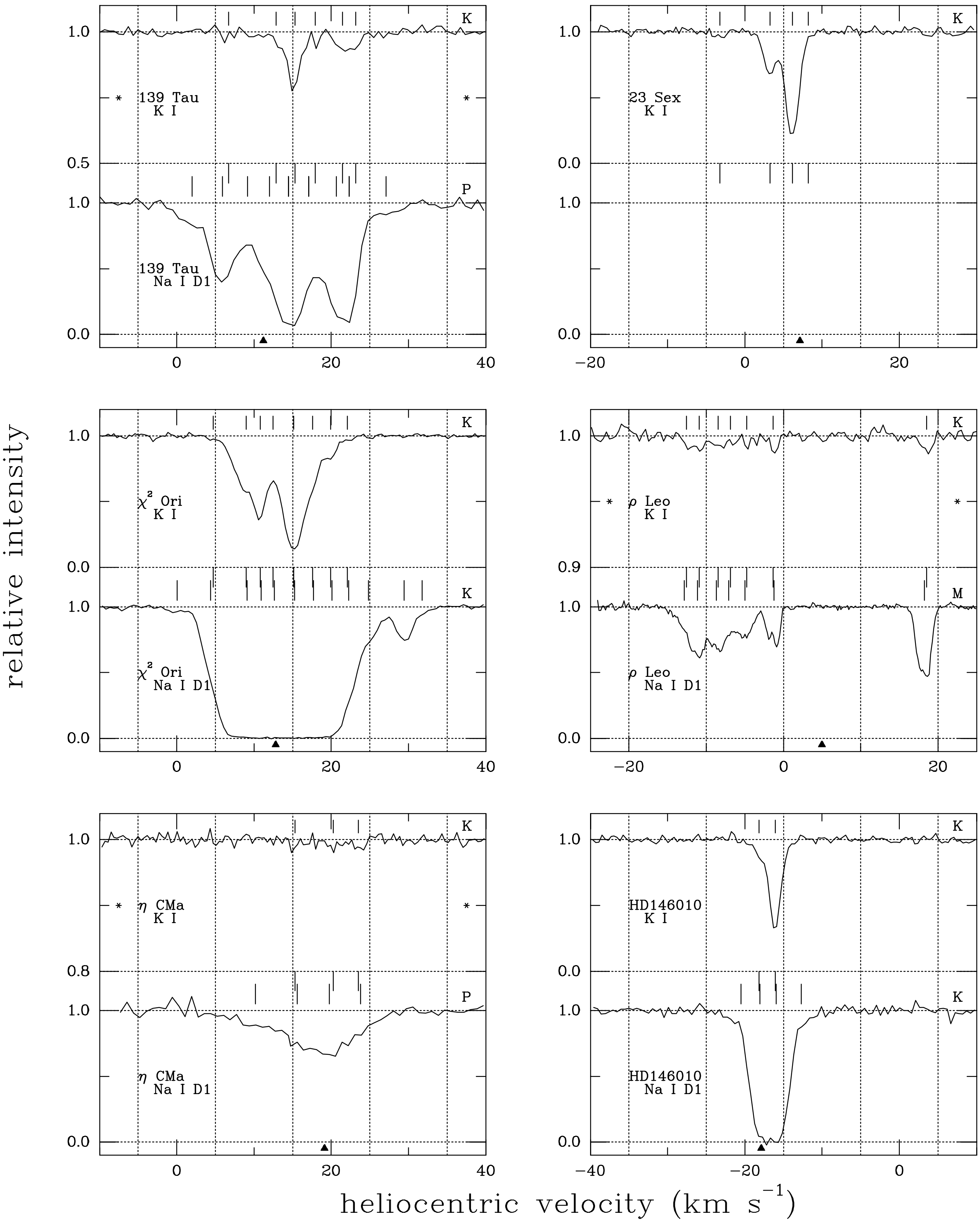

FIG. 4.—Interstellar K I and Na I profiles (as for Fig. 1)

widths of the narrowest lines. Since the K I lines are not as saturated as the Na I lines, acceptable fits were achieved for essentially all of the K I spectra, contrary to our experience with some of the stronger Na I absorption features. The individual components derived in the profile fits are noted in Figures 1–9 by tick marks above the spectra; the K I components are shown again just above the Na I components, to facilitate comparisons between the two species. Some of the Na I fits and column densities derived in this paper differ slightly from those obtained by WHK, who

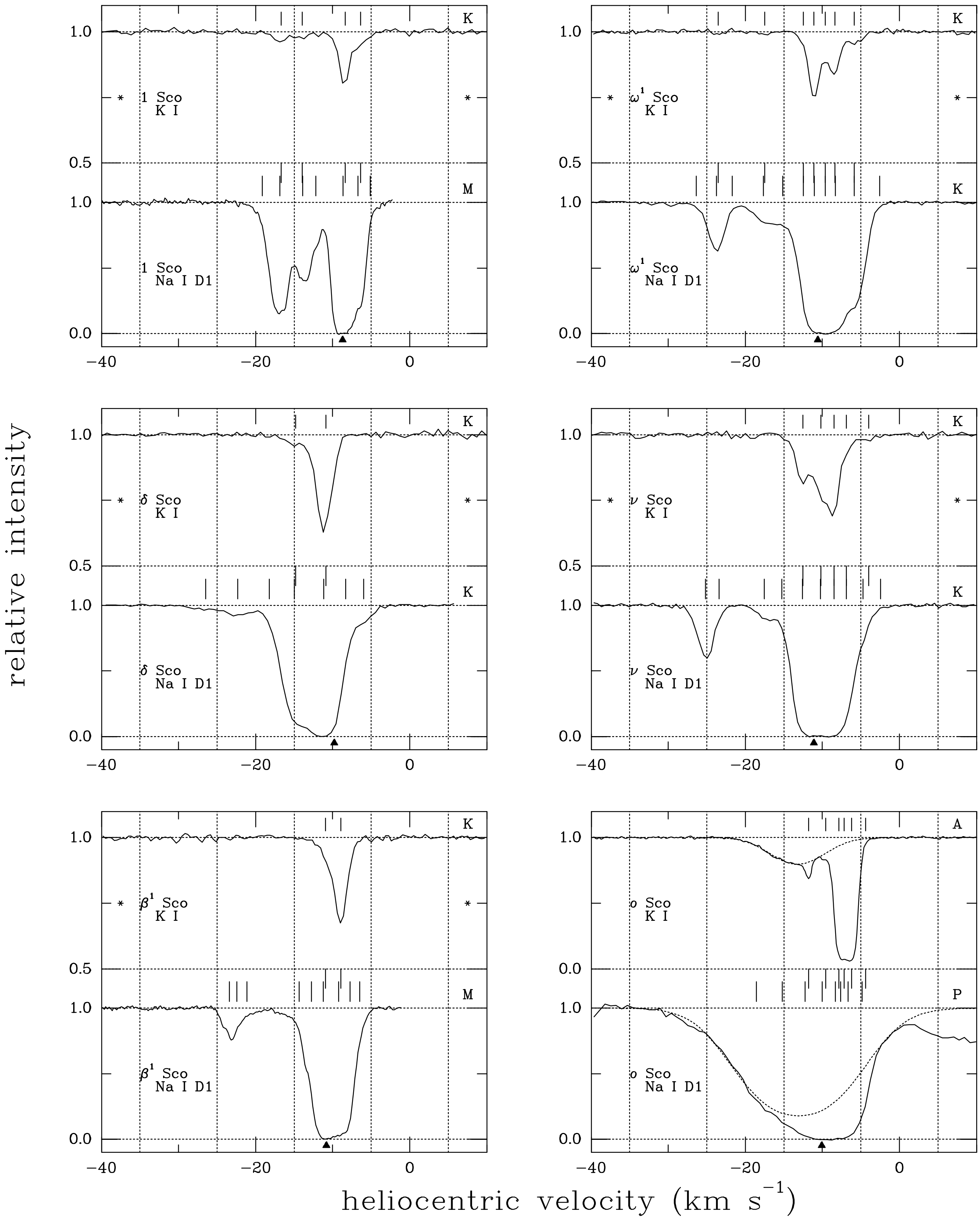

FIG. 5.—Interstellar K I and Na I profiles (as for Fig. 1). The dotted lines for o Sco indicate the stellar K I and Na I lines.

used preliminary versions of the K I component structures. The component structures for some of the PEPSIOS Na I profiles are not well determined, in view of the uncertainties in continuum and velocity zero point and the possible presence of telluric lines. The fits to saturated portions of the Na I D line profiles used the component structure found for K I, with the column densities scaled to yield the equivalent widths measured for the weaker Na I λ3302 doublet (which are available for nearly all such sight lines). Conversely, the fit to the very weak CF K I profile toward ρ Leo was guided

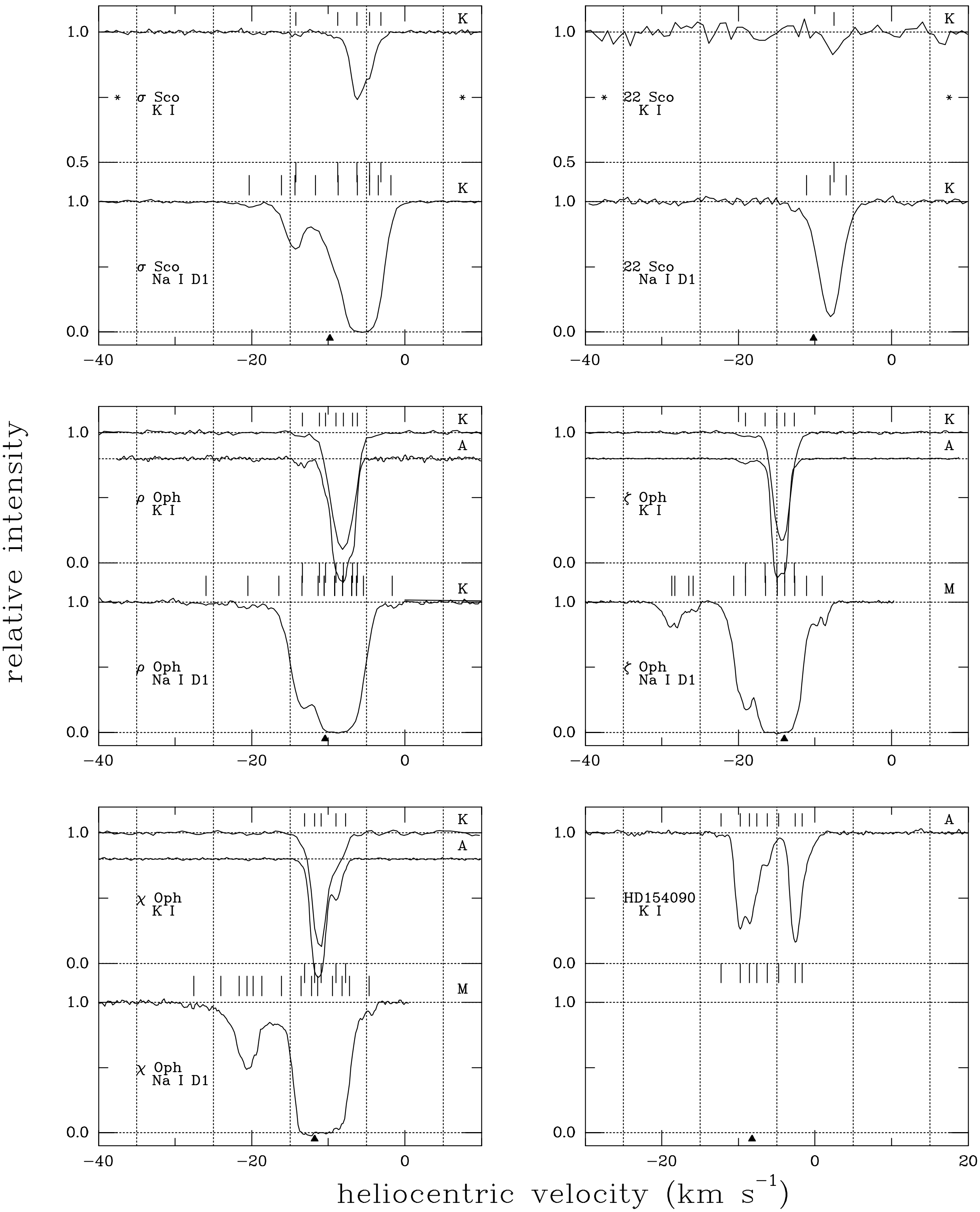

FIG. 6.—Interstellar K I and Na I profiles (as for Fig. 1)

by the component structure found for Na I; other weak K I lines observed with the CF could be fitted in this manner as well. The individual component parameters derived from the K I spectra are listed in Table 2, where successive columns give the star name, continuum S/N, equivalent width, component number, heliocentric velocity, column density, and *b*-value. The parameters derived from the higher resolution UHRF or McD spectra are given where available.

As was found in the Na I and Ca II surveys, these new higher resolution, higher S/N K I spectra show complex component structure in most lines of sight. Only five of the

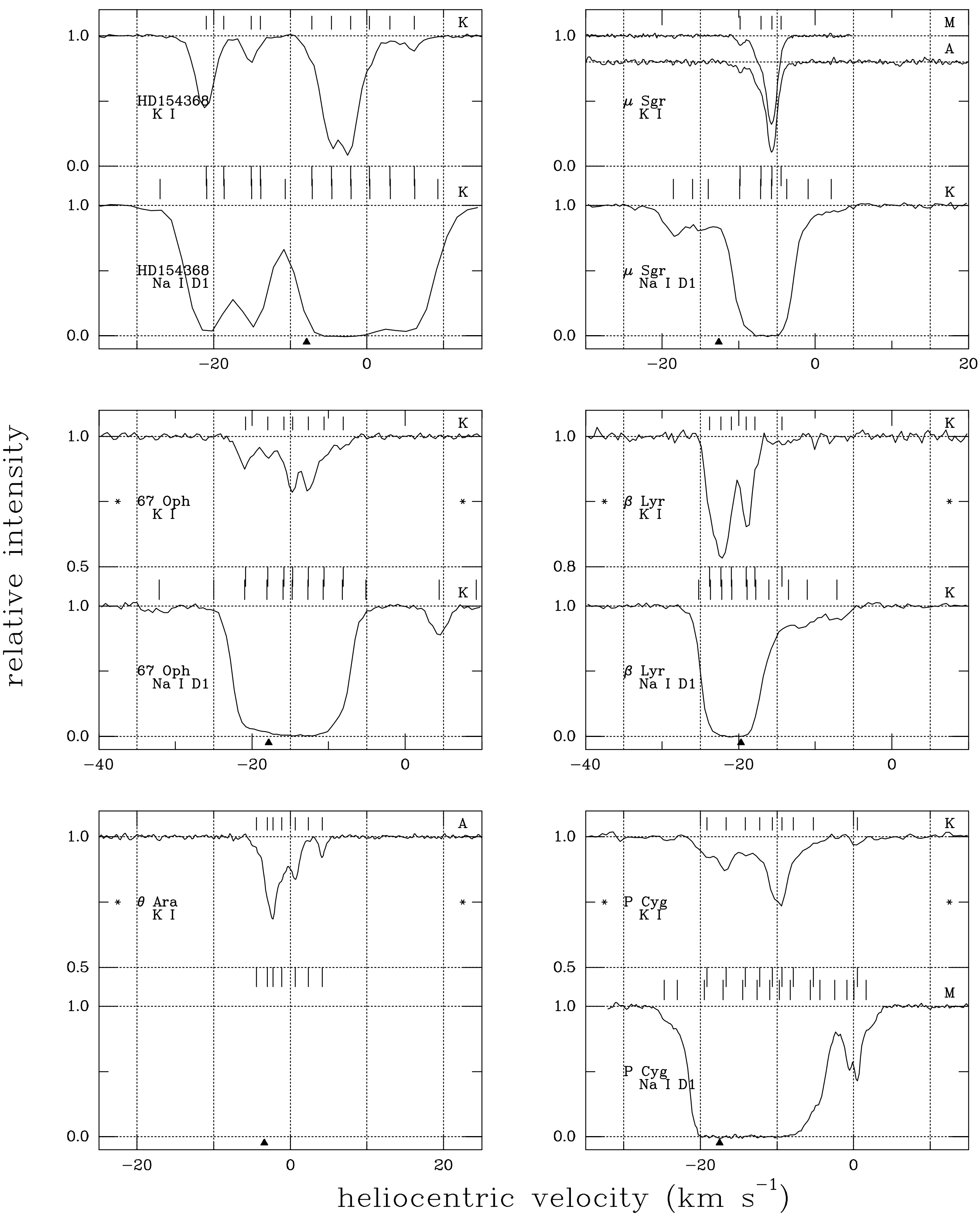

FIG. 7.—Interstellar K I and Na I profiles (as for Fig. 1)

54 K I profiles, those toward η Tau, 27 Tau, ϵ Per, 22 Sco, and λ Cyg, can be adequately fitted by a single component. All five were observed with the CF (i.e., at lower resolution), all five show weak lines (≤ 5 mÅ), and all five exhibit more complex structure in the stronger Na I and/or Ca II lines. The K I profiles observed toward 11 other stars at $d \lesssim 200$ pc each require 2–7 components, and those observed toward stars beyond 700 pc can require more than 10 components. Not surprisingly, the higher resolution UHRF/McD spectra often reveal more components than are discernible in the CF spectra—for the 13 lines of sight observed with both, a total of 95 components are found in

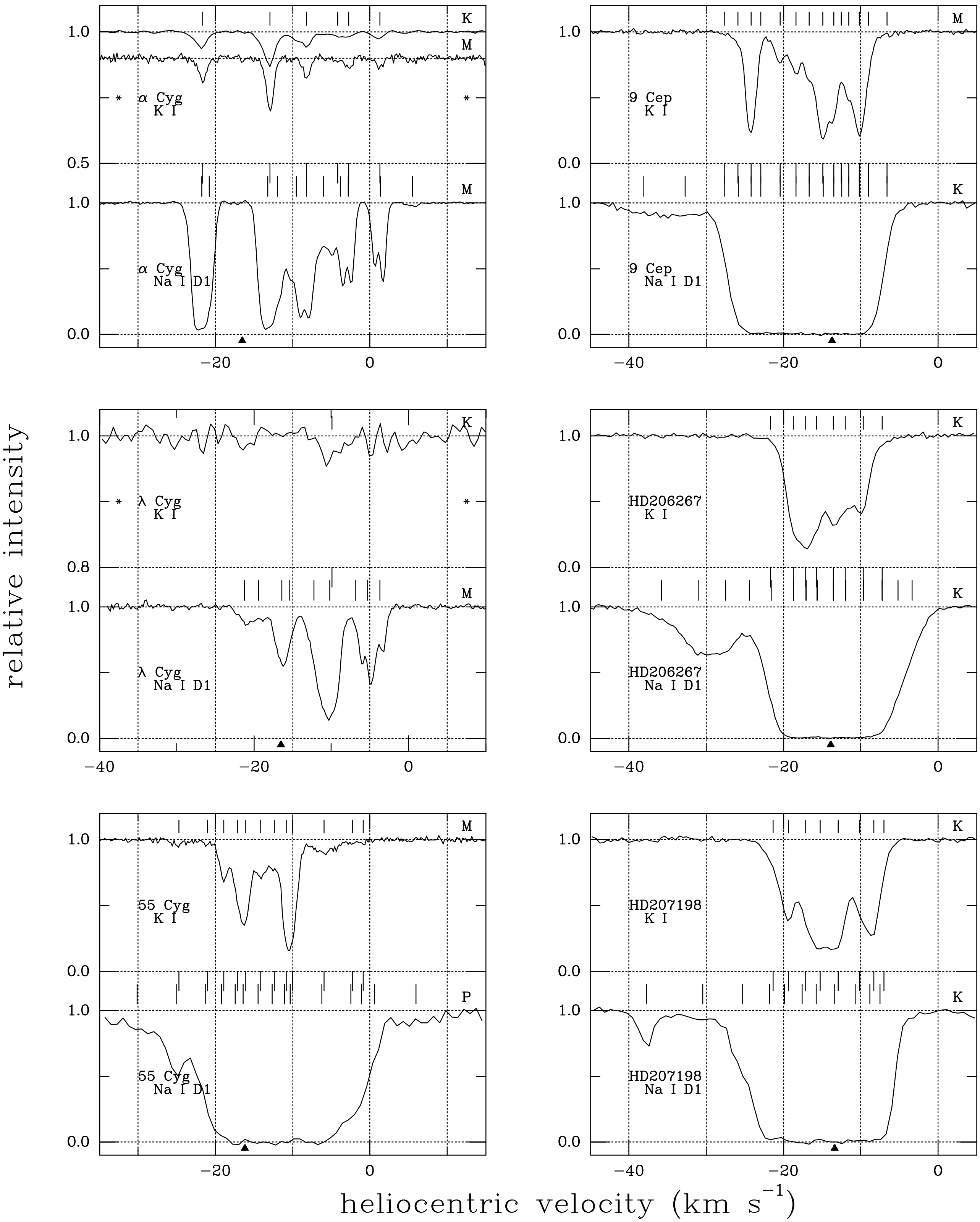

FIG. 8.—Interstellar K I and Na I profiles (as for Fig. 1)

the UHRF/McD spectra, while 74 are found in the CF spectra. For example, while the strong K I absorption toward ζ Oph and ρ Oph may be adequately fitted by single components in the CF spectra, the UHRF and McD spectra of those two stars require two and three narrow, closely spaced components, respectively. Comparisons of very weak K I features in some of the CF spectra (e.g., for 27 Tau, ϵ Per, ϵ Ori, σ Ori, κ Ori, λ Cyg, and π Aqr) with the corresponding strong, but unsaturated features in the higher resolution Na I spectra (WHK) suggest that the more complex structure seen in Na I is likely present in K I as well.

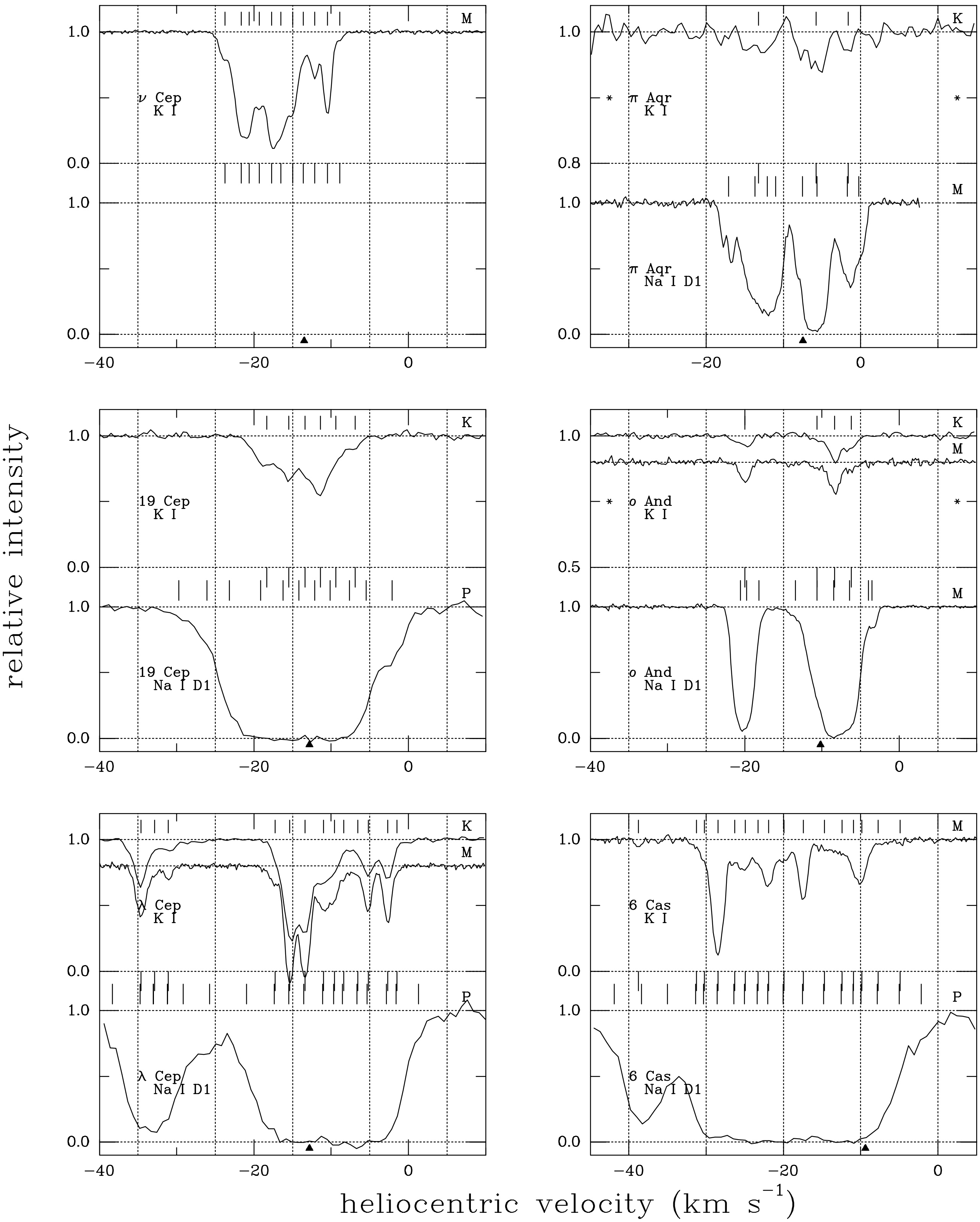

FIG. 9.—Interstellar K I and Na I profiles (as for Fig. 1)

Of the 319 individual interstellar cloud components listed in Table 2, 180 were derived from UHRF and/or McD spectra (23 stars), with the remaining 139 from the lower resolution CF spectra (31 stars). For well-defined components with $N \lesssim 10^{11}$ cm^{-2}, the formal 1 σ uncertainties in the column densities are typically a few times 10^9 cm^{-2}, comparable to the uncertainties that would be inferred from the error bars on the equivalent widths. The uncertainties in the column densities can be 10%–20% for stronger, but still well-defined components, and can be somewhat larger for significantly blended components. For most components, the derived velocities have formal uncertainties of less than

0.1 km s^{-1}, though the uncertainties can be larger for broader or more severely blended components. Comparisons among the CF, McD, UHRF, and Na I and Ca II spectra discussed above suggest that the absolute velocities for most well-defined components should be accurate to within about 0.2–0.3 km s^{-1}. Such comparisons also suggest that the parameters for some of the weak K I components (e.g., those needed to fit the wings of the stronger absorption) are less well determined. For some components, the b-values were not allowed to vary in the profile fitting. Those enclosed in square brackets were fixed to facilitate convergence of the fits and are about as well determined as the b-values allowed to vary—i.e., in general they could not be changed by more than about 15%–20% without noticeably degrading the fit. The 91 b-values enclosed in parentheses, often for weak and/or blended components, were essentially arbitrarily, though not unreasonably, fixed in the fitting and are less well determined. As for Na I and Ca II, uncertainties in the component parameters due to not discerning the full K I component structure (§ 4.1.4) may well be more significant than the formal uncertainties derived in the profile fits.

3.2. *Comparisons with Other* K I *Data*

Nineteen of the lines of sight in the present survey were also observed by Chaffee & White (1982, hereafter CW), at a resolution of about 8 km s^{-1} (FWHM). For those lines of sight, the ratio of equivalent widths is W(CW)/W(present) $= 1.09 \pm 0.20$ (mean $\pm$ standard deviation), and most of the integrated K I column densities agree within ± 0.2 dex.

Equivalent widths for the much weaker K I doublet at 4044 and 4047 Å have been measured for a few of the higher column density lines of sight. The equivalent widths of those weak K I lines and the corresponding column densities derived in the weak-line limit are listed in Table 3. The total line of sight column densities derived from the fits to the high-resolution λ7698 profiles, shown in the last column of the table, are quite consistent with those obtained from the weaker K I doublet. The good agreement in column density, for such strong λ7698 lines dominated by fairly narrow components (0.4 km s$^{-1} \lesssim b \lesssim$ 1.0 km s^{-1}), suggests (1) that we have accurately established the zero flux level in the λ7698 spectra and (2) that the derived component b-values (and thus the adopted instrumental FWHM) are also accurate.

Many of the lines of sight reported in this paper were observed previously with the PEPSIOS interferometric spectrometer, at an estimated resolution $\Delta v \sim 1.2$ km s^{-1} (FWHM) (Hobbs 1974a, 1974b, 1975, 1976); lower resolution spectra were obtained for a few other lines of sight. The present equivalent widths generally show good agreement with those from 1976 (and later), but the earlier PEPSIOS equivalent widths appear to be systematically higher by about 30% (for 10 lines of sight with $W_\lambda > 15$ mÅ; not including the much higher values for ψ Per, η CMa, and ρ Oph). Given the limited S/Ns, the uncertain backgrounds and continua, and the possible presence of weak telluric features in the PEPSIOS spectra, comparisons with the present spectra yield no strong evidence for time variable K I absorption. As for Na I and Ca II, there is a systematic offset in velocity zero point of approximately -0.55 ± 0.25 km s^{-1} (new minus PEPSIOS). Simulations using the profile fitting program and the K I component structures derived from the spectra presented here suggest that the effective resolution of the PEPSIOS K I spectra is closer to $\sim$1.8 km s^{-1}.

Sembach, Danks, & Lambert (1996) obtained a high-resolution (FWHM $\sim$ 0.56 km s^{-1}) K I spectrum of ζ Oph at McDonald, using an instrumental setup much like ours, for comparison with similar spectra of C_2. The component structure derived from that K I spectrum is very similar to ours—for the two strongest components, the velocities differ by 0.11–0.15 km s^{-1}, the b-values differ by 0.04–0.07 km s^{-1}, and the total column density differs by about 3%.

Lauroesch & Meyer (1999) obtained K I spectra of the individual stars in the β^1 Sco, ν Sco, HD 206267, and ρ Oph multiple stellar systems, using the CF and camera 6. For the brighter stars in each system, the Lauroesch & Meyer spectra are very similar to the CF spectra presented in this paper, though their resolution (FWHM $\sim$ 1.76 km s^{-1}) is slightly poorer. The UHRF spectra of ρ Oph A (Fig. 6), however, clearly reveal more complex structure within the strong absorption near -8 km s^{-1}. For the other three lines of sight, the component structures listed by Lauroesch & Meyer are similar to those given in Table 2, though some of their b-values are smaller and though the component velocities toward β^1 Sco and ν Sco appear to be about 0.8 km s^{-1} more negative.

4. DISCUSSION

4.1. *Component Statistics*

Much of the background for the following presentation of statistics derived from the ensemble of K I line component parameters was developed in our Na I and Ca II

TABLE 3

K I λ4044,4047 DATA[a]

Star	W_λ(4044) (mÅ)	W_λ(4047) (mÅ)	Reference	N(4044)[b] (cm^{-2})	N(7698)[c] (cm^{-2})
o Per	0.98 ± 0.04	...	1	$12.05^{+0.01}_{-0.02}$	$11.97^{+0.02}_{-0.03}$
ζ Per	0.61 ± 0.03	0.36 ± 0.02	1	$11.88^{+0.03}_{-0.04}$	$11.85^{+0.03}_{-0.03}$
HD 147889	3.1 ± 0.5	2.1 ± 0.5	2	$12.59^{+0.05}_{-0.06}$	...
ρ Oph	1.5 ± 0.5	...	3	$12.23^{+0.13}_{-0.18}$	$12.01^{+0.02}_{-0.02}$
ζ Oph	0.7 ± 0.3	...	3	$11.90^{+0.15}_{-0.25}$	$11.85^{+0.01}_{-0.01}$
HD 154368	2.4 ± 0.5	1.0 ± 0.5	4	$12.40^{+0.06}_{-0.08}$	$12.35^{+0.02}_{-0.02}$

[a] Uncertainties are 1 σ.
[b] Column density computed from λ4044 doublet equivalent widths, assuming weak-line limit.
[c] Column density computed from fits to λ7698 profiles.
REFERENCES.—(1) Knauth et al. 2000; (2) Haffner & Meyer 1995; (3) Crutcher 1978 (see also Shulman et al. 1974); (4) Snow et al. 1996.

TABLE 4

STATISTICS FOR K I, Ca II, AND Na I

Ion	Source[a]	Sample[b]	Lines of Sight	Clouds	b_{med} (km s^{-1})	$(\log N)_{med}$ (cm^{-2})	δv_{med} (km s^{-1})	$\langle v_{LSR} \rangle$ (km s^{-1})	$\langle v_{LSR}^2 \rangle^{1/2}$ (km s^{-1})	Comments
K I........	All	Full	54	319	0.77	10.54	1.9	1.67	7.45	
		Primary	54	228	0.71	...	...	...	...	
	CF	Full	45	210	0.85	10.50	2.2	1.24	7.06	
		Primary	45	135	0.82	...	...	...	...	
	McD, UHRF	Full	23	180	0.71	10.63	1.7	2.79	8.05	
		Primary	23	141	0.67	...	...	...	...	
Na I.......	McD	Full	38	276	0.81	11.09	2.0	−0.70	8.60	From WHK
		Primary	38	238	0.73	...	...	...	...	
		Full	38	101	...	...	...	2.06	6.59	log[N(Na I)] > 11.3
Ca II......	CF[c]	Full	39	336	1.48	10.70	2.9	−0.82	12.04	From WMH
		Primary	39	250	1.32	...	...	...	...	
	UHRF[c,d]	Full	14	181	1.40	10.61	2.4	−5.28	13.52	
		Primary	14	156	1.33	...	...	...	...	

[a] McD = McDonald 2.7 m (FWHM = 0.5–0.56 km s^{-1}); CF = KPNO coude feed (FWHM = 1.2–1.8 km s^{-1}); UHRF = AAT UHRF (FWHM = 0.3–0.55 km s^{-1}).
[b] Primary = components with well-determined b-values; Full = all components.
[c] HD 72127 A, HD 93521 omitted from $\langle v_{LSR} \rangle$, $\langle v_{LSR}^2 \rangle^{1/2}$.
[d] Using ζ Oph components from Barlow et al. 1995.

surveys (WHK; WMH). Those references also discuss the effects of limited samples, inhomogeneities in resolution and S/N, and the likelihood that we have not discerned all the components actually present. We will make comparisons between the statistics obtained for K I and those obtained for Na I and Ca II, but note that significant differences in the set of lines of sight observed for K I—as reflected in the larger median $E(B-V)$ and distances (§ 2.1)—suggest that some differences in statistical properties may be expected. On the other hand, some of the Na I component structures were constrained by preliminary fits to the corresponding K I spectra (where the Na I D1 line is saturated), so the K I and Na I component samples are not entirely independent.

Various statistics, for several subsets of the new high-resolution K I data, are listed in Table 4, illustrated in Figures 10–16, and discussed in the following sections. In the table and figures, the "primary" samples refer to the subsets of components for which b was either varied in the fits or fixed but well determined. Because the higher resolution McD and UHRF spectra generally reveal more of the apparently typically complex K I component structure, the 141 components comprising the "primary UHRF/McD" sample should provide the most accurate statistics, especially for line widths and component separations. The full component sample is generally used for statistics not involving b, however.

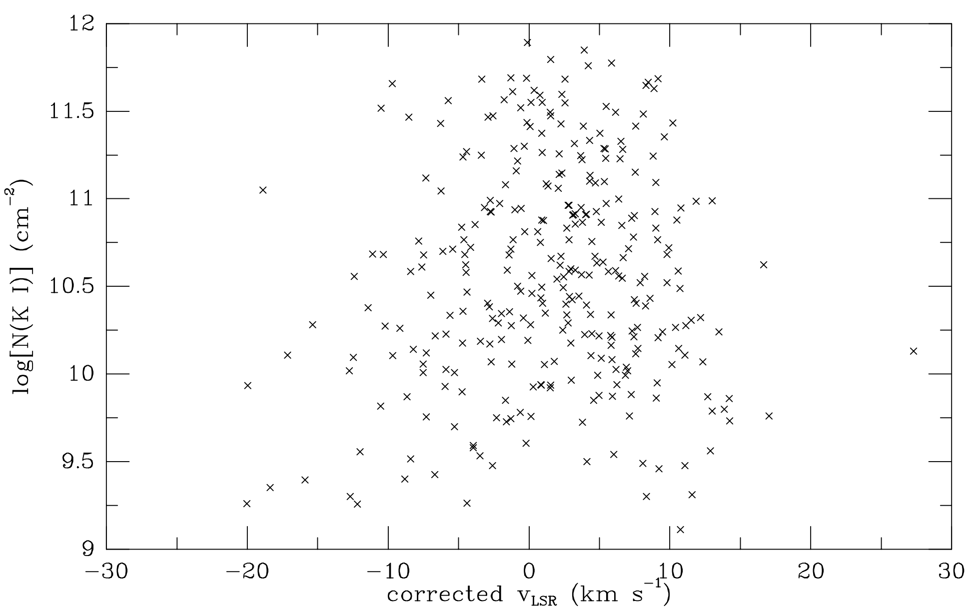

FIG. 10.—Distribution of log N(K I) vs. v_{LSR} for individual components. There is some tendency for the lower column density components to be more broadly distributed.

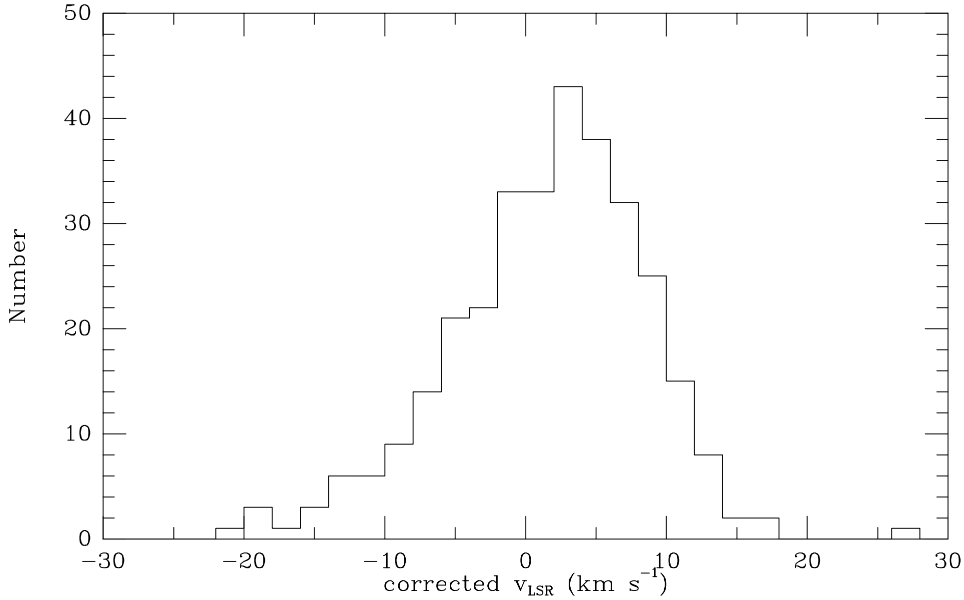

FIG. 11.—Distribution of K I component velocities, with respect to the LSR, corrected (approximately) for Galactic rotation

4.1.1. *Component Velocity Distribution*

Figures 10 and 11 show the distribution of K I component velocities, with respect to the local standard of rest. The LSR velocities have been corrected (approximately) for differential galactic rotation using $\Delta v = Ad \sin(2l) \cos^2(b)$, where we have used 15 km s^{-1} kpc^{-1} for Oort's constant A and have assumed a cloud distance d of half the distance to the star for each line of sight. The overall mean velocity $\langle v_{\rm LSR} \rangle \sim +1.7$ km s^{-1} is slightly larger than those found for Na I (-0.7 km s^{-1}) and Ca II (-1.7 km s^{-1}), perhaps due to the typically longer lines of sight probed in K I. There is a similar tendency for the lower column density components to be somewhat more broadly distributed than the higher column density components. For example, the velocity dispersion for the components with log $(N) < 11.3$ cm^{-2} is approximately 7.8 km s^{-1}, compared to 5.4 km s^{-1} for the stronger components. Part of that difference may be due to the difficulty in detecting weak components buried within stronger components at low velocities—which would also be the case for Na I and Ca II. The overall K I velocity distribution is, however, very similar to that for the stronger Na I components (those with log [N(Na I)] > 11.3 cm^{-2}), which have $\langle v_{\rm LSR} \rangle \sim +2.1$ km s^{-1} and $\langle v_{\rm LSR}^2 \rangle^{1/2} \sim 6.6$ km s^{-1}—consistent with the mean column density ratio N(Na I)/N(K I) ~ 85 (§ 4.2.2).

4.1.2. *Column Densities*

Figure 12 shows the distribution of K I column density (log N) versus line width parameter (b). Components in the primary sample, with well determined b-values (§ 3.1), are shown by the symbol "x," while components with less well determined b-values are shown by the symbol "o." As was

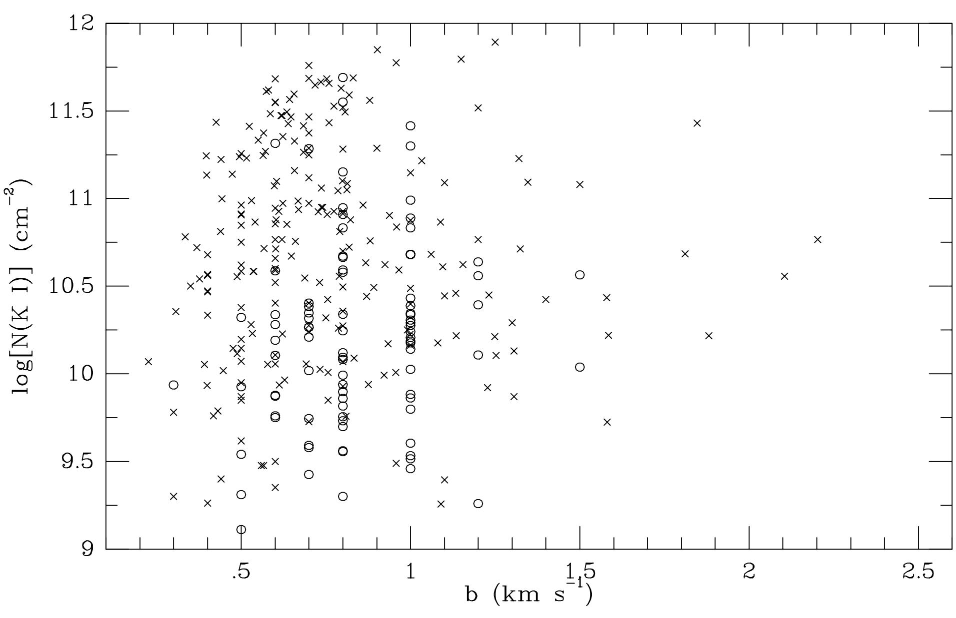

FIG. 12.—Distribution of log N(K I) vs. b for individual components. An "x" indicates that b is well determined; an "o" indicates that b was fixed somewhat arbitrarily in the fits and is less well determined. There is no apparent correlation between the two quantities.

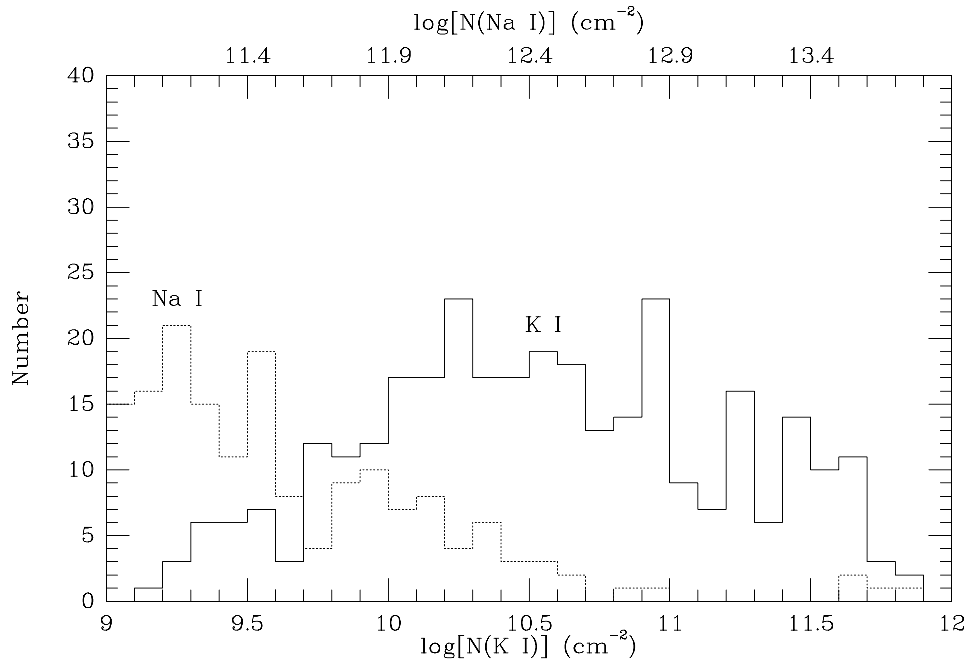

FIG. 13.—Distribution of K I component column densities (*solid line*). The corresponding distribution of Na I column densities (from WHK), shifted by 1.9 dex to account for the typical N(Na I)/N(K I) ratio, is also shown (*dotted line*; *scale at top*).

found for Na I and Ca II, $\log N$ and b do not show any obvious correlation, for the ranges in N and b sampled here. Only one cloud with $\log N > 12.0$ cm^{-2} does not appear in this figure. While the K I column density histogram shown in Figure 13 (*solid line*) bears a superficial resemblance to the corresponding histogram for Na I (Fig. 6 in WHK), we must recall that a given value of N(K I) actually corresponds to a Na I column density 30–200 times higher (§ 4.2.2). The dotted histogram in Figure 13 represents the Na I column density distribution from WHK, shifted by 1.90 dex to reflect the typical N(Na I)/N(K I) ratio. The low end of the K I distribution overlaps the high end of the Na I distribution—and the shapes of the two distributions may largely reflect the lines of sight included in the respective surveys, which were chosen to have detectable but (in most cases) not too heavily saturated absorption features. Comparison of the K I and Na I distributions does suggest, however, that the K I survey is probably incomplete for column densities below about 10^{10} cm^{-2}—some weak components are likely hidden within stronger ones, while others are below the detection limits for the lower S/N spectra. The median individual K I component column density in this survey is about 4×10^{10} cm^{-2}, which corresponds to an individual component hydrogen column density of about 2×10^{20} cm^{-2} (see below)—similar to that of the "standard cloud" defined by Spitzer (1968). The median individual component N(Na I) $\sim 1.3 \times 10^{11}$ cm^{-2} in the WHK sample, on the other hand, corresponds to N(H) $\sim 4 \times 10^{19}$ cm^{-2}. The properties of the clouds seen in K I—e.g., line widths and component separations—therefore should be more representative of the bulk of the cool, diffuse H I gas in the Galactic disk. [We would need a sight line sample not selected for K I absorption to obtain an accurate view of the distribution of individual cloud N(H), however.] The highest individual component K I column density, slightly larger than 10^{12} cm^{-2}, corresponds to a hydrogen column density of about 10^{21} cm^{-2}. Using the ratio $N(\mathrm{H})/E(B-V) = 5.8 \times 10^{21}$ cm^{-2} mag^{-1} found by Bohlin, Savage, & Drake (1979), the median and maximum column density K I components would have $E(B-V) = 0.03$ and 0.17, respectively.

Because very high spectral resolution observations are not always possible (e.g., in the UV), determination of the properties of individual interstellar clouds would be facilitated if we could identify lines of sight containing a single "sufficiently" dominant cloud. Unfortunately, the available high-resolution spectra of K I (and Na I) suggest that such sight lines are rare, especially for targets farther than 50–100 pc away. Only seven of the 54 lines of sight in this survey of K I, for example, have a single component containing more than 2/3 of the total N(K I) and/or N(Na I) (η Tau, 27 Tau, 23 Sex, HD 146010, δ Sco, β^1 Sco, 22 Sco). For all seven, we have only CF spectra of K I, so that more complex structure may be present in some cases. Furthermore, because of the quadratic (or steeper) dependence of the column densities of the trace neutral species on $N(\mathrm{H_{tot}})$ (see below), that single strongest component will be less prominent in H I and the various dominant ions.

4.1.3. *Line Widths*

The widths of individual absorption components seen for any individual species provide strict upper limits on the temperature and internal turbulent velocity (v_t) in the interstellar gas, since $b = (2kT/m + 2v_t^2)^{1/2}$. If two species of significantly different atomic weight m (e.g., K I and Na I) coexist in the same volume of gas, comparison of the widths of their corresponding absorption components can allow estimates of the relative contributions of thermal and turbulent broadening (e.g., Dunkin & Crawford 1999).

Figures 14 and 15 show the distribution of K I b-values, for the entire sample and for the UHRF/McD sample alone. In each figure, the solid histogram line refers to the primary

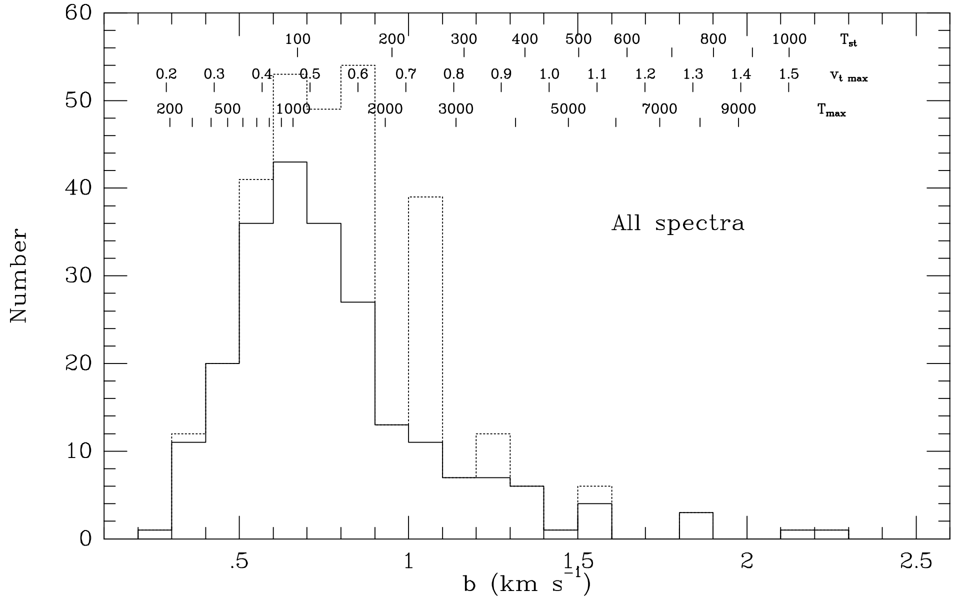

FIG. 14.—Distribution of K I component b-values (all spectra). The primary sample (b varied or fixed but well determined in the fits) is shown by the solid line; the dotted histogram includes also the less well determined fixed values. The scale at the top gives the maximum temperature and turbulent velocity corresponding to each b, as well as the temperature (T_{st}) for which the turbulence would be just sonic. The median b for the primary sample is 0.71 km s^{-1}.

sample; the dotted line refers to the full sample. Two additional scales near the top of the figures denote the maximum values of the temperature (T_{max}) and one-dimensional rms turbulent velocity ($v_{t\max}$) allowed for a given value of b; a third scale shows T for the case of sonic turbulence [$(3)^{1/2}v_t$ equal to the isothermal sound speed, $v_s \sim 0.7(T/80\ \mathrm{K})^{1/2}$ km s^{-1}]. The instrumental resolutions correspond to b-values of 0.24–0.33 km s^{-1} (UHRF), 0.34 km s^{-1} (McD), and 0.72–1.08 km s^{-1} (CF).

The median b for the primary sample of 141 well-determined b-values derived from the high-resolution UHRF and/or McD spectra is 0.67 km s^{-1}, which corresponds to $T_{max} \sim 1035$ K or to $v_{t\max} \sim 0.47$ km s^{-1}. The median values for the CF and combined samples are both somewhat larger, reflecting the less complete knowledge of the component structures in the lower resolution spectra. The larger median K I b-values found by Hobbs (1974d) (1.4 km s^{-1}, or 1.15 km s^{-1}, using the revised PEPSIOS resolution estimated above) and by Chaffee & White (1982) (1.8 km s^{-1} for their "Class A or B" components) also presumably are due to unrecognized complexity in the component structures. Nearly 80% of the primary b-values fall between 0.4 and 0.9 km s^{-1}, corresponding to values of T_{max} between 370 and 1870 K or values of $v_{t\max}$ between 0.28 and

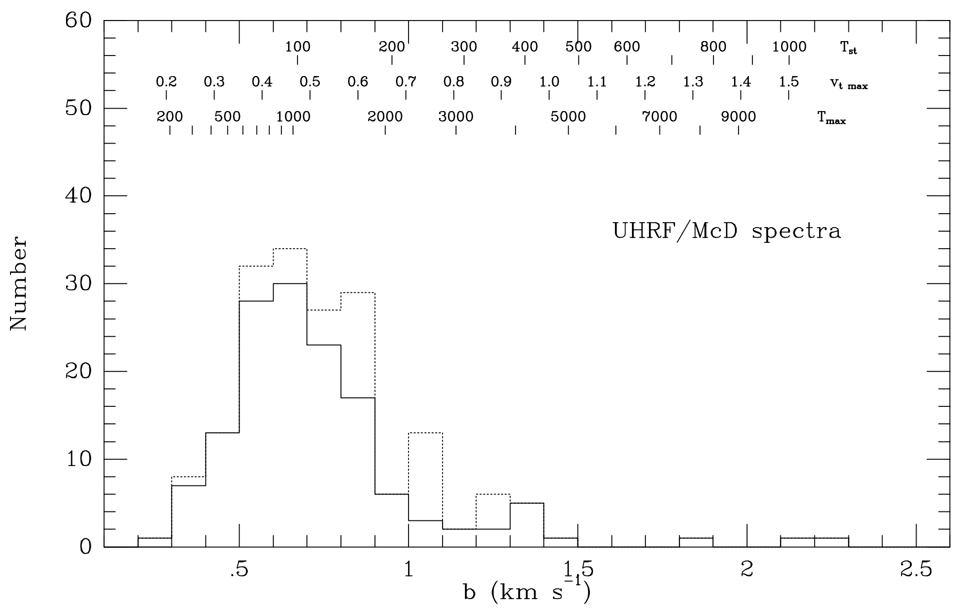

FIG. 15.—Distribution of K I component b-values (high-resolution UHRF/McD spectra only; otherwise as for Fig. 14). The median b for the primary sample is 0.67 km s^{-1}.

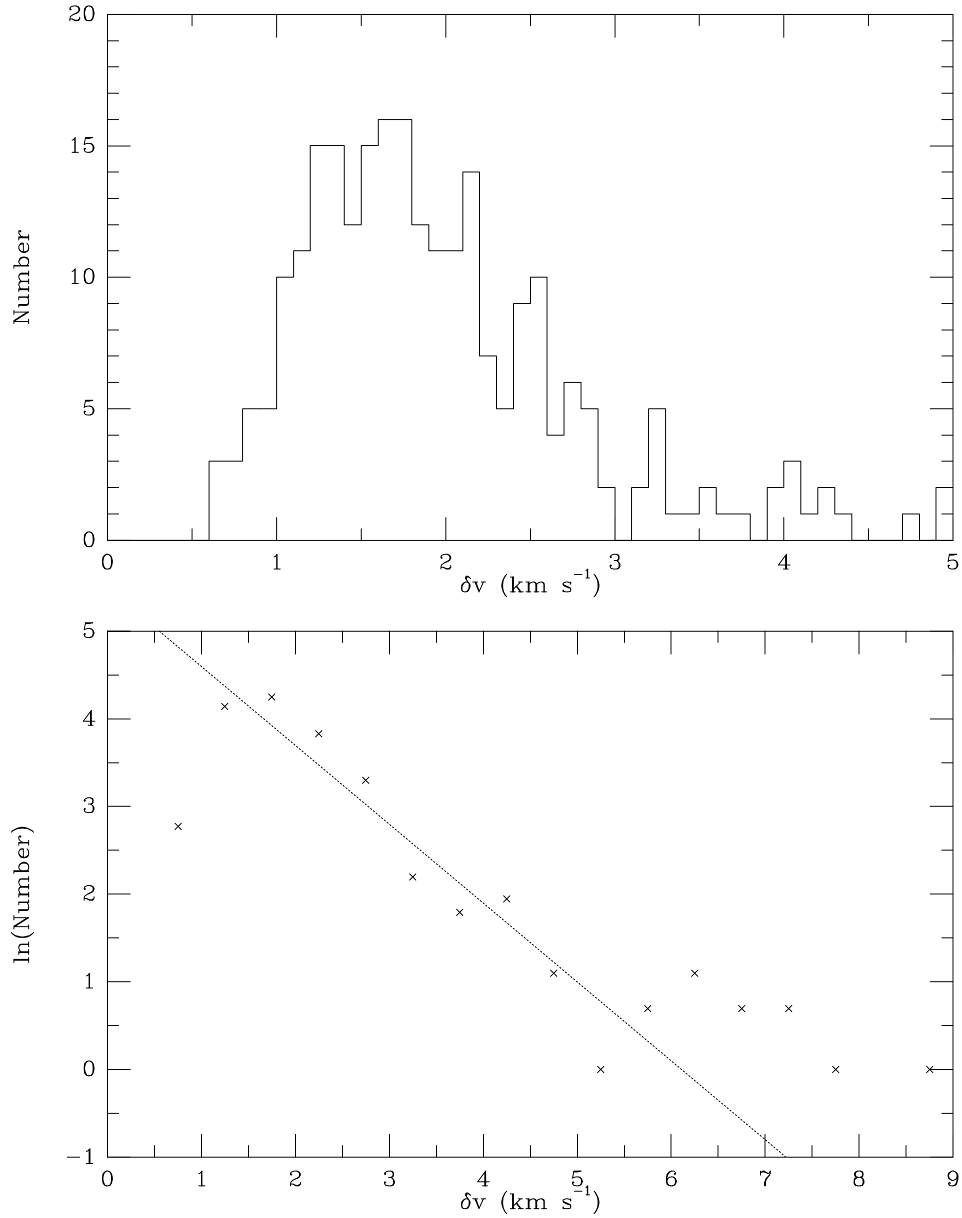

FIG. 16.—Distribution of velocity separations between adjacent K I components. In the lower panel, the dotted line shows the linear fit (with slope −0.9) over the range 1.5 km s^{-1} $\lesssim \delta v \lesssim$ 6.5 km s^{-1}.

0.64 km s^{-1}. If the isothermal sound speed is $v_s \sim 0.7(T/80\ \mathrm{K})^{1/2}$ km s^{-1} and if most of the clouds detected in K I have $T \sim 80$ K (100 K), then the distribution of b-values would also imply that the internal turbulence in at least 35% (50%) of the regions traced by K I is subsonic. Besides thermal and turbulent broadening, unresolved blends and cloud stratification may also contribute to the widths of the observed K I lines (see WHK and WMH). The "true" median b may therefore be somewhat smaller, and the minimum fraction of clouds with subsonic turbulence correspondingly larger.

If K I ($m = 39$) and Na I ($m = 23$) are coextensive in the interstellar gas, we would expect the ratio b(K I)/b(Na I) to lie between 1.00 (if turbulence dominates the line broadening) and 0.77 (if thermal broadening dominates). Under that assumption, Dunkin & Crawford (1999) have used b-values derived from K I and Na I spectra obtained with UHRF to estimate the temperature and turbulence in two clouds toward κ Vel. The distribution of K I b-values, for the high-resolution sample shown in Figure 15, is very similar to that of Na I (Fig. 5 of WHK). While that similarity may result in part from using the K I component structures to model the Na I D1 absorption where the latter is saturated, only about 10% of the Na I b-values were fixed in that way. The median b is slightly smaller for K I (0.67 vs. 0.73 km s^{-1}), consistent with the two species being coextensive (though the sight line samples are different for the two species). Unfortunately, there are very few cases of isolated, corresponding components in both species for which the K I line is strong enough but the Na I D1 line is not saturated, so that both b-values can be very precisely determined. For those cases (e.g., toward ζ Ori and α Cyg), the K I and Na I b-values are generally similar, within the mutual uncertainties. We note, however, that the Na I lines near 3302 Å ("U" lines) are much closer in strength to the K I λ7698 line. Compare, for example, the UHRF spectra of the Na I

λ3302 doublet toward ζ Oph shown by Barlow et al. (1995) with the K I spectra in Figure 6, or see Figure 3 of Hobbs (1978). High-resolution spectra of the Na I U lines would allow more extensive comparisons of the b-values of the two species—and thus estimates for T and v_t for more interstellar clouds.

If Ca II ($m = 40$) and K I are similarly distributed, we would expect that the respective b-values would be essentially identical, regardless of whether thermal broadening or turbulent broadening is dominant. We find, however, that the median b for K I is smaller than that for Ca II. For the components in the respective high-resolution primary samples, $b_{\rm med}$(K I) = 0.67 km s^{-1}, while $b_{\rm med}$(Ca II) = 1.33 km s^{-1}. The difference is reduced, but not eliminated, if outlying Ca II-only components are removed from the Ca II sample. We have identified 28 "corresponding" components in K I and Ca II for which the velocities agree to within 0.3 km s^{-1} (cf. the corresponding Na I and Ca II components discussed by WMH; again using the ζ Oph Ca II component parameters from Barlow et al. 1995). The median values of b are 0.79 and 0.96 km s^{-1} for the corresponding K I and Ca II components, respectively. While the typical uncertainties in the b-values would allow b(Ca II) $\sim b$(K I) for many of the corresponding components with b(Ca II) $\lesssim 1.2$ km s^{-1}, the data suggest that b(Ca II) is often greater than b(K I)—both globally and for individual components seen at the same velocity. As discussed by WMH (see also Barlow et al. 1995), the most straightforward explanation for this difference in b-values is that Ca II and K I are not identically distributed, even though similarities in component velocities suggest association of the two species. For a given velocity component, it is likely that Ca II occupies a somewhat larger volume, characterized by a larger temperature and/or greater internal turbulent motions, than does K I.

4.1.4. *Sample Completeness*

In the Na I and Ca II surveys, there were indications that we had not fully discerned all the individual components present, given our detection limits, even at resolutions of 0.3–0.5 km s^{-1}. Since many of the K I spectra in the present survey were obtained with the CF, at a resolution of 1.2–1.8 km s^{-1}, we have probably not resolved all the detectable K I components along the various lines of sight, either. As noted above (§ 3.1), additional components can often be discerned in the higher resolution McD/UHRF spectra (e.g., toward ϵ Aur and ρ Oph). When the K I component structures are compared with those derived for Na I and Ca II for the same lines of sight, a number of components do show good correspondence, but there are also many which do not line up, suggestive of unresolved structure in one or more of those species. The stronger Na I and Ca II lines also typically show additional components and more complex structure. While we have chosen in the present study to fit the K I profiles independently, without constraints from observations of other species, detailed studies of individual lines of sight will require a mutually consistent component model to be derived for all available species (cf. Welty et al. 1999b).

Additional information on possible unresolved structure can be obtained from the distribution of velocity separations δv between adjacent components, shown in Figure 16. The median δv is approximately 1.9 km s^{-1} for the full sample and 1.7 km s^{-1} for the higher resolution McD/UHRF spectra. Nearly 85% of the adjacent component separations are less than 3.0 km s^{-1}. Unresolved component structure probably accounts for the apparent fall-off in the distribution for $\delta v \lesssim 1.5$ km s^{-1}. As discussed in the Na I and Ca II surveys, if the component velocities for the true complete sample of clouds are both uncorrelated and taken from a single Poisson distribution, then the distribution of adjacent component separations will be an exponential function of δv: ln(number) $= \alpha + \beta\delta v$. In the bottom panel of Figure 16, we see that the distribution of δv, in 0.5 km s^{-1} bins, can be reasonably represented by an exponential for 1.5 km s^{-1} $\lesssim \delta v \lesssim$ 4.5 (or perhaps 7.0) km s^{-1}, with a significant deficit at smaller δv and a slight excess at larger δv. A least squares fit over the interval 1.5 km s^{-1} $\lesssim \delta v \lesssim$ 6.5 km s^{-1} yields ln(number) $\sim (5.6 \pm 0.5) - (0.9 \pm 0.1)\delta v$, if the points are given equal weight. If that best-fit exponential is extrapolated to $\delta v = 0.0$ km s^{-1}, we would predict $\sim$594 values of $\delta v \lesssim 6.5$ km s^{-1}, instead of the 253 observed, with the difference mainly at $\delta v \lesssim 1.0$ km s^{-1}. The 319 components comprising our full sample would thus represent only about 48% of the true complete sample of clouds which could have been detected along the 54 lines of sight, and the true median δv would be $\sim$1.2 km s^{-1}. The derived slope (-0.9 ± 0.1) is somewhat steeper than the slopes found in our surveys of Na I (-0.65 ± 0.05; WHK) and Ca II (-0.69 ± 0.05; WMH). The higher column density clouds detected in K I, which also have a somewhat smaller dispersion in $v_{\rm LSR}$ than those seen in Na I and Ca II (§ 4.1.1; Table 4), may also be more closely associated.

4.2. *Comparisons with Other Species*

Comparisons of N(K I) with N(H$_{\rm tot}$) and with the column densities of other trace neutral species have provided constraints on elemental depletions, the fractional ionization ($n_e/n_{\rm H}$), the processes contributing to the ionization in diffuse clouds, and dust grain properties (Hobbs 1974b, 1976; Jenkins & Shaya 1979; Chaffee & White 1982). Those studies have shown that while the column densities of K I, Na I, C I, and H$_{\rm tot}$ are generally well correlated, there do appear to be slight differences toward some stars in the Sco-Oph region (see also Crutcher 1976). The K I data reported in this paper, characterized by higher resolution, generally higher S/N, and a larger range in column density, provide a more accurate and more extensive view of the relationships among those various species. While we confirm the basic results of those previous studies, some details must be reconsidered. We also find evidence for variations in some of the column density ratios, similar to those found in Sco-Oph, in several additional regions.

In the following subsections, we examine some of the relationships between K I, Na I, C I, Li I, H$_{\rm tot}$, H$_2$, and CH. Unless otherwise noted, we compare total line of sight column densities, since individual component values are not available for hydrogen, C I, or (in most cases) for CH. The complete set of column densities used for these comparisons (with references) is given in the Appendix (Table 7). In each case, we perform least squares fits to log[N(Y)] versus log[N(X)], allowing for uncertainties (assumed comparable) in both quantities, to obtain both the slope of the "typical" relationship and an estimate of the scatter.[3] In some of the fits, we omitted the points from the Sco-Oph

[3] We used a slightly modified version of the subroutine regrwt.f, obtained from the statistical software archive maintained at Penn State (http://www.astro.psu.edu/statcodes), to perform the fits.

(and other "discrepant") sight lines; in all the fits, we made one pass through the data to eliminate greater than 2.5 σ outliers. The results of these fits, for different subsets of the data, are summarized in Table 5. The derived slopes (B) and intercepts (A) for the various relationships depend to some degree on the relatively small samples available for each comparison. In addition, the slopes found from fits to the total line of sight column densities may be somewhat smaller than the values which would be found from fits to the individual component column densities, when the slopes are greater than 1.0 (Hobbs 1974b; see § 4.3.1 below). Because most of the derived slopes were close to either 1.0 or 2.0, we have also performed fits holding the slopes fixed to those values, for comparison. In those cases (where B is given in parentheses), A is simply the mean of log $\{N(\mathrm{Y})/[N(\mathrm{X})]^{\mathrm{B}}\}$, and the uncertainty in A is just the standard deviation of the set of individual values. Possible implications of these empirical relationships will be discussed in § 4.3.

If photoionization and radiative recombination dominate the ionization balance for element X, then in equilibrium we have $\Gamma(\mathrm{X}^0)n(\mathrm{X}^0) = \alpha(\mathrm{X}^0, T)n_e n(\mathrm{X}^+)$, where Γ is the photoionization rate and α is the recombination rate. In most neutral (H I) gas, K, Na, and C are predominantly singly ionized. Because there are no ground state absorption lines in the optical or UV for either K II or Na II, and because the lines available for C II are either very strong or very weak, it has been difficult to determine reliable abundances for K, Na, and C for most lines of sight. Where column densities for the corresponding trace neutral species are available, however, we may determine *relative* abundances for those elements by taking ratios of the ionization equilibrium equation—where n_e is eliminated and the dependence on T and on the overall scale of the radiation field is substantially reduced (York 1980; Snow 1984). In the discussions below, we will generally use photoionization rates calculated for the WJ1 radiation field and recombination rates at $T = 100$

TABLE 5

Relationships among K I, Na I, Li I, C I, H_{tot}, and CH

Y	X	A[a]	B[b]	rms[c]	N[d]	Sample[e]
K I	H_{tot}	−26.93 ± 2.71	1.83 ± 0.13	0.13	29	1/1
		−27.21 ± 2.79	1.84 ± 0.13	0.15	39	2/1
		−26.30 ± 1.09	1.79 ± 0.16	0.18	46	2/3
		−30.61 ± 0.32	(2.00)	0.13	38	2/1
Na I	H_{tot}	−30.53 ± 2.08	2.09 ± 0.10	0.16	55	1/1
		−33.49 ± 2.36	2.23 ± 0.12	0.18	65	2/1
		−29.55 ± 2.25	2.03 ± 0.11	0.22	77	2/3
		−28.73 ± 0.42	(2.00)	0.19	65	2/1
Na I	K I	1.03 ± 0.32	1.08 ± 0.03	0.08	33	1/1
		0.94 ± 0.34	1.09 ± 0.03	0.08	37	2/1
		1.26 ± 0.39	1.06 ± 0.03	0.11	49	2/3
		1.96 ± 0.14	(1.00)	0.10	38	2/1
Li I	K I	−1.29 ± 1.80	0.92 ± 0.15	0.15	13	2/3
		−2.27 ± 0.22	(1.00)	0.15	13	2/3
Li I	Na I	−0.22 ± 2.46	0.72 ± 0.18	0.20	9	2/3
		−4.09 ± 0.31	(1.00)	0.22	9	2/3
C I	K I	−0.01 ± 1.05	1.30 ± 0.09	0.18	28	2/3
		3.36 ± 0.32	(1.00)	0.23	29	2/3
C I	Na I	−0.04 ± 0.55	1.12 ± 0.04	0.15	34	2/3
		1.42 ± 0.25	(1.00)	0.18	35	2/3
CH	K I	1.46 ± 1.36	0.99 ± 0.12	0.13	18	1/3
		0.86 ± 1.00	1.04 ± 0.08	0.14	36	2/3
		1.37 ± 0.20	(1.00)	0.14	36	2/3
K I	H_2	−3.75 ± 1.47	0.76 ± 0.07	0.17	28	2/3
		−8.58 ± 0.27	(1.00)	0.19	28	2/3
Na I	H_2	−9.34 ± 1.73	1.13 ± 0.09	0.15	22	2/3
		−6.78 ± 0.21	(1.00)	0.15	22	2/3

Note.—$\log[N(\mathrm{Y})] = \mathrm{A} + \mathrm{B} \times \log[N(\mathrm{X})]$

[a] Uncertainties in A were determined in the fits when B was varied but are the standard deviations of the set of values $\log\{N(\mathrm{Y})/[N(\mathrm{X})]^{\mathrm{B}}\}$ when B was fixed.

[b] Values in parentheses were fixed.

[c] Root mean square distance of points from best-fit line.

[d] Number of stars in sample.

[e] n/m: $n = 1$ includes high-resolution (FWHM < 2 km s^{-1}) data only; $n = 2$ includes also "reliable" lower resolution data; $m = 1$ excludes Sco-Oph and other "discrepant" stars; $m = 3$ includes all stars. Relationships with H_2 include only sight lines with $N(H_2) > 10^{18.5}$ cm^{-2}.

K, as tabulated by Péquignot & Aldrovandi (1986). We also adopt the solar system meteoritic reference abundances listed by Anders & Grevesse (1989) and Grevesse & Noels (1993).

4.2.1. K I *and* Na I *versus* H_{tot}

Figures 17 and 18 display the roughly quadratic dependences of both N(K I) and N(Na I) on $N(H_{tot})$, shown previously by Hobbs (1974b, 1974c, 1976). In both figures, the panel on the left shows only column densities derived from high-resolution spectra (FWHM $\lesssim 2$ km s^{-1}), while the panel on the right includes in addition values derived from "reliable" lower resolution spectra (*small filled circles*; see the Appendix). The best-fit slope for Na I may be slightly greater than 2.0 (*solid lines*), while the corresponding slope for K I may be slightly less than 2.0 (Table 5). In both cases, the scatter about the best-fit line is small, and the systematic differences for the "Sco-Oph" stars (*open circles*), Trapezium stars (*asterisks*), Pleiades stars (*open squares*), and other "discrepant" stars (*open triangles*) are clearly seen. The rms deviations (in distance from the best-fit line) are less than 0.15 dex for K I and less than 0.2 dex for Na I, when the points for the Sco-Oph and other discrepant stars are excluded; the rms deviations are only slightly higher if the slopes are fixed at 2.0 (*dotted lines*). The dashed line in Figure 18 shows the nearly linear relationship (slope = 1.04) between N(Na I) and $N(H_{tot})$ proposed by Ferlet, Vidal-Madjar, & Gry (1985) for $N(H_{tot}) \lesssim 10^{21}$ cm^{-2}. While that relationship has sometimes been used to estimate $N(H_{tot})$ from measured values of N(Na I), it is apparent that the hydrogen column density would be significantly overestimated for $N(\text{Na I}) \gtrsim 10^{13}$ cm^{-2} (as recognized by Ferlet et al.) and significantly underestimated for $N(\text{Na I}) \lesssim 10^{11}$ cm^{-2} (WHK). The dependence of N(Na I) on $N(H_{tot})$ appears to be reasonably approximated by a quadratic function over the full range of column densities shown in Figure 18, though the scatter about the best-fit line appears to be larger for $N(\text{Na I}) \lesssim 10^{11}$ cm^{-2}—making Na I less useful for predicting $N(H_{tot})$ in that regime.

The discrepant Sco-Oph stars include 1 Sco, δ Sco, β^1 Sco, ω^1 Sco, σ Sco, ν Sco, τ Sco, π Sco, 22 Sco and ρ Oph, but *not* χ Oph, ζ Oph, 67 Oph, ζ^1 Sco, HD 154090, or HD 154368. The differences seem to be confined to (but ubiquitous within) the region roughly bounded by $344° \lesssim l \lesssim 355°$ and $12° \lesssim b \lesssim 24°$, which also includes the sight lines toward the globular cluster M4 (Lyons et al. 1995) and toward more heavily reddened stars such as HD 147888 and HD 147889. For a given $N(H_{tot})$, N(K I) and N(Na I) are lower by (roughly) factors of 4 and 8, respectively, toward those Sco-Oph stars. Similar differences from the mean relationships are found toward P Cyg, υ Cyg, and some of the stars with very weak K I and/or Na I lines (e.g., δ Per, μ^1 Sco, η Cen, μ Cen). Even larger deficiencies of Na I and/or K I (factors of 50 or more) are found toward several stars in the Orion Trapezium region (θ^1 Ori C, θ^2 Ori A, and HD 37061; cf. Herbig 1993), toward several stars in Lupus (δ Lup, γ Lup; cf. Welsh, Crifo, & Lallement 1998), and (typically) for interstellar clouds in the LMC and SMC (Welty et al. 1999a, 2001a, in preparation). On the other hand, a few sight lines (e.g., toward 23 Ori, 23 Sex, HD 93521, η CMa, and α Vir) appear to exhibit somewhat enhanced K I and/or Na I absorption; in several other such cases (e.g., toward HD 154090), a significant amount of H_2 may be present, based on the observed N(CH).

4.2.2. Na I *versus* K I

Figure 19 shows an essentially linear relationship between N(Na I) and N(K I)—consistent with the expectation that these trace, neutral species of two alkali elements should have similar behavior and distribution in the ISM. The median N(Na I)/N(K I) ratio is about 85 for the full sample of sight lines but is slightly higher for the non Sco-Oph stars and about a factor of 2 lower for the Sco-Oph stars and P Cyg. We note, however, that the ratio

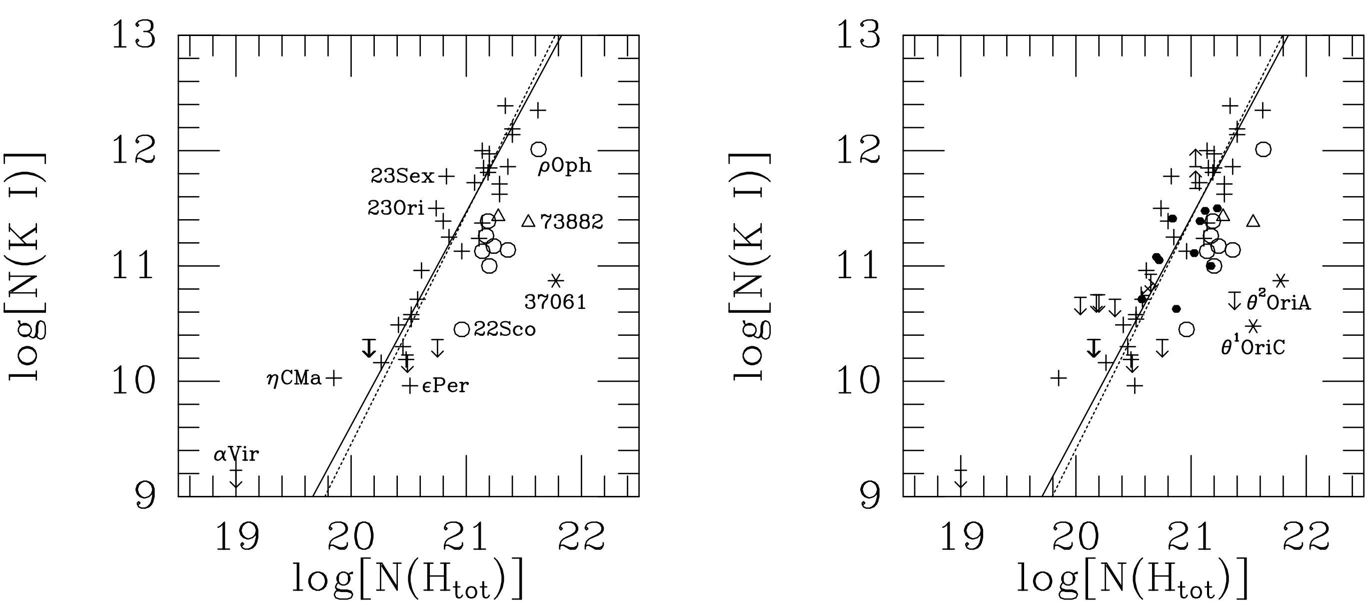

FIG. 17.—N(K I) vs. N(H). The plot at left shows the fit to the high-resolution data (*solid line*; slope = 1.83); the plot at right shows the fit to the high-resolution plus "good" lower resolution data (*small filled circles*) (slope = 1.84). In both cases, points corresponding to Sco-Oph sight lines (*open circles*), Pleiades sight lines (*squares*), Trapezium sight lines (*asterisks*), and other "discrepant" sight lines (*triangles*) were omitted from the fits. The dotted lines show the fits with the slope fixed at 2.0.

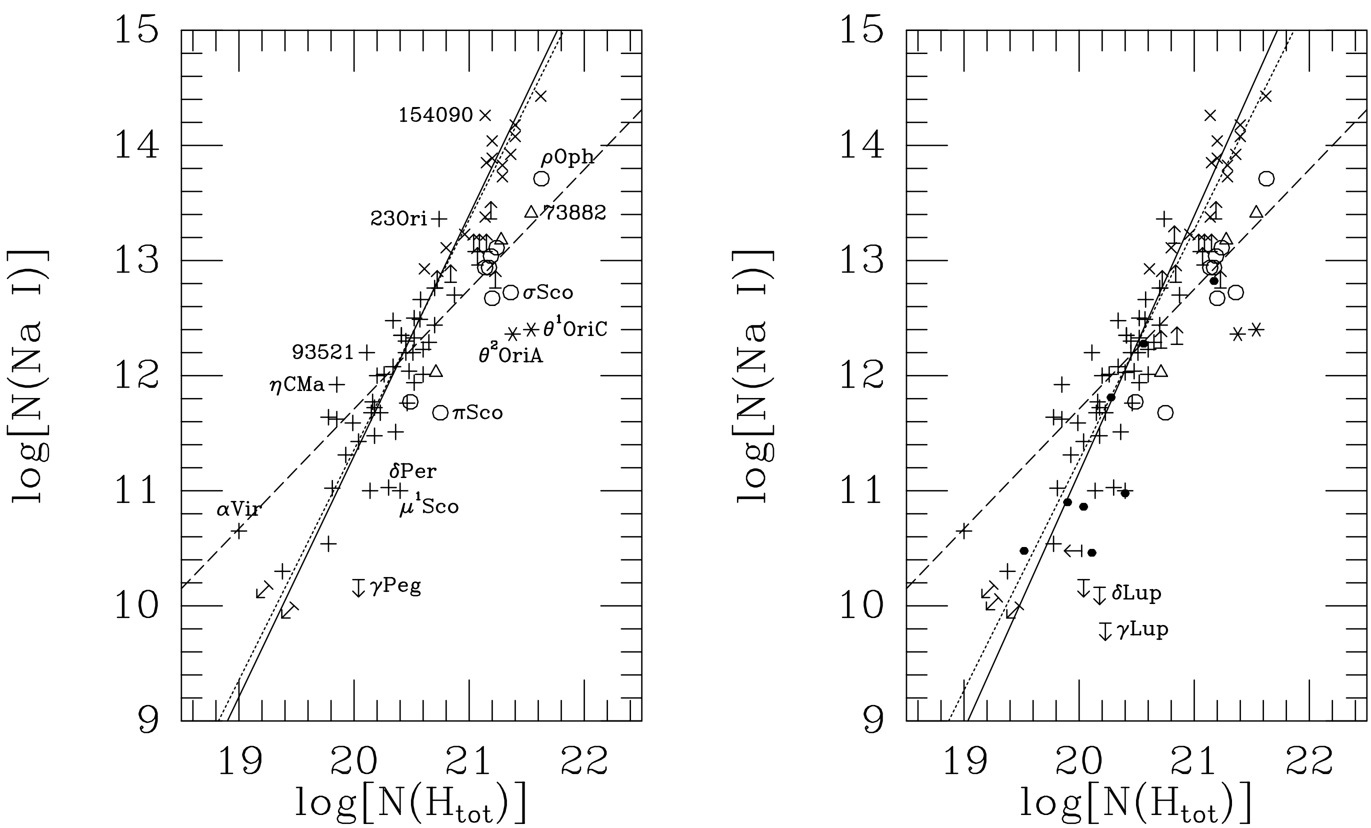

FIG. 18.—N(Na I) vs. N(H). The plot at left shows the fit to the high-resolution data (*solid line*; slope = 2.09); the plot at right shows the fit to the high-resolution plus "good" lower resolution data (*small filled circles*) (slope = 2.23). In both cases, points corresponding to Sco-Oph sight lines (*open circles*), Pleiades sight lines (*squares*), Trapezium sight lines (*asterisks*), and other "discrepant" sight lines (*triangles*) were omitted from the fits. Crosses denote sight lines where N(Na I) was determined from fits to the U line equivalent widths using the K I component structure. Plus signs denote sight lines where N(Na I) was determined from fits to the D1 line. The dashed line shows the relationship derived by Ferlet et al. (1985) for $N(\mathrm{H}) \lesssim 10^{21}$ cm^{-2} (slope = 1.04). The dotted lines show the fits with the slope fixed at 2.0.

is essentially normal toward θ^1 Ori C, where the individual K I and Na I column densities are both very low, relative to $N(\mathrm{H_{tot}})$. If we assume solar relative abundances for Na and K, then the ratio of ionization equilibrium equations for the two elements would predict N(Na I)/N(K I) ~ 70. The slightly larger value (~ 91) found for the linear fit to the sample which excludes the various discrepant sight lines (Table 5) suggests that K may generally be more severely depleted than Na by about 0.1 dex. The scatter about the best-fit relationship is only about 0.1 dex, if the various discrepant sight lines are excluded.

We may also examine the N(Na I)/N(K I) ratio (which we will call R_{NaK}) for individual components or groups of blended components, for sight lines where we have high-resolution spectra for both Na I and K I. For sight lines where Na I is detected over a wider velocity range than K I, R_{NaK} is (obviously) smaller for the components where K I is detected than for the sight line as a whole. In addition (and unsurprisingly), the ratios found for individual components in a given line of sight can span a considerable range. For example, toward 1 Sco, the components near -17 km s^{-1} have $R_{\mathrm{NaK}} \sim 86$, while the higher column density components near -8 km s^{-1} have $R_{\mathrm{NaK}} \sim 42$ (the latter value "typical" for stars in the Sco-Oph region). Both η Ori and α Cyg have components with $R_{\mathrm{NaK}} \sim 40$–45, similar to the ratios found in Sco-Oph, even though the ratios integrated over the two sight lines are 93 and 66, respectively. Evidently, low R_{NaK}-values are not confined to the Sco-Oph region—they are just more noticeable there because the sight lines are dominated by components with low R_{NaK}. Understanding the conditions in the main components toward Sco-Oph therefore may aid in understanding low-R_{NaK} components in other lines of sight.

4.2.3. Li I *versus* K I *and* Na I

White (1986) discussed the depletion behavior of the alkali elements Li, Na, and K based on comparisons of the interstellar gas phase abundances of the corresponding trace neutral species. The left panel of Figure 20 shows N(Li I) versus N(K I) for the relatively small number of sight lines for which data are available (including values from more recent work and reevaluation of some earlier limits, as discussed in the Appendix). The Sco-Oph lines of sight do not appear to be discrepant here. The slope of the unconstrained fit, 0.92 ± 0.15 (Table 5), is consistent with a linear relationship between the two species. A linear fit to the data yields a mean ratio N(Li I)/N(K I) ~ 0.0054, slightly greater than the value 0.0044 predicted from solar abundances and photoionization equilibrium—suggesting that the depletion of Li is generally ~ 0.1 dex less severe than that of K (cf. Hobbs 1984; White 1986; Steigman 1996). There are even fewer sight lines with measured column densities for both Li I and Na I (Fig. 20, *right*), and the slope of the unconstrained fit (0.72 ± 0.18) depends heavily on only three points (σ Sco, δ Sco, HD 154368). Additional data, for both higher and lower column densities, would be needed

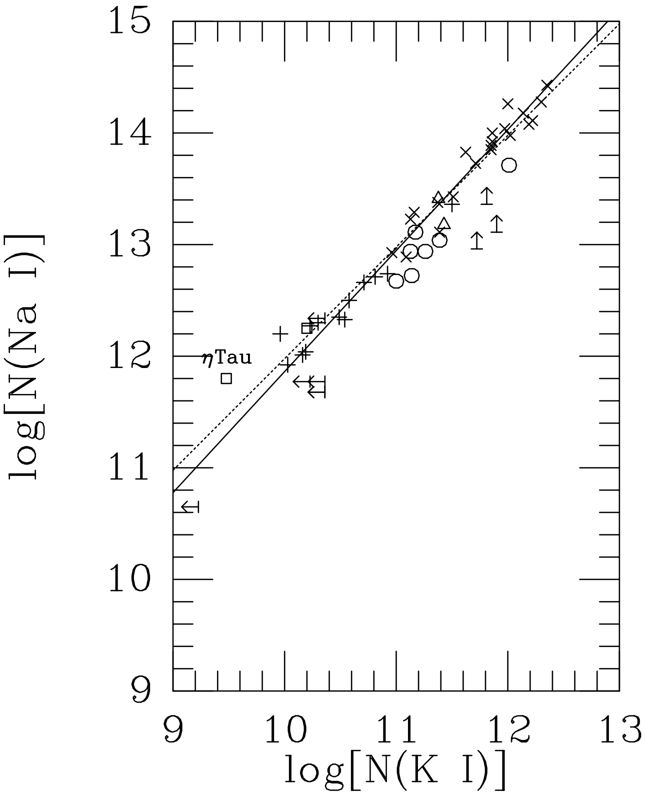

FIG. 19.—N(Na I) vs. N(K I). The plot at left shows the fit to the high-resolution data (*solid line*; slope = 1.08); the plot at right shows the fit to the high-resolution plus "good" lower resolution data (slope = 1.09). In both cases, points corresponding to Sco-Oph, Pleiades, Trapezium, and other "discrepant" sight lines were omitted from the fits. The symbols are as in Figs. 17 and 18. The dotted lines show the fits with the slope fixed at 1.0.

to confirm the proposed nonlinear relationship between N(Li I) and N(Na I) (White 1986).

The Li I absorption feature near 6707 Å is both weak (equivalent width generally less than 3 mÅ) and complex [the ^{7}Li I doublet lines at 6707.762 and 6707.913 Å each have hyperfine subcomponents separated by about 12 mÅ (WHK), and the weaker ^{6}Li I doublet is offset by only 0.160 Å]. Furthermore, because of the low atomic weight, the individual components are relatively broad—making it even more difficult to distinguish the contributions from individual interstellar clouds. Lemoine et al. (1993) and Lemoine, Ferlet, & Vidal-Madjar (1995) obtained high-resolution (FWHM = 3 km s^{-1}), very high S/N profiles of K I (λ7698) in an attempt to identify the individual com-

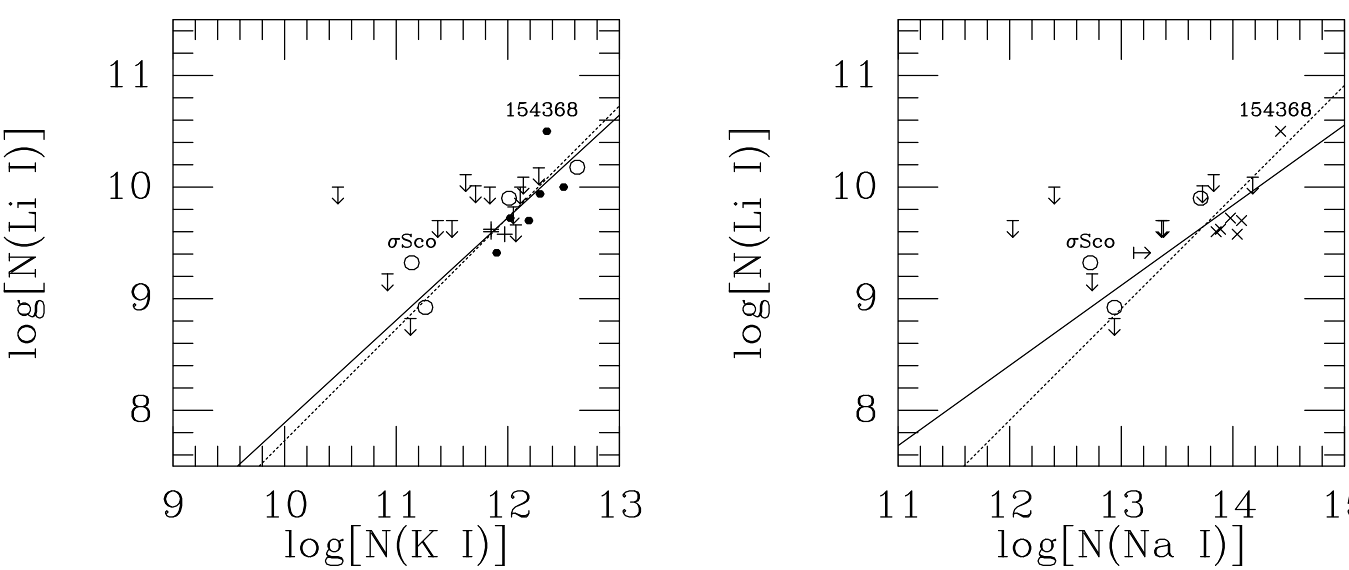

FIG. 20.—N(Li I) vs. N(K I) (*left*) and N(Na I) (*right*). All sight lines with Li I and K I or Na I data are included. The symbols are as in Figs. 17 and 18. Points corresponding to the various "discrepant" sight lines were included in the fits (*solid lines*; slope = 0.92 vs. K I; slope = 0.72 vs. Na I). The dotted lines show the fits with the slope fixed at 1.0.

ponents present in Li I toward ζ Oph and ρ Oph, in order to investigate possible differences in the Li isotope ratio in the different components. Knauth et al. (2000) obtained higher resolution (FWHM ∼ 2 km s^{-1}) spectra of the weaker K I line at 4044 Å (which is comparable in strength to the Li I lines) to aid in interpreting the Li I profiles toward ζ Per and o Per. The yet higher resolution (FWHM ∼ 0.4–0.56 km s^{-1}) K I spectra presented in this paper, however, reveal additional structure along each of those lines of sight. In all four cases, components previously thought to be single appear to consist of 2–3 narrow (b ∼ 0.4–0.8 km s^{-1}) subcomponents, of comparable strength, separated by $\lesssim$1.3 km s^{-1} (Table 2). While variations in the interstellar Li isotope ratio appear firmly established (Knauth et al. 2000), the precise values for individual clouds may need revision. Given the substantial difference in atomic weights, mutually consistent fits to high-resolution Li I and K I profiles should also yield better values for the temperature and turbulence in the individual clouds.

4.2.4. C I *versus* K I *and* Na I

Jenkins & Shaya (1979) compared the column densities of C I with those of K I and Na I, and found a slightly steeper than linear relationship in both cases (see also Chaffee & White 1982). They ascribed the apparent enhancement of C I in the higher column density lines of sight to preferential attenuation of the shorter wavelength photons needed to ionize C I, and estimated the required far-UV properties of the dust. In Figures 21 and 22, we revisit those relationships, making use of more accurate column densities for K I and Na I and additional C I column densities from Jenkins, Jura, & Loewenstein (1983). The N(C I)–N(K I) relationship is nearly linear for N(C I) less than about 2 × 10^{15} cm^{-2}, but the points for several stars with higher N(C I) (κ Cas, o Per, ζ Per, ζ Oph, HD 154368) fall significantly above the extrapolation of that relationship. C I also appears to be somewhat enhanced, relative to K I, toward η Tau and ϵ Per (at much lower column densities). There may be a weak tendency for the Sco-Oph stars to have slightly lower N(C I)/N(K I) ratios. The N(C I)–N(Na I) relationship appears more nearly linear, over the whole range sampled, with smaller scatter. Any enhancement of C I at higher column densities is much weaker [largely due to the higher N(Na I) adopted in this study for the higher column density sight lines], and the Sco-Oph stars generally do not appear to be offset from the overall mean relationship. If we assume solar relative abundances for Na, K, and C, then ratios of the ionization equilibrium equations would predict N(C I)/N(Na I) ∼ 16 and N(C I)/N(K I) ∼ 1100. The somewhat larger values (∼26 and ∼2290) found for the linear fits to the samples which exclude the various discrepant sight lines (Table 5) suggest that Na and K may generally be more severely depleted than C by about 0.2–0.3 dex.

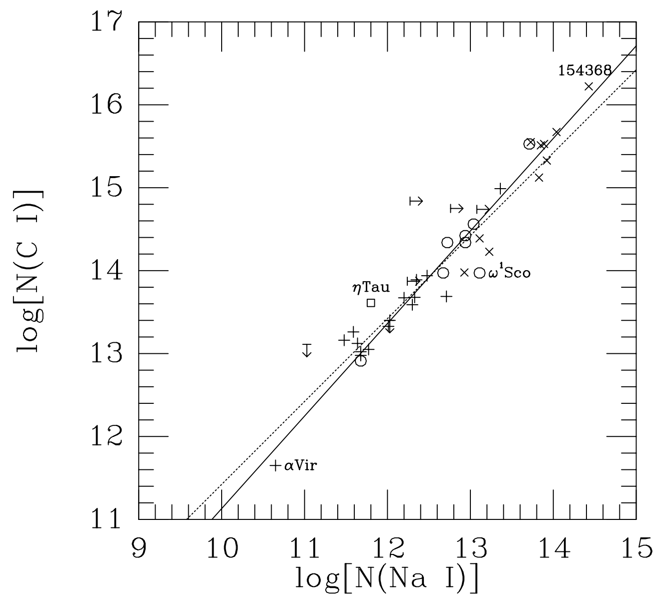

FIG. 22.—N(C I) vs. N(Na I). All sight lines with C I and Na I data are included. Points corresponding to the various "discrepant" sight lines were included in the fit (*solid line*). The symbols are as in Figs. 17 and 18. The C I–Na I relationship is more nearly linear (slope = 1.12) than the C I–K I relationship. The dotted line shows the fit with the slope fixed at 1.0.

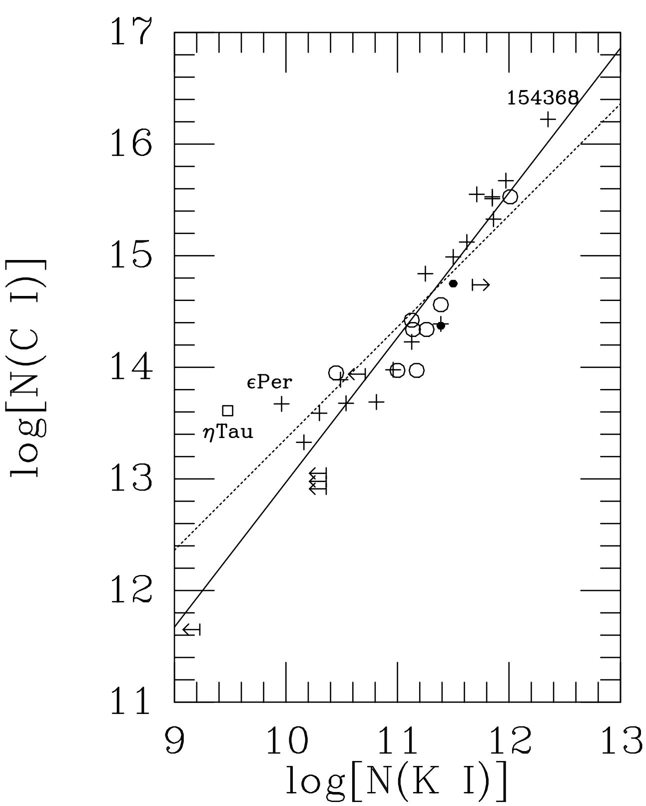

FIG. 21.—N(C I) vs. N(K I). All sight lines with C I and K I data are included. Points corresponding to the various "discrepant" sight lines were included in the fit (*solid line*). The symbols are as in Figs. 17 and 18. The slope of the best-fit line (1.30) would be smaller if the highest column density points were excluded. The dotted line shows the fit with the slope fixed at 1.0.

4.2.5. CH *versus* K I

Figure 23 shows an essentially linear relationship between N(CH) and N(K I), with very small scatter ($\lesssim$0.15 dex) about the mean N(CH)/N(K I) ratio of ∼23 (Table 5). In this comparison, the Sco-Oph sight lines are *not* discrepant, and the limits on N(CH) for θ^1 Ori C and HD 37061 are consistent with the mean relationship; CH data are not available for the other "discrepant" sight lines, however. We note as well that the N(CH)/N(K I) ratio toward 23 Ori falls right on the mean relationship—even though K I (and some other trace neutral species) are enhanced in the main absorbing clouds and though N(CH) is about 40 times larger than would be predicted by the usually tight corre-

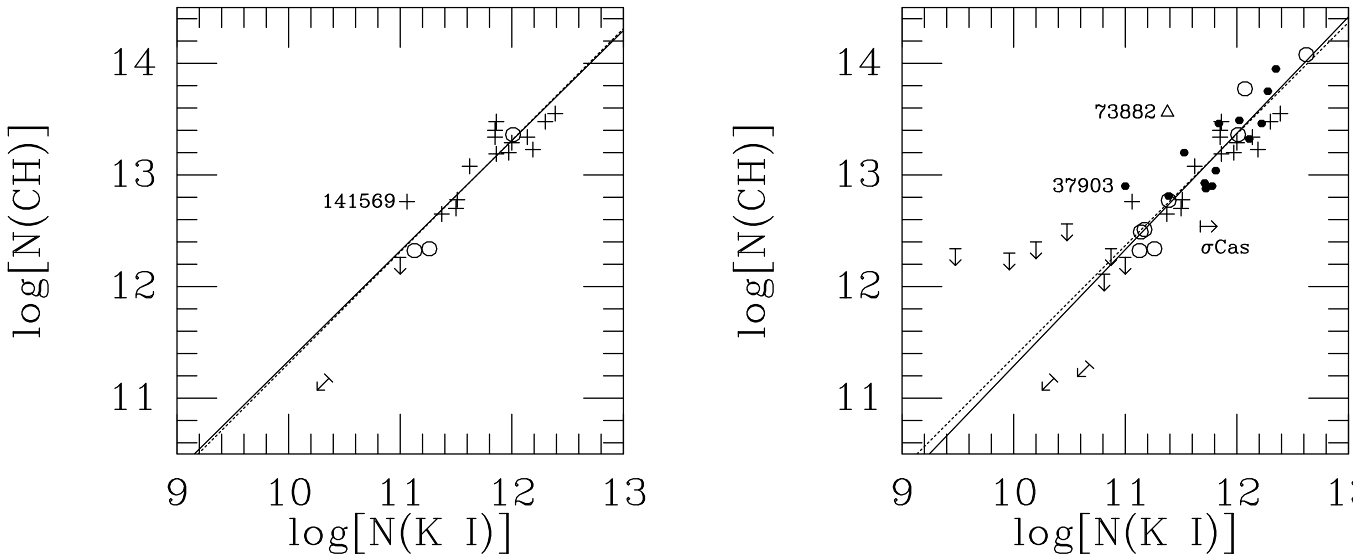

FIG. 23.—N(CH) vs. N(K I). The plot at left shows the fit to the high-resolution data (*solid line*; slope = 0.99); the plot at right shows the fit to the high-resolution plus "good" lower resolution data (slope = 1.04). Points corresponding to the various "discrepant" sight lines were included in the fits. The symbols are as in Figs. 17 and 18. The dotted lines show the fits with the slope fixed at 1.0.

lation between CH and H_2 (Welty et al. 1999b). The N(CH)/N(K I) ratio appears to be somewhat high toward HD 141569 and HD 37903, and low toward σ Cas. The very high value N(CH)/N(K I) $\gtrsim 150$ found for the translucent cloud(s) toward HD 73882 (Snow et al. 2000) will be considered in a future paper describing high-resolution spectra of more heavily reddened sight lines (Welty et al. 2001b, in preparation).

Crane, Lambert, & Sheffer (1995, hereafter CLS) had conjectured that CH and Na I were not entirely coextensive, based on differences in the distributions of component b-values obtained from fitting the ensembles of available high-resolution CH λ4300 and Na I D1 profiles (the latter from WHK). They noted, however, that detailed profile comparisons for individual lines of sight could not be made, since the Na I D1 line is typically very saturated for components in which CH is detected. The K I λ7698 line is much less saturated than the Na I D lines, and so provides a much better match to the CH profiles. We therefore included most of the stars observed by CLS in our K I program, so that we could compare the K I and CH profiles in detail—and thus gauge the degree of correspondence between the atomic and molecular gas.

In Figures 24 and 25, we compare high-resolution spectra of CH λ4300 and K I for twelve lines of sight. Seven of the CH spectra are from CLS, at a resolution of about 0.6 km s^{-1}; the other five were observed with the CF, at a resolution of about 1.3 km s^{-1}. The K I component structure is given by the tick marks above both spectra. In general, the high-resolution K I and CH λ4300 profiles appear very similar, when allowance is made for the larger atomic weight of K I and the Λ doubling present for CH (two subcomponents separated by about 1.4 km s^{-1}; see the CH profile for ζ Oph)—both of which imply that individual components will be broader in CH than in K I. The similar velocity extent and structure in the line profiles and the strong correlation between the overall N(CH) and N(K I) all suggest a general close association between the two species. We therefore fitted the CLS CH profiles for o Per, ζ Per, ξ Per, δ Sco, β^1 Sco, χ Oph, ζ Oph, and μ Sgr using the corresponding K I component structures listed in Table 2. The small velocity offsets between the K I and CH profiles obtained in these fits (generally less than about 0.6 km s^{-1}) have been applied to the CLS spectra in the figures. Because the CH lines are relatively weak and the individual components are relatively broad, CLS found only 1–3 components in each line of sight. The K I component structures are typically more complex, and so many of the "new" CH b-values are slightly smaller than those found by CLS—though the uncertainties are relatively large for such weak, blended lines. For most of the stronger individual components, b(K I) is less than 0.9 km s^{-1}; within the uncertainties, the ratio b(CH)/b(K I) generally lies between 1.0 (broadening dominated by turbulence) and 1.7 (thermal broadening). In principle, the two species therefore could generally be coextensive. If the gas is cold ($T < 100$ K), however, as suggested by the H_2 rotational level populations toward these stars (Savage et al. 1977), then the line widths may generally be dominated by turbulence, and b-value ratios greater than 1.0 may indicate that CH can be somewhat more widely distributed. We note as well that there are several clear cases of strong K I components with no (or very weak) corresponding CH—so the two species are not always associated. For example, the single strong, narrow CH components toward ρ Oph and λ Cep (CLS) each correspond to only one of several comparably strong, narrow K I components in those two lines of sight.

4.2.6. K I *and* Na I *versus* H_2

Figures 26 and 27 show the relationships N(K I) versus $N(H_2)$ and N(Na I) versus $N(H_2)$, respectively. Three regimes are represented for molecular hydrogen: (1) $N(H_2) \lesssim 10^{15}$ cm^{-2}, where the H_2 is dissociated by the ambient UV radiation field (attenuated only by dust); (2) $N(H_2) \gtrsim 10^{19}$ cm^{-2}, where the photodissociation is greatly reduced because of self-shielding (by the many strong H_2 absorption lines); (3) intermediate column densities, over which the transition to self-shielding occurs. Federman

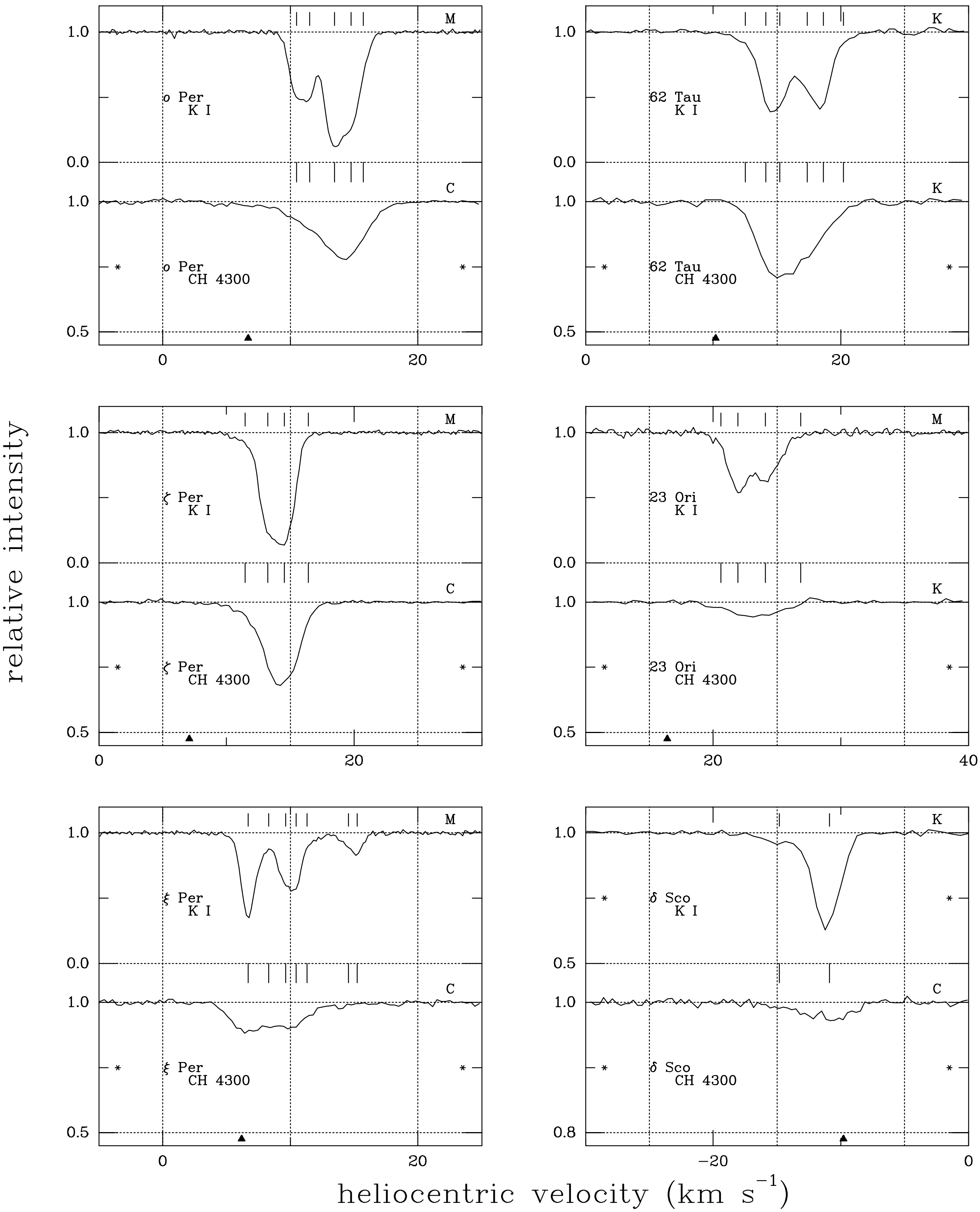

FIG. 24.—Comparison of high-resolution CH λ4300 and K I profiles. The vertical scale has been expanded in some cases to show weaker lines more clearly (noted by an asterisk near both vertical axes). The sources of the spectra have been noted at the right, just above the continuum [M = McDonald 2.7 m coudé (FWHM = 0.56 km s^{-1}); K = KPNO coudé feed (FWHM = 1.2–1.8 km s^{-1} for K I, FWHM = 1.3 km s^{-1} for CH); A = AAT UHRF (FWHM = 0.4–0.55 km s^{-1}); C = CLS (McDonald; FWHM = 0.6 km s^{-1})]. Tick marks above both K I and CH spectra indicate the components found in fitting the K I profiles. The solid triangles denote $v_{\mathrm{LSR}} = 0$ km s^{-1}.

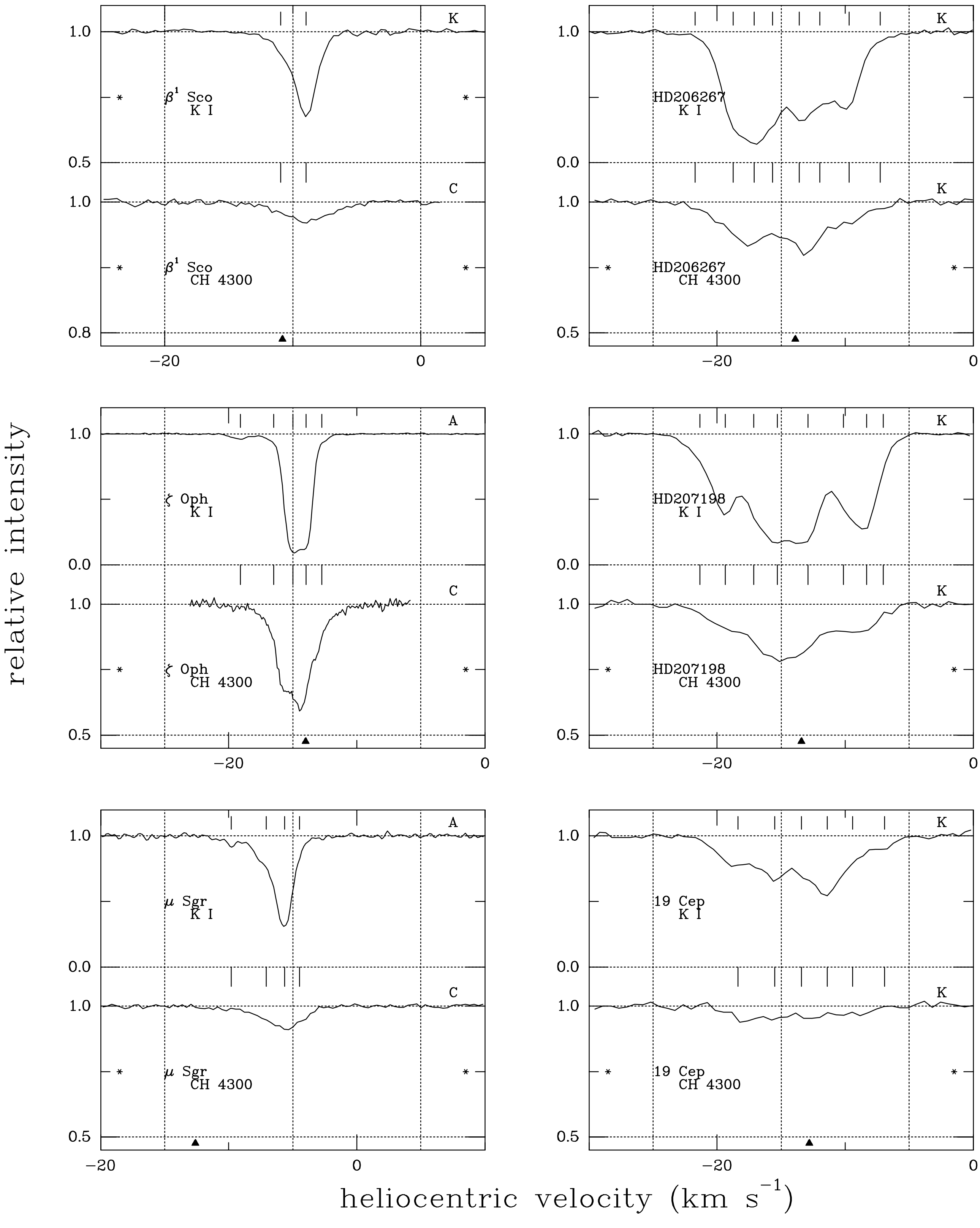

FIG. 25.—Comparison of individual CH and K I profiles (as for Fig. 24)

(1981) has shown that the roughly linear relationship between N(Na I) and $N(H_2)$ for $N(H_2) \gtrsim 10^{19}$ cm^{-2} follows naturally from the rate equations for the two species, if the formation rates of both species depend on the square of the local density and if the destruction is dominated by photo-ionization (Na I) or photodissociation (H_2). The scatter about that mean relationship then arises from differences in the fractional ionization (n_e/n_H), temperature, radiation field shape, Na abundance, H_2 formation rate, and H_2 self-shielding among the various lines of sight. Those same rate

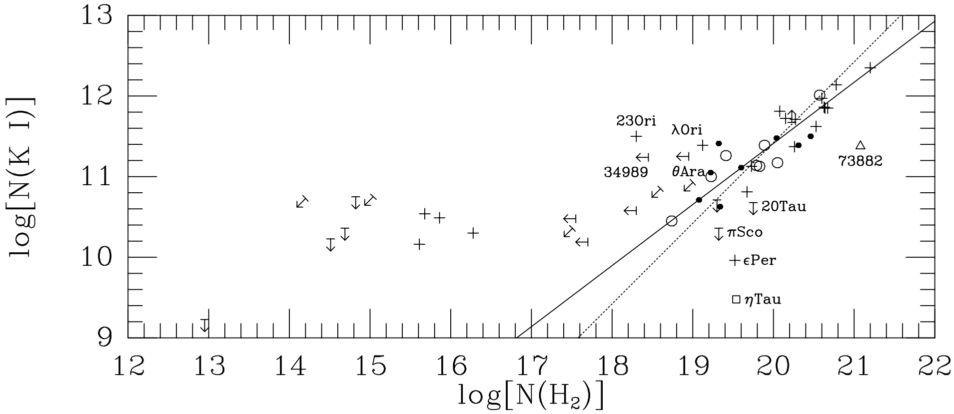

FIG. 26.—N(K I) vs. $N(H_2)$. All sight lines with K I and H_2 data are included. The symbols are as in Figs. 17 and 18. The relationship is complicated by the transition of H_2 to the self-shielded regime (10^{15} cm^{-2} $\lesssim N(H_2) \lesssim 10^{19}$ cm^{-2}), but may be slightly shallower than linear (*solid line*; slope = 0.76) above that transition region. The dotted line shows the fit [for $N(H_2) > 10^{18.5}$ cm^{-2}] with the slope fixed at 1.0.

equations suggest a similar, roughly linear relationship for $N(H_2) \lesssim 10^{15}$ cm^{-2}, as long as the local density is not too high—as seems to be indicated by the data in Figure 27. Higher resolution far-UV spectra of H_2 absorption toward ζ, δ, and ϵ Ori obtained with IMAPS (Jenkins & Peimbert 1996; Jenkins et al. 2000) indicate that the general Na I–H_2 relationship shown in Figure 27 holds as well for each of several groups of components along those three lines of sight. Figure 26 shows similar behavior for N(K I) versus $N(H_2)$, though only the higher column density regime is well sampled.

These observed relationships suggest that high-resolution spectra of K I and Na I should be very useful for modeling the line profiles of H_2 observed at lower resolution with *Copernicus* and/or *FUSE*—particularly for $N(H_2) \gtrsim 10^{19}$ cm^{-2}. Because the relationship between N(CH) and $N(H_2)$ is even tighter, this modeling will be most reliable when relatively high-resolution spectra of CH are also available. The component structure is most clearly seen in K I and Na I; using that structure to model the CH profile yields the atomic/molecular ratio for the individual components. The relative column densities found for CH may then be scaled to fit the H_2 lines. Such modeling will be particularly important for obtaining more accurate column densities from saturated H_2 lines (from various rotational levels) on the flat part of the curve of growth (e.g., Snow et al. 2000).

While the Sco-Oph sight lines generally do not appear to be discrepant in these relationships, there are a number of other sight lines which do not lie along the general mean curves in Figures 26 and 27. Toward 23 Ori, both N(K I)/$N(H_2)$ and N(Na I)/$N(H_2)$ are higher, by roughly an order of magnitude, than would be expected from the general mean relationships. The strong absorption from trace neutral species may imply a fractional ionization as high as 0.01 (i.e., significantly higher than the 0.0002 expected from photoionization of heavy elements alone) in the main "strong, low-velocity" clouds along that line of sight (Welty et al. 1999b). In addition, the molecular hydrogen may not have reached its equilibrium abundance, if those clouds lie at the boundary of the Orion-Eridanus bubble. Several

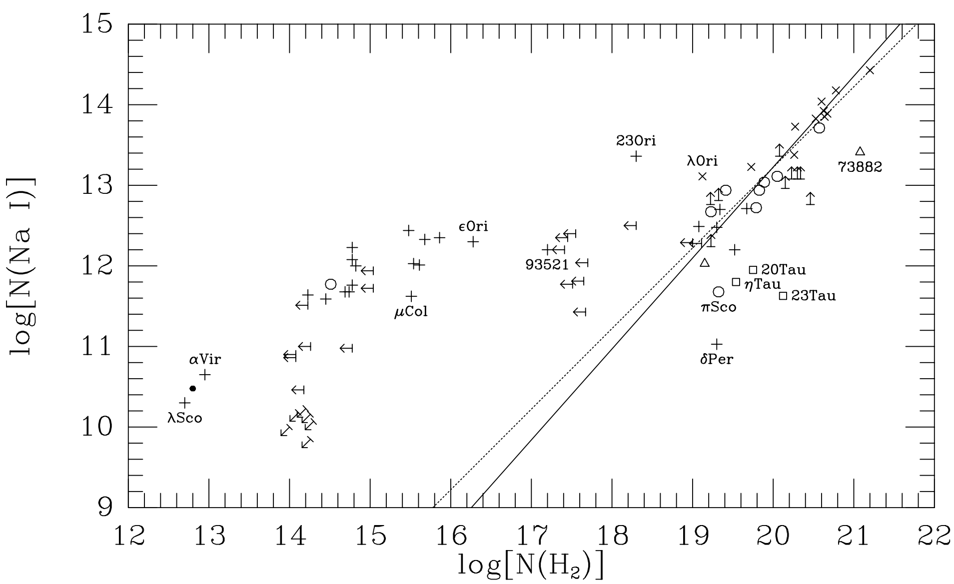

FIG. 27.—N(Na I) vs. $N(H_2)$. All sight lines with data are included. The symbols are as in Figs. 17 and 18. The relationship is complicated by the transition of H_2 to the self-shielded regime (10^{15} cm^{-2} $\lesssim N(H_2) \lesssim 10^{19}$ cm^{-2}), but may be slightly steeper than linear above (*solid line*; slope = 1.13) and slightly shallower than linear below that transition region. The dotted line shows the fit [for $N(H_2) > 10^{18.5}$ cm^{-2}] with the slope fixed at 1.0.

other stars in that general region (λ Ori, ϕ^1 Ori, HD 34989) also exhibit somewhat enhanced N(K I)/$N(H_2)$ and/or N(Na I)/$N(H_2)$ ratios. On the other hand, N(K I)/$N(H_2)$ and/or N(Na I)/$N(H_2)$ are lower than expected toward several Pleiades stars (η Tau, 20 Tau, 23 Tau), δ Per, π Sco, and (perhaps) ϵ Per. All but ϵ Per have much higher $N(H_2)$ than would be expected from their small $E(B-V) < 0.04$ (Savage et al. 1977); several of the other ratios discussed above appear to be somewhat discrepant toward some of these stars. The N(K I)/$N(H_2)$ and N(Na I)/$N(H_2)$ ratios are also low in the translucent cloud(s) toward HD 73882, where roughly 2/3 of the hydrogen is in molecular form (Snow et al. 2000; Welty et al. 2001b, in preparation).

4.3. *Depletions and Ionization*

4.3.1. *Mean Relationships/Typical Properties*

The strong correlations among the total column densities of K I, Na I, Li I, and C I—characterized by small scatter about nearly linear mean relationships—suggest that both the relative depletions and the relative ionization of K, Na, Li, and C are generally very similar (on average) along most of the sight lines for which data are available. In this section, we will use the observed relative gas phase abundances of these trace neutral species, together with recent results on the depletion of C, to determine depletions for Li, Na, and K. We will then examine the ionization equilibria for those elements and make rough estimates for n_e, $n_{\rm H}$, and the thermal pressure for individual clouds with different N(H). Differences between these estimated densities and pressures and those inferred from analyses of the fine-structure excitation equilibrium of C I suggest that some additional process(es) besides photoionization and radiative recombination may commonly and significantly affect the ionization balance of these and other elements in cool H I clouds. Charge exchange reactions between dominant singly ionized atomic species and neutral and/or negatively charged large molecules may provide the requisite enhancement of the trace neutral species.

Previous studies (e.g., Hobbs 1974c, 1976; CW) used either assumed or estimated values for n_e, T, and the radiation field in order to estimate the depletions of C, Na, and/or K. Recently, however, accurate abundances for C, based on measurements of the weak C II] λ2325 line, have been obtained for a set of sight lines characterized by wide ranges in mean density ($\langle n_{\rm H} \rangle$) and in the fraction of hydrogen in molecular form [$f(H_2) = 2N(H_2)/N(H_{\rm tot})$] (Cardelli et al. 1996; Sofia et al. 1997; Sofia, Fitzpatrick, & Meyer 1998). In all those sight lines, carbon is depleted by about -0.4 dex (relative to the assumed solar reference abundance). Because the lines of sight listed in Tables 1 and 7 cover similar ranges in $\langle n_{\rm H} \rangle$ and $f(H_2)$ to those of the C II] sample, we will assume a uniform carbon depletion $D({\rm C}) = \log(\delta_{\rm C})$ of -0.4 dex. If we also assume photoionization equilibrium, then the observed mean ratios N(Na I)/N(K I), N(Li I)/N(K I), N(C I)/N(Na I), and N(C I)/N(K I) noted above (§§ 4.2.2, 4.2.3, and 4.2.4) imply $D({\rm K}) \sim -0.7$ dex and $D({\rm Li}) \sim D({\rm Na}) \sim -0.6$ dex—at least in the (presumably) cooler, denser regions where the trace neutral species are predominantly located. The depletion values for Na and K are 0.1–0.2 dex more severe than those estimated by Hobbs (1976) and by CW—and depend relatively weakly on the assumed T and radiation field. For example, they would be more severe by about 0.15 dex if photoionization rates corresponding to the Draine (1978) radiation field were used (essentially due to the higher rate for C in that somewhat harder radiation field).

The relationships between the column densities of the trace neutral species (Li I, C I, Na I, and K I) and N(H) depend on the specific processes involved in the ionization equilibria of Li, C, Na, and K. The tight, nearly linear mean relationships among the trace neutral species suggest that those processes must not be highly element-specific or selective. For the general diffuse ISM, the obvious candidates are photoionization by the average interstellar radiation field (with shape relatively independent of location) and radiative recombination (with rate varying as $T^{-\beta}$; $\beta \sim 0.6$–0.7 for most elements of interest). Hobbs (1974b) recognized that the observed roughly quadratic relationships between the trace neutral species and H could arise if those two processes dominated the ionization equilibria, if $n_e/n_{\rm H}$ were roughly constant (as would be the case, for example, if photoionization of carbon were the main source of electrons), and if the individual clouds were characterized by a roughly uniform thickness. Other ionization processes (e.g., via cosmic rays, X-rays, or charge exchange with C II) would yield noticeably shallower relationships, and so must not be significant in most cases (Hobbs 1974b, 1974c, 1976).

In principle, we would like to know the relationships among these various species not just averaged over complex lines of sight, but for individual clouds and (ultimately) locally within each cloud. Where the integrated line of sight relationships are linear [e.g., for N(Na I) versus N(K I)], it is not unreasonable to assume linearity as well for the individual clouds (with a similar mean ratio but with greater scatter about the mean). Component analyses of the available high-resolution spectra of Na I and K I seem reasonably consistent with that assumption. As noted by Hobbs (1974b) and by Tarafdar (1977), however, the individual cloud column densities of the trace neutral species could have a steeper dependence on N(H) than the roughly quadratic relationships found for the total line of sight values. For example, if the individual clouds were generally in thermal pressure equilibrium and if $n_e/n_{\rm H} \sim$ constant, then the local densities of the trace neutral species could be roughly proportional to $n_{\rm H}^{2.7}$, since the recombination rates typically vary as $T^{-0.7}$ (e.g., Tarafdar 1977). Unfortunately, there are at present very few lines of sight for which N(H) is known (or reliably estimated) for the constituent individual clouds (e.g., Fitzpatrick & Spitzer 1997; Welty et al. 1999b).

In an attempt to determine what range of individual cloud dependences could yield the observed integrated (total line of sight) N(X I) versus N(H) relationships, we have performed two sets of simulations. In the first set, we constructed 55 lines of sight by assigning to each a random number of components, each component having a randomly assigned N(K I). The overall distributions of components per sight line and individual component column densities were both constrained to mimic those observed in our K I sample. In the second set of simulations, we used the K I component structures derived for the observed sample (54 lines of sight). In both cases, we predicted individual component N(H) from the relationship $N({\rm K\ I}) = N_0\,[N({\rm H})]^\gamma$, where the normalization was fixed (for each choice of γ) to reproduce the observed overall integrated N(K I) versus N(H). For both sets of simulations, the slope predicted for the integrated $\log[N({\rm K\ I})]$ versus $\log[N({\rm H})]$ is relatively insensitive to the individual component slope γ. For γ

ranging from 2.0 to 4.0, the predicted integrated slope varied only from about 1.7 to about 2.0 (vs. the observed values near 1.8 for K I and near 2.1 for Na I). The normalizations for the various simulations suggest that the median individual component $N(\mathrm{K\ I}) \sim 4 \times 10^{10}$ cm^{-2} corresponds to an individual component $N(\mathrm{H}) \sim 2 \times 10^{20}$ cm^{-2}—about a factor 2 smaller than the integrated N(H) that would correspond to a total sight line $N(\mathrm{K\ I}) = 4 \times 10^{10}$ cm^{-2}. Comparisons of the predicted integrated N(H) and $E(B-V)$ with those observed for some of the individual sight lines in the K I sample generally gave better agreement for γ between 2.0 and 3.0—consistent with the results for the integrated slopes. While these results seem to be consistent with thermal pressure equilibrium in the individual clouds, the weak dependence of the integrated slope on γ and the somewhat larger slope observed for N(Na I) versus N(H) preclude firm conclusions.

In principle, extinction effects could also steepen the predicted dependences of N(Na I) and N(K I) on N(H) by progressively reducing the photoionization rates in the thicker clouds (e.g., Tarafdar 1977). The complex component structure found in most lines of sight, however, means that the total $E(B-V)$ is generally due to contributions from a number of clouds. The reduction in the photoionization rates (Γs) within each individual cloud thus will be much smaller than if all the material were in a single cloud. As noted above, the median and maximum individual cloud column densities in the K I sample have corresponding $E(B-V)$ of about 0.03 and 0.17, respectively. For a cloud with total visual extinction $A_V = 0.6$ mag [slightly thicker than the maximum column density K I cloud, for $R_V = A_V/E(B-V) = 3.1$], the calculations of Roberge, Dalgarno, & Flannery (1981) (for grain model 2, with albedo $= 0.6$ and asymmetry factor $= 0.5$ for $\lambda < 1500$ Å) suggest that the photoionization rates for C I, Na I, and K I will be reduced by factors of 2.0–2.5 at the center (and by smaller factors, when integrated over the whole cloud). The reductions in Γ thus will be very slight for most of the individual clouds detected in K I.

As noted by Hobbs (1974a), the range of detectability of K I via the λ7698 line corresponds very well to that for which N(H I) can be accurately measured via damped Lyα absorption. If we assume an individual cloud slope $\gamma = 2.0$, then the minimum/median/maximum individual component $\log[N(\mathrm{K\ I})] \sim 9.2/10.6/12.0$ have corresponding $\log[N(\mathrm{H})] \sim 19.6/20.3/21.0$. If we further assume the depletions derived above, the WJ1 radiation field, $T = 100$ K, and that photoionization and radiative recombination dominate the ionization balance (reducing Γ by about 40% for the maximum column density clouds), then the corresponding electron densities (for uniform clouds) are 0.015/0.08/0.23 cm^{-3}. If the electrons come primarily from photoionization of C, then the fractional ionization $n_e/n_{\mathrm{H}} \sim 1.4 \times 10^{-4}$ (the gas phase abundance of C), yields local densities $n_H \sim 115/540/1600$ cm^{-3} and thermal pressures $\log(n_{\mathrm{H}} T) \sim 4.0/4.7/5.2$. The cloud thicknesses (uniform, as noted above) are all of order 0.1 pc. Assuming a slope $\gamma = 3.0$ does not affect the median values, and changes the various minimum and maximum values by less than a factor of 2. The assumed n_e/n_{H} represents a minimum fractional ionization due to photoionization, but it should be close to the true value if other sources of ionization (e.g., X-rays, cosmic rays) are generally not important. These rough predicted densities and pressures are significantly larger than the $\log(n_{\mathrm{H}} T) \sim 3.4 \pm 0.4$ typically inferred from analyses of the C I fine-structure excitation (Jenkins & Shaya 1979; Jenkins, Jura, & Loewenstein 1983; see also next sections below), with T determined from observations of H_2 (e.g., Savage et al. 1977). These systematic differences are puzzling, as there is significant overlap in the sight lines sampled in C I and K I, and as the two trace neutral species should be very similarly distributed. We note, however, that Fitzpatrick & Spitzer (1997) found that electron densities inferred from trace/dominant ratios seemed to be systematically higher than those derived from C II excitation equilibrium in the clouds toward HD 215733. In order to bring the values predicted from K I into better agreement with those inferred from C I, we would have to reduce T, reduce the radiation field, and/or increase the fractional ionization—but "reasonable" adjustments to these parameters may not be sufficient.

4.3.2. *Charge Exchange with Large Molecules*

Alternatively, those apparent discrepancies may provide evidence that charge exchange with neutral and/or negatively charged large molecules (LM) may play a significant role in the neutralization of singly ionized heavy elements even in relatively diffuse clouds (Omont 1986; Lepp et al. 1988; Welty et al. 1999b). The photoejection of electrons from such large molecules (e.g., 50 atom PAHs) may contribute significantly to the heating of diffuse clouds (Lepp & Dalgarno 1988b; Bakes & Tielens 1994); charge exchange reactions between the LM and various other molecular species may play a significant role in the cloud chemistry (Omont 1986; Lepp & Dalgarno 1988a; Bakes & Tielens 1998). Comparing the current best values for various N(X I)/N(X II) ratios for the main components toward ζ Oph with the cloud models computed by Lepp et al. (1988), most trace neutral species (C I, Mg I, S I, Ca I, but not Fe I) appear to be enhanced by a factor of about 3 over the values expected from radiative recombination alone. The models suggest that a fractional abundance of LM (relative to H) of about 3×10^{-7} could produce such an enhancement. For $T \sim 100$ K, the charge exchange rate for $\mathrm{LM}^- + \mathrm{X}^+$ is of order 10^{-7} cm^3 s^{-1}, with relatively weak dependences on T and the mass of element X; the rate for $\mathrm{LM}^0 + \mathrm{X}^+$ is much smaller, of order 10^{-9} cm^3 s^{-1} (Omont 1986; Lepp & Dalgarno 1988a). If the fractional abundance of large molecules is as high as 3×10^{-7} (and if all LM exist as LM$^-$), then charge exchange with LM$^-$ would be about 30 times faster than radiative recombination (for a fractional ionization 1.3×10^{-4} and rates typically of order 8×10^{-12} cm^3 s^{-1} at $T \sim 100$ K; e.g., Péquignot & Aldrovandi 1986), which in turn would be several times faster than charge exchange with LM^0 (even if all LM exist as LM^0). A factor 3 enhancement in the trace neutral species would thus require less than 10% of the LM to be negatively charged. The relative abundances of LM$^+$, LM^0, and LM$^-$ depend on the ratio n_e/F, where F is the scale factor relative to the Draine (1978) radiation field; the calculations of Lepp & Dalgarno (1988b) suggest that the fraction in LM$^-$ will be $\gtrsim$10% for $\log(n_e/F) \gtrsim -2$ (e.g., $n_e \gtrsim 0.01$ cm^{-3} for $F = 1$). For the main clouds toward ζ Oph, if $n_e \sim 0.1$ cm^{-3} [about 1/3 the value inferred from various N(X I)/N(X II) ratios assuming only radiative recombination, with $T \sim 20$–30 K and $F = 3.5$ as in the Lepp et al. models], then about 25% of the LM would be negatively charged. With the model central densities $n_{\mathrm{H}} \sim 350$–800 cm^{-3}, the electron density $n_e \sim 0.1$

cm^{-3} gives a fractional ionization of $2.9\text{–}1.3 \times 10^{-4}$—consistent with the electrons coming from photoionization of C. The thermal pressures implied by those models exceed the value $\log(n_H T) \sim 3.8$ inferred from C I fine-structure excitation (Jenkins et al. 1983) by factors of about 2. Similar calculations of the LM ionization state by Bakes & Tielens (1994) predict that roughly 30% of the 5 Å ($\sim$50 atom) LM will be negatively charged in their representative cold, diffuse cloud ($T = 100$ K, $n_e = 0.008$ cm^{-3}, $n_H = 25$ cm^{-3}, $G = 1$, where G is the scale factor for the somewhat weaker Habing radiation field)—i.e., about twice the fraction in LM^- predicted for those conditions by Lepp & Dalgarno (1988b). If the overall abundance of LM is of order 10^{-7} (containing about 4% of the gas phase C), then diffuse clouds therefore may well harbor quantities of LM^- sufficient to significantly affect the ionization balance of various heavy elements.

For a constant fractional abundance of LM, the density dependence of the neutralization of X^+ will be very similar to the dependence for radiative recombination with a constant fractional ionization. We consider only negatively charged LM, as the rates for LM^0 are likely smaller than those for radiative recombination. The models of Lepp & Dalgarno (1988b) suggest that the fractional abundance of LM^- (relative to all LM) increases from about 10% to about 90% as $\log(n_e/F)$ increases from about -1.95 to about -0.15. Over that range, the overall neutralization rate will thus go as approximately $n_H^{2.2}$, compared to $n_H^{2.0}$ for radiative recombination. If the cloud is in thermal pressure equilibrium, and if the charge exchange rate varies as $T^{-1/2}$ (Omont 1986), then the overall neutralization rate will go as roughly $n_H^{2.7}$, the same as for radiative recombination.

Because the rates for both charge exchange with LM^- and radiative recombination are only weakly dependent on element, inclusion of charge exchange neutralization does not significantly change the depletions estimated for Li, Na, and K. If charge exchange dominates (with rates proportional to $m^{-1/2}$), then all three elements would be depleted by about 0.6 dex.

Where the conversion of X^+ to X^0 is dominated by charge exchange with LM, the true n_e will be smaller than the values inferred from the various N(X I)/N(X II) ratios assuming only radiative recombination; the corresponding reductions in n_H and the pressure (assuming constant fractional ionization) then should generally yield better agreement with the values inferred from C I fine-structure excitation. Unless the abundance of LM^- and the relevant charge exchange rates are well known, however, the true n_e will be difficult to determine from the various N(X I)/N(X II) ratios alone. It may actually be best to estimate n_e from n_H, assuming a fractional ionization equal to the gas phase abundance of C—instead of the other way around.

If charge exchange with LM^- dominates the neutralization of various singly ionized species, it would be of interest to compare the column densities of the resulting neutral species with the strengths of the diffuse interstellar bands (DIBs), which also have been attributed to neutral and/or ionized large molecules (e.g., Allamandola, Tielens, & Barker 1985; Léger & d'Hendecourt 1985; Snow & Seab 1991). For example, Salama et al. (1996) have proposed that some of the stronger, broader DIBs might be due to positively charged "compact" PAHs, while some of the weaker, narrower DIBs might be due to positively or negatively charged "noncompact" PAHs. There is some question, however, as to whether the smaller PAHs (with fewer than about 30 carbon atoms), would survive in typical diffuse interstellar clouds (e.g., Allain, Leach, & Sedlmayr 1996). In principle, somewhat larger planar and/or spherical PAHs (neutral or charged) might also be responsible for some DIBs (Salama et al. 1996). If the abundances of the trace neutral species are set by charge exchange with LM^-, and if the stronger DIBs are due to LM^+, then we might expect a general anticorrelation between the strength of those DIBs and N(X I), in view of calculations of the LM ionization equilibrium (e.g., Lepp & Dalgarno 1988b; Bakes & Tielens 1994; Salama et al. 1996). Herbig (1993), however, reported positive correlations between the equivalent widths of the DIBs at 5780 and 5797 Å and the column densities of Na I, K I, and C I, with the slopes of the best-fit lines for log [W(DIB)] versus log [N(X I)] ranging from about 0.5 to 0.9 (see also Krelowski, Galazutdinov, & Musaev 1998). Comparing the column densities for those three trace neutral species given in Table 7 with equivalent widths for the 5780 and 5797 Å DIBs listed by Josafatsson & Snow (1987), Herbig (1993), and/or Krelowski et al. (1999) (for 72 sight lines in common), we find similar correlations, but with the slopes of the best-fit lines all between 0.3 and 0.6. The shallower slopes found here are likely due to the generally higher (and more accurate) values of N(X I) for the higher column density lines of sight listed in Table 7, but may also reflect the somewhat different sight line samples. The nearly linear correlations between both DIBs and log [$N(H_{tot})$] suggest that these DIBs behave more like dominant species in diffuse clouds (cf. Herbig 1993). We note, however, that there appears to be a weak anticorrelation between the ratios W(5780)/W(5797) and N(K I)/N(H)—suggestive of differences in ionization behavior for the two DIBs (cf. Sonnentrucker et al. 1997). Furthermore, the weakness of these two DIBs, relative to N(H), for the Sco-Oph and Trapezium sight lines—reminiscent of the corresponding weakness of the trace neutral species—suggests some modification and/or destruction of the DIB carriers there. These issues will be explored in more detail in a future paper.

4.3.3. *Discrepant Sight Lines*

While atypical values for such ratios as N(Na I)/N(H) and N(Na I)/N(K I) toward some stars in the Sco-Oph region have been recognized for some time (Hobbs 1976; Crutcher 1976), the explanation for those "discrepant" ratios has remained elusive. Crutcher proposed (1) that the Na I, K I, and C I absorption toward σ Sco arises in a cold cloud containing roughly half the observed H I and (2) that Na might be preferentially depleted, if the dust grains are positively charged, since the relatively small Γ/α for Na I implies that a larger fraction of the Na will be neutral. Crutcher noted that corresponding enhancements in the depletions of O and N (for which the neutral species are dominant in H I regions) might not be discernible in the existing *Copernicus* data. Chaffee & White (1982) also placed the trace neutral species seen toward the Sco-Oph stars in a cold, dense (a few $\times 10^3$ cm^{-3}) core containing only about 10% of the observed hydrogen.

Additional optical and UV data obtained since those early studies allow a reassessment of the "discrepant" ratios observed toward Sco-Oph. Reliable column densities are now available for H I, H_2, and various neutral and singly ionized species for many more lines of sight (see, e.g., the Appendix to this paper). As discussed above (§ 4.2), these data yield more extensive and accurate information on the abundances and depletions of a number of elements, more precise definition of various mean relationships, and the identification of additional deviations from those mean relationships (some of which are more extreme than those seen toward Sco-Oph). In addition:

1. High-resolution and/or high-S/N spectra of weak lines due to C II, N I, O I, and Kr I (all dominant in H I regions) obtained with the *HST* GHRS for sight lines characterized by wide ranges in location, $f(H_2)$, and $\langle n_H \rangle$ have revealed no significant variations in the (mild-to-negligible) depletions of C, N, O, or Kr (Sofia et al. 1997; Meyer, Cardelli, & Sofia 1997; Meyer, Jura, & Cardelli 1998; Cardelli & Meyer 1997). That apparent uniformity, for elements with different nucleosynthetic origins, suggests that abundance anomalies are not the reason for the observed discrepant ratios. Several of the Sco-Oph stars are included in those studies; there is no indication of enhanced depletions for O or N.

2. Comparisons of N(Ti II) with $N(H_{tot})$ yield depletion values for an element which can be very severely depleted (e.g., Stokes 1978; Albert et al. 1993; Welsh et al. 1997). The Sco-Oph stars exhibit both severe Ti depletion and low N(Na I)/N(K I) ratios, but there are other cases where those two properties do not go together—so that low N(Na I) is not necessarily associated with generally severe depletions. And while the depletions of both Ti and Fe toward Sco-Oph are more severe than for other lines of sight with similar $f(H_2)$, they are unexceptional when plotted versus $\langle n_H \rangle$. The difference is most likely due to the lower $f(H_2)$ in Sco-Oph (see below), rather than to anomalously severe depletions there. The N(Ti II)/N(Fe II) ratio appears to be somewhat low toward at least several of the Sco-Oph stars (cf. the apparent differences in depletion of several elements between 1 Sco and ζ Oph noted by Welty et al. 1995).

3. Analyses of the C I fine-structure excitation toward a small number of stars observed with GHRS, together with temperatures derived from H_2 (Savage et al. 1977), generally yield much smaller densities and pressures than would be predicted by the K I–H_{tot} relationship and assumptions discussed above (§ 4.3.1). In the main clouds toward 23 Ori, $n_H \sim$ 10–15 cm^{-3} and $\log(n_H T) \sim 3.1$ (Welty et al. 1999b)—much smaller than the $n_H \sim 1000$ cm^{-3} and $\log(n_H T) \sim 5.0$ that would be predicted from the observed N(K I). Toward the Sco-Oph stars π Sco, 1 Sco, β^1 Sco, and δ Sco, the n_H inferred from C I fine-structure excitation range from about 15 to about 150 cm^{-3} (cf. Federman, Welty, & Cardelli 1997)—again, much smaller than the values predicted from K I (or proposed by CW).

4. GHRS echelle profiles (FWHM $\sim$ 3.5 km s^{-1}) of the Zn II lines at 2026 and 2062 Å generally are very similar to the corresponding (higher resolution) Na I profiles (including those toward several of the Sco-Oph stars). As Zn II should be a good tracer of the total hydrogen, that general similarity suggests that if Na I is to be associated with only a fraction of the H (as proposed for the Sco-Oph stars), then it must be largely due to stratification within individual clouds. We expect some differences in distribution between the various trace and dominant species, due to the steeper density dependence of the trace species. To yield discrepant ratios for N(Na I)/N(K I), however, that stratification would have to be different for the two trace neutral species. If differences in cloud structure are responsible for the discrepant ratios in some lines of sight, then what is responsible for those differences?

As noted above, the Sco-Oph region is not alone in exhibiting discrepant ratios. In Table 6, we summarize the average values found for various ratios toward the Sco-Oph stars and toward stars in several other regions. The mean values listed in the second column are the values obtained by fixing the slopes of the various relationships to either 1.0 or 2.0 (see Table 5). For N(Na I)/$[N(H_{tot})]^2$, N(K I)/$[N(H_{tot})]^2$, N(Na I)/N(K I), and $f(H_2)$, the mean values exclude the various discrepant sight lines; the mean values for the other ratios include all sight lines except those discrepant by more than 2.5 σ. The values in the second line for each ratio are the differences with respect to the mean values. The ratios involving trace neutral species and H_2 include only sight lines for which $\log[N(H_2)] \geq 18.5$. In summary:

1. The Sco-Oph sight lines (listed in § 4.2.1) exhibit low N(X I)/$[N(H_{tot})]^2$, low $f(H_2)$, and slightly low N(Na I)/N(K I). The N(S I)/N(K I) and N(C I)/N(K I) ratios are also low toward several of the Sco-Oph stars (Welty 1989). The other ratios [e.g., N(X I)/$N(H_2)$] are within factors of 2 of the mean values.

2. The Trapezium sight lines include those toward θ^1 Ori C, θ^2 Ori A, and HD 37061. The N(X I)/$[N(H_{tot})]^2$ ratios and $f(H_2)$ are both very low, but N(Na I)/N(K I) appears normal.

3. The line of sight to 23 Ori exhibits enhanced abundances of various trace neutral species and of CH, relative to H_{tot} and H_2, and a relatively low $f(H_2)$ (Welty et al. 1999b). The N(X I)/N(Y I) and N(K I)/N(CH) ratios listed in Table 6, however, are within factors of 2 of the mean values.

4. The Pleiades sight lines (20 Tau, 23 Tau, 27 Tau, η Tau) appear to have C I and H_2 enhanced, relative to Na I and K I; N(CH)/$N(H_2)$ is low. Estimates of $N(H_{tot})$ toward η Tau based on column densities of O I, N I, P II, Zn II, and other dominant species suggest that N(K I)/$[N(H_{tot})]^2$ is slightly low, N(Na I)/$[N(H_{tot})]^2$ is fairly typical, and $f(H_2)$ is rather high in that line of sight.

5. In the ISM in the Magellanic Clouds, the N(X I)/$[N(H_{tot})]^2$ ratios are generally very low (except for K I in one SMC sight line); only a small part of those deficits can be attributed to the lower overall metallicities of the LMC (-0.3 dex) and SMC (-0.6 dex). The N(Na I)/N(K I) ratio also is typically rather low; the N(C I)/N(K I) ratio is low toward SN 1987A. The N(X I)/$N(H_2)$ ratios [toward one LMC star with $N(H_2) > 10^{19}$ cm^{-2}] are slightly lower than the mean Galactic values—consistent with the lower metallicity. The Magellanic Clouds sight lines will be discussed by Welty et al. (2001a, in preparation); see also Welty et al. (1999a) for analysis of the line of sight to SN 1987A in the LMC.

4.3.4. *Abundance Anomalies or Radiation Field Effects?*

The recognition of additional sight lines/regions with discrepant ratios provides an opportunity to look for common environmental factors that might be related to the observed differences in the relative abundances of the various trace neutral and molecular species. The two most obvious factors to consider are (1) the overall elemental abundances and depletions and (2) the strength and shape of the ambient radiation field.

TABLE 6

COLUMN DENSITY RATIOS FOR "DISCREPANT" REGIONS[a]

	Mean[b]		Sco-Oph[c]		Trapezium[d]		23 Ori[e]		Pleiades[f]		LMC[g]		SMC[h]	
Ratio	Ratio	Sight Lines	Ratio	Sight Lines	Ratio	Sight Lines	Ratio	Sight Lines	Ratio	Sight Lines	Ratio	Sight Lines	Ratio	Sight Lines
Na I/H^2_{tot}	−28.73	65	−29.53	9	−30.54	2	−28.12	1	...	0	−30.63	5	−30.98	6
	...		**−0.80**		**−1.81**		**+0.61**		...		**−1.90**		**−2.25**	
K I/H^2_{tot}	−30.61	36	−31.27	7	−32.65	2	−29.98	1	...	0	−31.62	2	−32.8/−30.6	2
	...		**−0.66**		**−2.04**		**+0.63**		...		**−1.01**		**−2.2**/0.0	
Na I/K I	1.96	38	1.67	6	1.92	1	1.86	1	2.19	2	1.19	3	1.25/0.50	2
	...		−0.29		−0.04		−0.10		+0.23		**−0.77**		**−0.7/−1.5**	
C I/K I	3.36	27	3.23	7	...	0	3.49	1	4.13	1	2.62	1	...	0
	...		−0.13		...		+0.13		**+0.77**		**−0.74**		...	
C I/Na I	1.42	34	1.40	8	...	0	1.63	1	1.81	1	1.29	1	...	0
	...		−0.02		...		+0.21		**+0.39**		−0.13		...	0
CH/K I	1.37	35	1.36	7	...	0	1.20	1	...	0	1.04	1	...	0
	...		−0.01		...		−0.17		...		**−0.33**		...	
K I/H_2	−8.58	27	−8.43	7	...	0	−6.80	1	−10.06	1	−8.38	1	...	0
	...		+0.15		...		**+1.78**		**−1.48**		+0.20		...	
Na I/H_2	−6.78	22	−6.91	8	...	0	−4.94	1	−8.01	3	−7.11	1	...	0
	...		−0.13		...		**+1.84**		**−1.23**		**−0.33**		...	
$f(H_2)$	−0.72	33	−1.23	9	< −3.69	1	−2.14	1	...	0	...	0	...	0
	...		**−0.52**		**< −2.97**		**−1.42**		...		...		...	

[a] For each region, the two columns are average logarithmic ratio and number of sight lines contributing; see Table 7 (see Appendix) for values and references. The second line for each ratio gives the difference with respect to the mean value in the the second column; entries in bold type denote differences greater than 0.3 dex. Ratios involving H_2 include only sight lines with $\log[N(H_2)] \geq 18.5$.

[b] For slope fixed at 1.0 or 2.0; see Table 5.

[c] 1 Sco, π Sco, δ Sco, β^1 Sco, ω^1 Sco, ν Sco, o Sco, σ Sco, HD 147889, ρ Oph, 22 Sco, τ Sco.

[d] θ^1 Ori C, θ^2 Ori A, HD 37061.

[e] Welty et al. 1999b. Some similar values are found also for λ Ori, HD 34989, and ϕ^1 Ori.

[f] 20 Tau, 23 Tau, η Tau, 27 Tau.

[g] SN 1987A, Sk −67 5, Sk −68 73, Sk −69 203, Sk −69 213, Sk −69 243 (Welty et al. 1999a, 2001a, in preparation).

[h] Sk 13, Sk 40, Sk 78, Sk 80, Sk 82, Sk 143, Sk 155 (Welty et al. 2001a, in preparation); individual values are given for ratios involving K I.

While the abundance results for C, N, O, and Kr noted above suggest that the overall total (gas + dust) abundances of most elements are fairly uniform in the Galactic ISM, the main clouds in the regions listed in Table 6 are characterized by a range in overall elemental depletions. If we use $N(\text{Ti II})/N(H_{tot})$ as a depletion index, with the Ti II column densities taken from Stokes (1978), Albert (1983), Hobbs (1978), Albert et al. (1993), and Welsh et al. (1997), the overall depletions are most severe toward the Sco-Oph stars, slightly less severe toward the Trapezium stars (e.g., Shuping & Snow 1997), 23 Ori (Welty et al. 1999b), and the Pleiades, and least severe in the Magellanic Clouds (Welty et al. 1997, 1999a). The differences in $N(\text{X I})/[N(H_{tot})]^2$ do not appear to be correlated with the overall depletions, however.

While the generally fairly tight relationships between the various trace neutral species, H_{tot}, CH, and H_2 discussed above (§ 4.3.1) suggest that the majority of Galactic clouds are immersed in a fairly uniform average radiation field, we suspect that the strength and/or shape of the radiation field in at least several of the regions listed in Table 6 may depart significantly from that average. In particular, the far-UV field may well be significantly enhanced for the main clouds toward Sco-Oph, toward the Trapezium stars, and in the Magellanic Clouds. An enhanced far-UV radiation field would reduce the abundances of trace neutral species, CH, and H_2 (via increased photoionization and photodissociation), as observed for the clouds in each of those regions.

1. The main neutral components toward the Trapezium stars may form a "neutral lid," located between the Trapezium stars and ι Ori along the line of sight (O'Dell et al. 1993), and therefore close to those (and other) hot, bright, early-type stars. In addition, the far-UV extinction in that region is fairly shallow (e.g., Fitzpatrick & Massa 1990), enabling the far-UV radiation to penetrate further into the clouds.

2. The interstellar radiation field in both the LMC and the SMC appears to be stronger than the typical Galactic field by a factor $\gtrsim 5$ (Lequeux 1989; Pak et al. 1998). The far-UV extinction curves are generally steep (in the SMC and near 30 Dor in the LMC), but the dust-to-gas ratios are typically smaller than those found in the Galactic ISM (due

to the lower metallicities and relatively mild depletions), again allowing the radiation to penetrate.

3. The main neutral components toward Sco-Oph also are likely to be located relatively close to the numerous early-type stars in that region (e.g., de Geus, de Zeeuw, & Lub 1989; de Geus & Burton 1991). The far-UV extinction for at least some of the Sco-Oph stars is relatively shallow; a harder UV radiation field may be responsible for the low N(S I)/N(K I) and N(C I)/N(K I) ratios, given the higher ionization potentials of S I and C I (Welty 1989; Welty, Hobbs, & York 1991).

4. Toward the Pleiades, the main neutral components once again appear to be located close to the background stars (White 1984), but in this case those stars are of somewhat later type, so that the mid-UV part of the radiation field is enhanced. An enhanced mid-UV field would reduce the abundances of K I and Na I, but might not significantly affect C I and H_2, whose thresholds for photoionization or photodissociation are at significantly shorter wavelengths. Such a change in field shape thus might produce higher N(C I)/N(K I) ratios and lower N(K I)/N(H_2) ratios, as observed; the N(K I)/$[N(H_{tot})]^2$ ratio is slightly low, but the N(Na I)/$[N(H_{tot})]^2$ ratio is normal toward η Tau, however.

5. Finally, we note that the N(Na I)/$[N(H_{tot})]^2$ ratios found for two groups of Galactic halo clouds toward SN 1987A [with $N(H) \sim 10^{19}$ cm^{-2}; Welty et al. 1999a] are at least a factor of 5 higher than the mean value found for disk clouds—which might, in principle, be due to a somewhat weaker ambient radiation field in the halo and/or to slight ionization of H (and consequent increased n_e) in those relatively thin clouds.

While variations in the strength and/or shape of the radiation field appear to provide a plausible qualitative explanation for the differences observed in the various ratios (particularly for N(X I)/$[N(H_{tot})]^2$ and for ratios of species with significantly different ionization potentials), can they account quantitatively for the observed differences? For example, is the radiation field at the main neutral clouds toward the Trapezium enhanced by two orders of magnitude over the typical average field (to yield the observed low N(X I)/$[N(H_{tot})]^2$ ratios) and could the field at the halo clouds toward SN 1987A be only of order one-tenth the average field in the disk? Here again, neutralization of singly ionized species via charge exchange with negatively charged large molecules may provide a reasonable explanation. If n_e/F lies in the range for which changes in F produce appreciable changes in the fraction in LM$^-$, then the effects of changes in the radiation field on the ionization balance will be amplified. If the radiation field is reduced, not only is the photoionization of X I decreased, but the relative abundance of LM$^-$ is increased—increasing the neutralization of X II and thus enhancing the neutral species even more. Conversely, increasing the radiation field both increases the photoionization and decreases the abundance of LM$^-$—both of which will act to reduce N(X I)/N(X II). For example, if the overall abundance of large molecules is 3×10^{-7}, with 30% in LM$^-$ [for $\log(n_e/F) \sim -1.4$ (Fig. 1 of Lepp & Dalgarno 1988b); cf. the "cold neutral cloud" value for 5 Å LM in Bakes & Tielens 1994], then the neutral species will be enhanced by about a factor of 10, relative to the abundances that would be produced by radiative recombination alone. If the radiation field is then increased by a factor of 10, the fractional abundance of LM$^-$ would be reduced to about 2%–3% (where the charge exchange rate would be comparable to the radiative recombination rate), and the various N(X I)/N(X II) ratios would decrease by a factor of order 50. The combination of a stronger radiation field, charge exchange with LM, and lower metallicities might thus account for the typically very low N(X I)/$[N(H_{tot})]^2$ ratios in the LMC and SMC.

Variations in the strength of the radiation field—even if augmented by charge exchange with LM—would not account for differences in the relative abundances of trace neutral species, however. Differences in the shape of the radiation field—due to local stellar sources and/or UV extinction properties—can produce differences in the ratios of trace species with very different ionization potentials [e.g., N(C I)/N(K I)] (Jenkins & Shaya 1979; Roberge et al. 1981; Welty 1989). It seems unlikely, however, that differences in either the strength or shape of the field could significantly affect the N(Na I)/N(K I) ratio, as the two species have similar ionization potentials (5.1 and 4.3 eV) and as their photoionization cross sections appear to behave similarly in the wavelength region most important for their photoionization (roughly from 1100 to 1700 Å). A significantly harder field might produce a slightly smaller N(Na I)/N(K I) ratio, but probably not the factor of 2 smaller value found toward Sco-Oph. It is intriguing that Na I appears to behave more similarly to C I than to K I—even though considerations of ionization potential and chemical properties would suggest the opposite should be true.

5. SUMMARY

We have analyzed high-resolution (FWHM $\sim$ 0.40–0.56 or 1.2–1.8 km s^{-1}) spectra of interstellar K I λ7698 absorption toward 54 Galactic stars. Typical S/Ns of 100–200 for the spectra yield 2 σ equivalent width limits of 0.25–1.0 mÅ, which correspond to K I column density limits of 1.4–5.6×10^9 cm^{-2}. These spectra are thus characterized by higher resolution, S/N, and sensitivity than the K I spectra previously available for most of these lines of sight.

Voigt profile fits to the observed line profiles yielded a total of 319 individual K I components—enabling estimates of the statistical properties of the component velocities, column densities, and line widths. The distribution of component velocities is similar to that of the stronger Na I components discussed by WHK, with mean $v_{LSR} = 1.7$ km s^{-1} and dispersion $\langle v^2 \rangle^{1/2} = 7.5$ km s^{-1}. The median and maximum individual component K I column densities are about 4×10^{10} cm^{-2} and 10^{12} cm^{-2}, respectively. In view of the good correlation between N(K I) and $N(H_{tot})$, those median and maximum individual cloud N(K I) correspond to individual cloud hydrogen column densities of about 2×10^{20} cm^{-2} and 10^{21} cm^{-2} [and $E(B-V)$ of about 0.03 and 0.17], respectively. As for Na I and Ca II, the K I component line widths show no apparent correlation with column density. The median K I b-value for the highest resolution spectra is 0.67 km s^{-1}—smaller than previous estimates based on lower resolution spectra by factors of 2–3. If T = 80–100 K in the gas traced by K I, then at least 35%–50% of the components have subsonic internal turbulent velocities. The median K I b-value is slightly smaller than the median b found for Na I (0.73 km s^{-1}; WHK), as would be expected if the two species are generally coextensive. The generally larger b-values found for Ca II (WMH) suggest that Ca II may be more broadly distributed, in gas characterized by somewhat higher T and/or v_t. The distribution of adjacent component separations δv, somewhat steeper than those found for Na I and Ca II and with true median value less than about 1.2 km s^{-1}, suggests that we may have discerned only about half of the K I components actually present. The general complexity of the component structures seen in K I and/or Na I suggests both that shielding effects for individual clouds are smaller than previously thought and that sight lines dominated by a single cloud are rare.

Using the high-resolution, high S/N spectra of K I, Na I (WHK), and CH (CLS) now available, we have reexamined some of the relationships among the total line of sight column densities of K I, Na I, C I, Li I, H_{tot}, H_2, and CH. In general, pairwise comparisons among these species yield well-defined mean relationships with relatively small scatter (though in some cases only over restricted ranges in column density):

1. We confirm the essentially linear relationships between the total column densities of the trace neutral species Li I, C I, Na I, and K I. The mean N(Na I)/N(K I) ratio is about 85—though it can vary by factors of 2–3 among the individual components or component groups along a given line of sight. The mean N(C I)/N(Na I) and N(C I)/N(K I) ratios are about 26 and about 2300, respectively—though the latter ratio is somewhat higher for the few highest column density sight lines. The average N(Li I)/N(K I) ratio is about 0.0054. The small scatter about these well-defined mean relationships suggests that there are typically only modest variations both in the shape of the interstellar radiation field and in the relative depletions of Li, C, Na, and K. Since carbon is generally depleted by about 0.4 dex (relative to solar reference abundances), Li, Na, and K are likely depleted by about 0.6, 0.6, and 0.7 dex, respectively, in the relatively cool, dense regions where the neutral species are concentrated.

2. We also confirm the roughly quadratic dependence of the total column densities of C I, Na I, and K I on $N(H_{tot})$. For Na I in particular, a quadratic relationship appears to apply over the full range of column densities so far explored—though the scatter increases significantly for $N(\text{Na I}) \lesssim 10^{11}$ cm^{-2}. As discussed by Hobbs (1974b, 1976), a quadratic relationship could result if the ionization balance is dominated by photoionization and radiative recombination, with an approximately constant fractional ionization n_e/n_H and a uniform cloud thickness. Ionization by cosmic rays or X-rays, which would yield somewhat shallower relationships between the trace neutral species and H_{tot}, must not (in general) significantly affect the ionization balance. Simulations suggest that the corresponding relationships for *individual* clouds are likely somewhat steeper, with an exponent γ between 2 and 3; γ would be 2.7 if the clouds are in thermal pressure equilibrium and if $n_e/n_H \sim$ constant. The small scatter about the mean relationships suggests that the overall strength of the interstellar radiation field is typically close to its mean value (except, perhaps, for clouds in the various "discrepant" sight lines). If we assume the above depletions, the WJ1 radiation field, $T = 100$ K, $n_e/n_H = 1.4 \times 10^{-4}$, and that photoionization and radiative recombination dominate the ionization equilibria, the resulting inferred local densities and thermal pressures are systematically higher than those determined from analyses of C I fine-structure excitation.

3. There is an approximately linear relationship between N(K I) and N(CH), with very small scatter, which holds even for many sight lines that are "discrepant" in other relationships. High-resolution profiles of K I and CH absorption are in many cases very similar—suggesting close association between the two species (though perhaps not complete coexistence). The total column densities of both K I and Na I exhibit a roughly linear dependence on $N(H_2)$, for $N(H_2) \lesssim 10^{15}$ cm^{-2} and for $N(H_2) \gtrsim 10^{19}$ cm^{-2} (though there are a number of discrepant sight lines). High-resolution absorption-line profiles for K I and Na I therefore should be very useful for determining more accurate H_2 column densities from the lower resolution far-UV spectra obtained with *Copernicus* and *FUSE*.

4. The lower abundances of various trace neutral species (relative to H_{tot}) and the lower $f(H_2)$ toward Sco-Oph, toward the Orion Trapezium, and in the ISM of the Magellanic Clouds may be ascribed to the generally stronger interstellar radiation fields in those regions. Conversely, weaker fields may be responsible for the higher relative abundances of the trace neutrals observed for clouds in the Galactic halo. Toward the Pleiades, lower abundances of K I and CH, relative to C I and H_2, may be due to an enhanced mid-UV radiation field in clouds close to the late B type background stars. Changes in the strength and/or shape of the radiation field would not explain the anomalous N(Na I)/N(K I) ratios seen in several of these regions, however.

We concur with the suggestion of Lepp et al. (1988) that charge exchange between singly ionized atomic species and negatively charged large molecules (e.g., 50 atom PAHs) may be more important than radiative recombination for maintaining the abundances of the corresponding trace neutral atomic species, even in relatively diffuse clouds. The required fractional abundance of LM$^-$, a few times 10^{-8} relative to H, can apparently be present in clouds of modest density bathed in the average interstellar radiation field (Lepp & Dalgarno 1988b; Bakes & Tielens 1994). The true electron densities would thus be smaller than those derived assuming only radiative recombination; the corresponding smaller inferred local hydrogen densities and thermal pressures would be more consistent with those determined from analyses of the C I and C II excitation equilibria. Unless the abundance of LM and the relevant charge exchange rates can be accurately determined, however, it will be difficult to determine precise values for n_e directly from the various trace neutral species. In addition, charge exchange with LM$^-$ would tend to amplify the effects on the ionization balance of changes in the strength of the radiation field—making it easier to account for the various "discrepant" $N(\text{X I})/[N(H_{tot})]^2$ ratios. Finally, comparisons between the column densities of trace neutral species and the strengths of various diffuse interstellar bands, in different environments, may help to clarify the (possible) role of large molecules in producing both the neutral species and the DIBs.

We are grateful to M. Lemoine and R. Ferlet for contributing their UHRF K I spectra to this survey, to D. Willmarth (KPNO) and D. Doss (McDonald) for their help in setting up the spectrographs, to P. Crane for providing some of the CLS CH spectra in digital form, to S. Federman and D. Knauth for communicating λ4044 equivalent widths, to J. Lauroesch and D. Meyer for providing Na I spectra of several stars, and to S. Federman and E. Jenkins for comments on an earlier version of the paper. J. Fowler obtained some of the KPNO K I spectra; J. Trapero assisted with some of the McDonald K I observations. Support for this work has been provided by NASA LTSA grant NAGW-4445 and by NASA grant GO-2251.01-87A from the Space Telescope Science Institute, which is operated by AURA, Inc., under NASA contract NAS5-26555.

APPENDIX

COLUMN DENSITIES FOR H_{tot}, H_2, Na I, K I, Li I, C I, AND CH

In Table 7, we list total line of sight column densities for H_{tot} (i.e., H I + 2 H_2), H_2, Na I, K I, Li I, C I, and/or CH, for 147 sight lines for which data for at least two of the species (at least one besides H_{tot} and H_2) are available. We have tried to include all available column densities of Na I, K I, and CH derived from high-resolution spectra (FWHM $\lesssim 2$ km s^{-1}). In general, we include values obtained from lower resolution spectra only for cases where the corresponding absorption lines are relatively weak or (for H_{tot}, H_2, and C I) where no high-resolution spectra are available. A catalog of high-resolution optical spectra obtained since about 1980 (by us and by others, including some unpublished) may be found at http://astro.uchicago.edu/home/web/welty/hicat.html; plots of the spectra are available for many of the lines of sight.

H_{tot} *and* H_2.—We have taken H I column densities primarily from Bohlin, Savage, & Drake (1978), Shull & Van Steenberg (1985), Jenkins, Savage, & Spitzer (1986), and Diplas & Savage (1994)—all based on fits to the damped interstellar Lyα absorption profiles. In general, we prefer the values derived from *Copernicus* spectra, except for ρ Oph, where the Bohlin et al. value appears to be an overestimate. Some of the N(H I) values for some sight lines toward early B stars with N(Na I) $\lesssim 10^{11}$ cm^{-2} might, in principle, include a noticeable contribution from stellar Lyα absorption (see, e.g., Diplas & Savage 1994). We therefore checked the available data for interstellar N I, O I, S II, and P II (which are dominant species in H I gas and which typically are at most mildly depleted) (York et al. 1983; Jenkins et al. 1986). We conclude that the listed N(H I) are unlikely to be more than a factor 2 higher than the true interstellar values for those sight lines. The increased scatter in $N(H_{tot})$ for those low Na I column densities is therefore real.

Most of the H_2 column densities are from Savage et al. (1977) and Jenkins et al. (1986). The values for δ Ori, ϵ Ori, and ζ Ori are from higher resolution spectra obtained with IMAPS (Jenkins & Peimbert 1996; Jenkins et al. 2000). There are a number of sight lines for which H_2 has not been measured, but may well be significant, based on the available CH column densities and the generally tight N(CH)–$N(H_2)$ relationship found by Danks, Federman, & Lambert (1984) (e.g., for AE Aur, χ^2 Ori, ζ^1 Sco). In most of those cases, however, the increase in log [$N(H_{tot})$] is likely to be less than 0.2 dex. The $N(H_2)$ listed for HD 154368, an indirect estimate reported by Snow et al. (1996), is not used in any of the correlation fits.

Na I.—Most of the Na I column densities are from WHK or from Hobbs (1974c, 1976), though values based on somewhat lower resolution spectra (mostly for relatively weak D lines) were taken from Ferlet et al. (1985), Crawford (1991), and Centurion & Vladilo (1991). We have not included sight lines with very strong D lines observed only at lower resolution (FWHM $\gtrsim 4$ km s^{-1}), for which only lower limits to N(Na I) are generally available. Observations of the weaker Na I doublet at 3302 Å are available for most of the sight lines with N(Na I) $\gtrsim 10^{13}$ cm^{-2} (de Boer & Pottasch 1974; Crutcher 1975; Hobbs 1978; Chaffee & Dunham 1979; Crawford 1992). The species K I and Na I appear to be very similarly distributed in the ISM, and the K I line at 7698 Å is generally similar in strength (W_λ/λ) to the Na I λ3302 doublet lines. We therefore used the component structure derived from the high-resolution K I spectra, assuming $T \sim 100$ K and uniformly scaling the individual component column densities, to match the equivalent widths observed for the λ3302 doublet. The resulting Na I column densities differ slightly in some cases from those tabulated by WHK, which were based on preliminary versions of the K I component structures. Because the individual component b-values are typically smaller than the "effective" line of sight b-values used in previous analyses of the weaker doublet, and because we have used the slightly smaller (by 0.17 dex) f-values tabulated by Morton (1991), the resulting Na I column densities are generally somewhat higher than the previous estimates for these higher column density lines of sight.

K I.—Most of the K I column densities are from the present survey, from Hobbs (1974a, 1976), or from the lower resolution survey of Chaffee & White (1982); some previously unpublished values derived from lower resolution (FWHM ~ 2.5 km s^{-1}) CF spectra are also included. As noted in § 3.2, column densities derived from the weak K I doublet at 4044 and 4047 Å have been used to check the values derived from the much stronger λ7698 line for a few high column density lines of sight.

Li I.—Most of the Li I column densities are from Hobbs (1984) and White (1986), who also included several lines of sight from earlier studies. We have increased some of the upper limits listed by Hobbs (which were computed for single, unresolved components) to reflect the wider velocity range spanned by strong, multicomponent K I absorption. The values for ζ Per, o Per, ρ Oph, and ζ Oph are from more recent high-resolution, high S/N spectra reported by Meyer, Hawkins, & Wright (1993), Lemoine et al. (1993, 1995), and Knauth et al. (2000). The equivalent width and column density for HD 154368 given by Snow et al. (1996) are too high, by a factor of about 5 (J. Black 2000, private communication). Several values derived from recent very high S/N but lower resolution spectra obtained with the ARC echelle spectrograph are also included (J. Thorburn 2000, private communication).

C I.—Nearly all of the C I column densities are from Jenkins et al. (1983) or Jenkins & Shaya (1979), who attempted to account for saturation in the C I lines using the high-resolution Na I profiles available at that time. A new survey of C I, using higher resolution UV spectra obtained with GHRS and STIS and making use of improved f-values, would be valuable (e.g., Zsargó, Federman, & Cardelli 1997; Jenkins 2000).

CH.—Most of the CH column densities are from the high-resolution survey of Crane et al. (1995) or from an update to the compilation of molecular column densities in Federman et al. (1994) (S. Federman 2000, private communication). Some of the

TABLE 7

COLUMN DENSITIES FOR H_{tot}, H_2, Na I, K I, Li I, C I, AND CH[a]

Star	H_{tot}	Reference[b]	H_2	Reference[c]	Na I	Reference[d]	K I	Reference[e]	Li I	Reference[f]	C I	Reference[g]	CH	Reference[h]
γ Peg	20.04	1	<14.20	1	<10.23	1	<10.73	1						
κ Cas	21.29	1	20.27	1	13.73	2	11.71	2	<10.01	1	15.55	1	12.93	1
γ Cas	20.16	1	<17.51	1	11.77	3	<10.36	3			13.05	1		
ϕ Per	20.57	1	19.08	1	12.49	1	10.71	1						
HD 14633	20.56	1	<19.11	1	12.28	1								
HD 18100	20.14	2			11.00	4								
HD 21291							12.11	2	<10.00	2			13.32	1
HD 21856	21.12	1	20.04	1			11.48	1						
ψ Per					12.89	2	11.09	2						
17 Tau					11.30	3							<12.20	2
20 Tau			19.75	2	11.95	1	<10.68	1					<11.30	3
23 Tau			20.12	2	11.63	1							<12.34	2
η Tau			19.54	2	11.80	3	9.48	2			13.61	3	<12.34	1
27 Tau					12.25	3	10.20	2					<12.40	2
δ Per	20.30	3	19.30	2	11.03	3					<13.11	1		
40 Per	21.23	1	20.46	1	>12.76	1	11.50	1			14.75	1		
o Per	21.20	1	20.60	1	14.04	2	11.97	2	9.58	3	15.67	2	13.20	3
ζ Per	21.20	1	20.67	1	13.89	2	11.85	2	9.62	3	15.53	2	13.34	3
ξ Per	21.29	1	20.53	1	13.83	2	11.62	2	<10.11	1	15.12	1	13.08	3
ϵ Per	20.51	1	19.52	1	12.20	3	9.96	2			13.73	3	<12.30	1
62 Tau							11.83	2	<10.00	4			13.46	1
HD 28497	20.20	1	14.82	1	12.00	1	<10.75	1						
ν Eri	20.45	1	<17.41	2	12.20	1								
α Cam	21.09	1	20.34	1	>13.08	1					>15.17	1	12.83	3
π^4 Ori	20.60	2			12.01	3								
π^5 Ori	20.41	1	<17.45	2	12.35	3								
ϵ Aur					>13.11	1	11.90	2	9.41	5				
AE Aur	21.20	2			14.27	5	12.17	1	<10.00	2			13.90	1
β Ori					11.60	1	<10.68	1						
λ Lep	20.18	1	<15.04	2	11.72	1	<10.75	1						
HD 34989	21.11	1	<18.45	1			11.24	2						
23 Ori	20.74	1	18.30	3	13.36	3	11.50	2	<9.70	4	14.99	4	12.70	4
25 Ori	20.46	1	14.78	2	11.76	1								
ψ Ori	20.60	1	14.78	2	12.23	1								
η Ori	20.61	2			12.93	2	10.96	2			13.98	3		
χ Aur					14.09	5	12.01	1	<10.14	2				
γ Ori	19.81	3			11.02	6								
δ Ori	20.23	1	14.74	4	11.68	3					13.02	1		
ϕ^1 Ori	20.84	1	19.32	1	>12.81	1	11.41	1						
λ Ori	20.80	1	19.12	1	13.11	2	11.39	2			14.39	1		
HD 36982	21.55	2					11.89	2						
θ^1OriC	21.54	2			12.40	1	10.48	2	<10.00	4			<12.56	5
θ^2OriA	21.38	2			12.36	1	<10.77	1						
HD 37061	21.78	2					10.87	2					<12.34	4
ι Ori	20.15	1	14.69	1	11.68	3	<10.36	3			13.12	3		
ϵ Ori	20.45	1	16.28	4	12.30	3	10.30	2			13.69	3		

TABLE 7—*Continued*

Star	H_{tot}	Reference[b]	H_2	Reference[c]	Na I	Reference[d]	K I	Reference[e]	Li I	Reference[f]	C I	Reference[g]	CH	Reference[h]
ζ Tau	20.04	1	<17.67	1	11.43	1								
σ Ori	20.52	1	<18.30	2	12.50	3	10.58	2						
ζ Ori	20.41	1	15.86	4	12.35	3	10.49	2			13.88	4		
HD 37903	21.17	2			12.82	6	11.00	2					12.90	1
μ Col	19.85	1	15.51	1	11.62	6								
κ Ori	20.52	1	15.68	1	12.33	3	10.54	2			13.68	1		
139 Tau	20.96	1	19.73	1	13.23	2	11.13	2			14.28	3		
χ^2 Ori	21.40	2			14.08	2	12.20	2	9.70	2			13.23	3
S Mon A	20.40	1	15.54	1	12.03	3			<9.70	4	13.40	2		
κ CMa	19.78	2			10.54	1								
19 Mon	20.34	1	14.78	2	12.08	1								
o^2 CMa	20.18	1			11.48	3					13.16	2		
τ CMa	20.70	1	15.48	1	12.44	3								
η CMa	19.85	1			11.92	1	10.03	2						
ζ Pup	19.99	1	14.45	1	11.59	3					13.26	2		
γ^2 Vel	19.78	1	14.23	1	11.64	3					13.12	2		
HD 73882	21.54	4	21.08	5	13.41	7	11.38	4					13.56	6
α Pyx	20.52	1	<15.04	2	11.94	1								
κ Vel	20.48	1	<17.70	2	12.04	3	10.19	5						
23 Sex	20.83	2			>13.15	8	11.78	2					12.90	7
ρ Leo	20.26	1	15.61	1	12.01	3	10.16	2			13.33	2		
θ Car	20.28	1	<17.65	1	11.81	9					>13.12	2		
HD 93521	20.11	1	17.20	6	12.20	6								
δ Cru	20.04	1	<14.08	2	10.86	10								
HD 110432					14.00	2	11.86	6					13.19	3
α Vir	19.00	1	12.95	1	10.65	6	<9.23	2			11.65	5		
ϵ Cen	19.90	1	<14.08	2	10.90	10								
μ Cen	20.40	1	<14.78	2	10.98	10								
ζ Cen	<20.02	1	12.80	1	10.48	10								
β Cen	19.52	1	12.80	1	10.48	9								
η Cen	20.11	1	<14.18	2	10.46	10								
δ Lup	20.18	1	<14.26	2	<10.16	10								
γ Lup	20.23	1	<14.26	2	<9.85	10								
HD 141569							11.06	7					12.76	8
1 Sco	21.20	1	19.23	1	12.67	3	11.00	2			13.97	1	<12.26	4
π Sco	20.75	1	19.32	1	11.68	3	<10.36	3			12.91	2	<11.18	4
δ Sco	21.17	1	19.41	1	12.94	2	11.26	2	8.92	6	14.30	4	12.34	3
β^1 Sco	21.14	1	19.83	1	12.94	2	11.13	2	<8.82	5	14.42	6	12.32	3
ω^1 Sco	21.24	1	20.05	1	13.11	2	11.17	2			13.97	1	12.51	1
ν Sco	21.19	1	19.89	1	13.04	2	11.39	2			14.56	1	12.77	1
HD 146010					>12.52	8	11.53	2					11.40	7
o Sco							12.07	2	<9.66	1			13.77	1
σ Sco	21.36	1	19.79	1	12.72	2	11.14	2	9.32	5	14.34	1	12.49	1
HD 147889							12.59	8	10.18	4			14.08	1
ρ Oph	21.63	5	20.57	1	13.71	2	12.01	2	9.90	7	15.53	6	13.36	3

TABLE 7—*Continued*

Star	H_{tot}	Reference[b]	H_2	Reference[c]	Na I	Reference[d]	K I	Reference[e]	Li I	Reference[f]	C I	Reference[g]	CH	Reference[h]
χ Oph	21.36	1	20.63	1	13.92	2	11.86	2			15.33	6	13.48	3
22 Sco	20.96	1	18.74	1			10.45	2			13.95	1		
μ Nor	21.19	1	20.45	1	13.64	5					>15.31	1	13.00	1
τ Sco	20.49	1	14.51	1	11.77	3	<10.23	3						
ζ Oph	21.15	1	20.64	1	13.85	2	11.85	2	9.60	7	15.51	2	13.40	3
HD 149881	20.65	1	<19.00	1	12.29	6	<10.93	1						
μ^1 Sco	20.40	1	<14.26	2	11.00	1								
HD 151804	21.01	1	20.26	1	13.54	5							12.70	1
ζ^1 Sco	21.77	2			14.38	5							13.38	9
HD 152249	21.41	2			13.56	5							12.65	1
HD 152270					13.84	5							13.10	9
HD 154090	21.14	2			14.26	2	12.00	2						
HD 154368	21.62	6	21.20	7	14.43	2	12.35	2	10.50	8	16.22	7	13.95	1
HD 155806	21.14	1	19.92	1			11.73	1						
γ Ara	20.71	1	19.23	1	>12.24	9					13.87	1	<11.78	1
HD 157841							12.00	7					13.29	8
λ Sco	19.38	1	12.70	1	10.30	6								
κ Sco	20.36	1	<14.23	2	11.51	1								
67 Oph	21.14	1	20.26	1	13.38	2	11.37	2	<9.70	4			12.65	3
θ Ara	20.85	1	<18.95	1	>12.27	9	11.25	2			14.84	1		
HD 164402	21.13	1	19.49	1			11.55	1						
μ Sgr					13.43	2	11.51	2					12.78	3
15 Sgr	21.25	1	20.28	1			11.60	1					12.69	1
HD 169454							12.28	9	<10.17	2			13.75	1
β Lyr					13.25	2	11.16	2						
κ Aql	21.08	1	20.31	1			11.39	1			14.37	1	12.81	3
9 Sge	21.04	1					>11.86	1						
HD 187982							12.50	1	10.00	2				
HD 188209	21.00	1	20.01	1	13.73	5	11.66	1						
HD 188439	20.89	1	19.95	1			11.61	1						
P Cyg	21.28	2			13.18	2	11.43	2						
HD 193322	21.16	1	20.08	1			11.94	1					13.23	1
γ Cyg					12.34	1	<10.36	3						
α Cyg					12.74	3	10.92	2	<9.22	2				
λ Cyg					12.27	3	10.23	2						
55 Cyg					13.98	2	12.02	2	9.72	2			13.49	1
59 Cyg	20.34	1	19.30	1	12.48	3	<10.71	1			13.94	1		
υ Cyg	20.71	1	19.15	2	12.03	3					<13.40	2		
68 Cyg	21.15	1	20.30	1	>13.08	1							12.92	3
69 Cyg	21.03	1	19.60	1			11.11	1						
β Cep	19.93	2			11.31	1								
9 Cep					14.11	2	12.22	2					13.46	1
HD 206267					14.28	2	12.30	2					13.41	1
HD 207198	21.34	2					12.39	2					13.66	1
ν Cep							12.28	2	9.94	2				
19 Cep	21.19	1	20.08	1	>13.36	1	11.81	2					13.04	1

TABLE 7—*Continued*

Star	H_{tot}	Reference[b]	H_2	Reference[c]	Na I	Reference[d]	K I	Reference[e]	Li I	Reference[f]	C I	Reference[g]	CH	Reference[h]
λ Cep	21.40	1	20.78	1	14.18	2	12.14	2	< 10.09	1			13.34	3
π Aqr	20.58	2			12.66	3	10.71	2						
HD 214080......	20.64	1	< 19.00	1	12.76	4								
10 Lac	20.72	1	19.22	1	> 12.76	1	11.05	1						
HD 215733......	20.70	1			12.76	6	11.08	2						
1 Cas	21.07	1	20.15	1	> 12.96	1	11.72	3					12.88	1
HD 219188......	20.87	1	19.34	1	12.70	6	10.63	2						
o And............			19.67	2	12.71	3	10.81	2			13.60	3	< 12.11	1
6 Cas					> 13.56	1	12.05	2	< 9.82	2				
σ Cas	21.04	1	20.23	1	> 13.08	1	> 11.67	1			14.74	1	12.54	1

NOTE.—Table 7 is also available in machine-readable form in the electronic edition of the *Astrophysical Journal*.

[a] Entries are log (N) (cm^{-2}). Numbers following each entry give reference (see subsequent notes).

[b] H_{tot}: (1) Bohlin et al. 1978; (2) Diplas & Savage 1994; (3) Savage & Jenkins 1972; Spitzer et al. 1973; (4) Snow et al. 2000; (5) Shull & Van Steenberg 1985; (6) Snow et al. 1996.

[c] H_2: (1) Savage et al. 1977; (2) Jenkins et al. 1986; (3) Welty et al. 1999b; (4) Jenkins & Peimbert 1996; Jenkins et al. 2000; (5) Snow et al. 2000; (6) Caldwell 1979; (7) Snow et al. 1996.

[d] Na I: (1) Hobbs 1974c, 1978; (2) this paper (U lines fitted using K I component structure); (3) Welty et al. 1994, 1996, 1999b; (4) Ryans et al. 1996, Sembach et al. 1993; (5) U lines (see text for references); (6) Welty, unpublished; (7) Snow et al. 2000; (8) Penprase 1993; (9) Ferlet et al. 1985; (10) Crawford 1991, Centurion & Vladilo 1991, Welsh et al. 1990, 1991.

[e] K I: (1) Chaffee & White 1982; (2) this paper, Welty, unpublished; (3) Hobbs 1974c, 1978; (4) Snow et al. 2000; (5) Dunkin & Crawford 1999; (6) Crawford 1995; (7) Sahu et al. 1998; (8) Haffner & Meyer 1995; (9) Federman & Lambert 1992.

[f] Li I: (1) Hobbs 1984 (see text); (2) White 1986; (3) Knauth et al. 2000; (4) J. Thorburn 2000, private communication; (5) Vanden Bout et al. 1978, Snell & Vanden Bout 1981; (6) Ferlet & Dennefeld 1984; (7) Lemoine et al. 1993, 1995, Meyer et al. 1993; (8) Snow et al. 1996, J. Black 2000, private communication.

[g] C I: (1) Jenkins et al. 1983; (2) Jenkins & Shaya 1979; (3) Welty et al. 1991; (4) Welty et al. 1999b, Welty, unpublished; (5) York & Kinahan 1979; (6) Zsargó et al. 1997; (7) Snow et al. 1996.

[h] CH: (1) Federman et al. 1994, S. Federman 2000, private communication; (2) White 1984; (3) Crane et al. 1995; (4) Welty et al. 1999b, Welty, unpublished; (5) Jenniskens et al. 1992; (6) Snow et al. 2000; (7) Penprase 1993; (8) Sahu et al. 1998; (9) Crawford 1995.

CH column densities in the latter compilation were derived from equivalent widths for the relatively strong λ4300 line using a curve of growth corresponding to a single component with $b = 1.0$ km s^{-1}. Those column densities therefore may be overestimated for sight lines where the CH component structure is more complex. For example, the N(CH) listed in Table 7 for AE Aur, based on higher resolution CH spectra subsequently obtained by S. Federman (2000, private communication), is 0.42 dex lower than the value listed in the compilation.

REFERENCES

Albert, C. E. 1983, ApJ, 272, 509
Albert, C. E., Blades, J. C., Morton, D. C., Lockman, F. J., Proulx, M., & Ferrarese, L. 1993, ApJS, 88, 81
Allain, T., Leach, S., & Sedlmayr, E. 1996, A&A, 305, 616
Allamandola, L. J., Tielens, A. G. G. M., & Barker, J. R. 1985, ApJ, 290, L25
Anders, E., & Grevesse, N. 1989, Geochim. Cosmochim. Acta, 53, 197
Bakes, E. L. O., & Tielens, A. G. G. M. 1994, ApJ, 427, 822
———. 1998, ApJ, 499, 258
Barlow, M. J., Crawford, I. A., Diego, F., Dryburgh, M., Fish, A. C., Howarth, I. A., Spyromilio, J., & Walker, D. D. 1995, MNRAS, 272, 333
Blauuw, A. 1963, in Stars and Stellar Systems 3, Basic Astronomical Data, ed. K. Aa. Strand (Chicago: Univ. Chicago Press), 401
Bohlin, R. C., Savage, B. D., & Drake, J. F. 1978, ApJ, 224, 132
Caldwell, J. A. R. 1979, Ph.D. thesis, Princeton Univ.
Cardelli, J. A., & Meyer, D. M. 1997, ApJ, 477, L57
Cardelli, J. A., Meyer, D. M., Jura, M., & Savage, B. D. 1996, ApJ, 467, 334
Centurion, M., & Vladilo, G. 1991, ApJ, 372, 494
Chaffee, F. H., & Dunham, T. 1979, ApJ, 233, 568
Chaffee, F. H., & White, R. E. 1982, ApJS, 50, 169 (CW)
Crane, P., Lambert, D. L., & Sheffer, Y. 1995, ApJS, 99, 107 (CLS)
Crawford, I. A. 1991, A&A, 247, 183
———. 1992, MNRAS, 259, 47
———. 1995, MNRAS, 277, 458
Crutcher, R. M. 1975, ApJ, 202, 634
———. 1976, ApJ, 208, 382
———. 1978, ApJ, 219, 72
Danks, A. C., Federman, S. R., & Lambert, D. L. 1984, A&A, 130, 62
de Boer, K. S., & Pottasch, S. R. 1974, A&A, 32, 1
de Geus, E. J., & Burton, W. B. 1991, A&A, 246, 559
de Geus, E. J., de Zeeuw, P. T., & Lub, J. 1989, A&A, 216, 44
Diego, F. 1993, Appl. Opt., 32, 6284
Diego, F., et al. 1995, MNRAS, 272, 323
Diplas, A., & Savage, B. D. 1994, ApJS, 93, 211
Draine, B. T. 1978, ApJS, 36, 595
Dunkin, S. K., & Crawford, I. A. 1999, MNRAS, 302, 197
ESA. 1997, The *Hipparcos* and Tycho Catalogues (ESA SP-1200) (Noordwijk: ESA)
Federman, S. R. 1981, A&A, 96, 198
Federman, S. R., & Lambert, D. L. 1992, AJ, 104, 691
Federman, S. R., Strom, C. J., Lambert, D. L., Cardelli, J. A., Smith, V. V., & Joseph, C. L. 1994, ApJ, 424, 772
Federman, S. R., Welty, D. E., & Cardelli, J. A. 1997, ApJ, 481, 795
Ferlet, R., & Dennefeld, M. 1984, A&A, 138, 303
Ferlet, R., Vidal-Madjar, A., & Gry, C. 1985, ApJ, 298, 838
Fitzpatrick, E. L., & Massa, D. 1990, ApJS, 72, 163
Fitzpatrick, E. L., & Spitzer, L. 1997, ApJ, 475, 623
Grevesse, N., & Noels, A. 1993, in Origin of the Elements, ed. N. Prantzos et al. (Cambridge: Cambridge Univ. Press), 15
Haffner, L. M., & Meyer, D. M. 1995, ApJ, 453, 450
Herbig, G. H. 1993, ApJ, 407, 142
Hobbs, L. M. 1969, ApJ, 157, 135
———. 1974a, ApJ, 188, L67
———. 1974b, ApJ, 188, L107
———. 1974c, ApJ, 191, 381
———. 1974d, ApJ, 191, 395
———. 1975, ApJ, 200, 621
———. 1976, ApJ, 203, 143
———. 1978, ApJS, 38, 129
———. 1984, ApJ, 286, 252
Hoffleit, D. 1982, The Bright Star Catalogue (New Haven: Yale Univ. Obs.)
Hoffleit, D., Saladyga, M., & Wlasuk, P. 1983, A Supplement to the Bright Star Catalogue (New Haven: Yale Univ. Obs.)
Jenkins, E. B. 2000, BAAS, 196, 3518
Jenkins, E. B., Jura, M., & Loewenstein, M. 1983, ApJ, 270, 88
Jenkins, E. B., & Peimbert, A. 1996, ApJ, 477, 265
Jenkins, E. B., Savage, B. D., & Spitzer, L. 1986, ApJ, 301, 355
Jenkins, E. B., & Shaya, E. J. 1979, ApJ, 231, 55
Jenkins, E. B., Woźniak, P. R., Sofia, U. J., Sonneborn, G., & Tripp, T. M. 2000, ApJ, 538, 275
Jenniskens, P., Ehrenfreund, P., & Désert, F.-X. 1992, A&A, 265, L1
Johnson, H. L. 1963, in Stars and Stellar Systems 3, Basic Astronomical Data, ed. K. Aa. Strand (Chicago: Univ. Chicago Press), 214
Josafatsson, K., & Snow, T. P. 1987, ApJ, 319, 436
Krelowski, J., Ehrenfreund, P., Foing, B. H., Snow, T. P., Weselak, T., Tuairisg, S. Ó., Galazutdinov, G. A., & Musaev, F. A. 1999, A&A, 317, 235
Krelowski, J., Galazutdinov, G. A., & Musaev, F. A. 1998, ApJ, 493, 217
Knauth, D. C., Federman, S. R., Lambert, D. L., & Crane, P. 2000, Nature, 405, 656
Lauroesch, J. T., & Meyer, D. M. 1999, ApJ, 519, L181
Léger, A., & d'Hendecourt, L. B. 1985, A&A, 146, 81
Lemoine, M., Ferlet, R., & Vidal-Madjar, A. 1995, A&A, 298, 879
Lemoine, M., Ferlet, R., Vidal-Madjar, A., Emerich, C., & Bertin, P. 1993, A&A, 269, 469
Lepp, S., & Dalgarno, A. 1988a, ApJ, 324, 553
———. 1988b, ApJ, 335, 769
Lepp, S., Dalgarno, A., van Dishoeck, E. F., & Black, J. H. 1988, ApJ, 329, 418
Lequeux, J. 1989, in Recent Developments of Magellanic Cloud Research, ed. K. S. de Boer, F. Spite, & G. Stasinska (Paris: Paris Obs.), 119
Lyons, M. A., Bates, B., Kemp, S. N., & Davies, R. D. 1995, MNRAS, 277, 113
Meyer, D. M., Cardelli, J. A., & Sofia, U. J. 1997, ApJ, 490, L103
Meyer, D. M., Hawkins, I., & Wright, E. L. 1993, ApJ, 409, L61
Meyer, D. M., Jura, M., & Cardelli, J. A. 1998, ApJ, 493, 222
Morton, D. C. 1991, ApJS, 77, 119
O'Dell, C. R., Valk, J. H., Wen, Z., & Meyer, D. M. 1993, ApJ, 403, 678
Omont, A. 1986, A&A, 164, 159
Pak, S., Jaffe, D. T., van Dishoeck, E. F., Johansson, L. E. B., & Booth, R. S. 1998, ApJ, 498, 735
Palmer, B. A., & Engelman, R. 1983, Atlas of the Thorium Spectrum (Los Alamos Nat. Lab. Rep. LA-9615)
Penprase, B. E. 1993, ApJS, 88, 433
Péquignot, D., & Aldrovandi, S. M. V. 1986, A&A, 161, 169
Roberge, W. G., Dalgarno, A., & Flannery, B. P. 1981, ApJ, 243, 817
Ryans, R. S. I., Sembach, K. R., & Keenan, F. P. 1996, A&A, 314, 609
Sahu, M. S., Blades, J. C., He, L., Hartmann, D., Barlow, M. J., & Crawford, I. A. 1998, ApJ, 504, 522
Salama, F., Bakes, E. L. O., Allamandola, L. J., & Tielens, A. G. G. M. 1996, ApJ, 458, 621
Savage, B. D., Bohlin, R. C., Drake, J. F., & Budich, W. 1977, ApJ, 216, 291
Savage, B. D., & Jenkins, E. B. 1972, ApJ, 172, 491
Sembach, K. R., Danks, A. C., & Lambert, D. L. 1996, ApJ, 460, L61
Sembach, K. R., Danks, A. C., & Savage, B. D. 1993, A&AS, 100, 107
Shulman, S., Bortolot, V. J., & Thaddeus, P. 1974, ApJ, 193, 97
Shull, J. M., & Van Steenberg, M. E. 1985, ApJ, 294, 599
Shuping, R. Y., & Snow, T. P. 1997, ApJ, 480, 272
Snell, R. L., & Vanden Bout, P. A. 1981, ApJ, 250, 160
Snow, T. P. 1984, ApJ, 287, 238
Snow, T. P., Black, J. H., van Dishoeck, E. F., Burks, G., Crutcher, R. M., Lutz, B. L., Hanson, M. M., & Shuping, R. Y. 1996, ApJ, 465, 245
Snow, T. P., et al. 2000, ApJ, 538, L65
Snow, T. P., & Seab, C. G. 1991, ApJ, 382, 189
Sofia, U. J., Cardelli, J. A., Guerin, K. P., & Meyer, D. M. 1997, ApJ, 482, L105
Sofia, U. J., Fitzpatrick, E. L., & Meyer, D. M. 1998, ApJ, 504, L47
Sonnentrucker, P., Cami, J., Ehrenfreund, P., & Foing, B. H. 1997, A&A, 327, 1215
Spitzer, L. 1968, Diffuse Matter in Space (New York: Wiley)
Spitzer, L., Drake, J. F., Jenkins, E. B., Morton, D. C., Rogerson, J. B., & York, D. G. 1973, ApJ, 181, L116
Steigman, G. 1996, ApJ, 457, 737
Stokes, G. M. 1978, ApJS, 36, 115
Tarafdar, S. P. 1977, A&A, 61, 755
Trapero, J., Beckman, J. E., Genova, R., & McKeith, C. D. 1992, ApJ, 394, 552
Trapero, J., Beckman, J. E., Serra-Ricart, M., Davies, R. D., Watson, R. A., & Lopez, R. J. G. 1995, ApJ, 445, 231
Vanden Bout, P. A., Snell, R. L., Vogt, S. S., & Tull, R. G. 1978, ApJ, 221, 598
Watson, J. K., & Meyer, D. M. 1996, ApJ, 473, L127
Welsh, B. Y., Crifo, F., & Lallement, R. 1998, A&A, 333, 101
Welsh, B. Y., Sasseen, T., Craig, N., Jelinsky, S., & Albert, C. E. 1997, ApJS, 112, 507
Welsh, B. Y., Vedder, P. W., & Vallerga, J. V. 1990, ApJ, 358, 473
Welsh, B. Y., Vedder, P. W., Vallerga, J. V., & Craig, N. 1991, ApJ, 381, 462
Welty, D. E. 1989, in The Interstellar Medium in External Galaxies, ed. D. J. Hollenbach & H. A. Thronson (NASA Conf. Publ. CP-3084), 42
Welty, D. E., Frisch, P. C., Sonneborn, G., & York, D. G. 1999a, ApJ, 512, 636
Welty, D. E., Hobbs, L. M., & Kulkarni, V. P. 1994, ApJ, 436, 152 (WHK)
Welty, D. E., Hobbs, L. M., Lauroesch, J. T., Morton, D. C., Spitzer, L., & York, D. G. 1999b, ApJS, 124, 465

Welty, D. E., Hobbs, L. M., Lauroesch, J. T., Morton, D. C., & York, D. G. 1995, ApJ, 449, L135
Welty, D. E., Hobbs, L. M., & York, D. G. 1991, ApJS, 75, 425
Welty, D. E., Lauroesch, J. T., Blades, J. C., Hobbs, L. M., & York, D. G. 1997, ApJ, 489, 672
Welty, D. E., Lauroesch, J. T., Sembach, K. R., & York, D. G. 2001a, in preparation
Welty, D. E., Morton, D. C., & Hobbs, L. M. 1996, ApJS, 106, 533 (WMH)
Welty, D. E., Morton, D. C., & Snow, T. P. 2001b, in preparation
White, R. E. 1984, ApJ, 284, 685
White, R. E. 1986, ApJ, 307, 777
York, D. G. 1980, in Astrophysics from Spacelab, ed. P. L. Bernacca & R. Ruffini (Dordrecht: Reidel), 609
York, D. G., & Kinahan, B. F. 1979, ApJ, 228, 127
York, D. G., Spitzer, L., Bohlin, R. C., Hill, J., Jenkins, E. B., Savage, B. D., & Snow, T. P. 1983, ApJ, 266, L55
Zsargó, J., Federman, S. R., & Cardelli, J. A. 1997, ApJ, 484, 820